

LA-UR-97-4423

Approved for public release;  
distribution is unlimited.

*Title:* **Nuclear Fuels Technologies  
Fiscal Year 1997 Research and  
Development Test Results**

*Author(s):* H. R. Trelue  
T. Baros  
H. T. Blair  
J. J. Buksa  
D. P. Butt  
K. Chidester  
S. F. DeMuth  
S. L. Eaton  
G. J. Havrilla  
R. J. Hanrahan, Jr.  
C. A. James  
D. G. Kolman  
R. E. Mason  
Y. Park  
M. Stan  
J. H. Steele, Jr.  
S. S. Voss  
T. C. Wallace, Sr.  
C. G. Worley

**Los Alamos**  
NATIONAL LABORATORY

Los Alamos National Laboratory, an affirmative action/equal opportunity employer, is operated by the University of California for the U.S. Department of Energy under contract W-7405-ENG-36. By acceptance of this article, the publisher recognizes that the U.S. Government retains a nonexclusive, royalty-free license to publish or reproduce the published form of this contribution, or to allow others to do so, for U.S. Government purposes. Los Alamos National Laboratory requests that the publisher identify this article as work performed under the auspices of the U.S. Department of Energy. Los Alamos National Laboratory strongly supports academic freedom and a researcher's right to publish; as an institution, however, the Laboratory does not endorse the viewpoint of a publication or guarantee its technical correctness.

**Nuclear Fuels Technologies**  
**Fiscal Year 1997 Research and Development Test Results**

H. R. Trellue, T. Baros, H. T. Blair, J. J. Buksa, D. P. Butt,  
K. Chidester, S. F. DeMuth, S. L. Eaton, G. J. Havrilla,  
R. J. Hanrahan, Jr., C. A. James, D. G. Kolman, R. E. Mason, Y. Park,  
M. Stan, J. H. Steele, Jr., S. S. Voss, T. C. Wallace, Sr., and C. G. Worley

**Los Alamos National Laboratory**

November 1997



## Table of Contents

List of Tables.....	vii
List of Figures.....	viii
EXECUTIVE SUMMARY .....	1
1.0. INTRODUCTION.....	3
2.0. FEED QUALIFICATION.....	4
2.1. PuO <sub>2</sub> Production .....	4
2.1.1. HYDOX-Derived PuO <sub>2</sub> .....	4
2.1.2. Aqueous-Derived PuO <sub>2</sub> .....	10
2.2. Ga Removal.....	10
2.2.1. Thermodynamics and Phase Relationships .....	11
2.2.1.1. Development of a Relational Thermodynamic Database.....	12
2.2.1.2. Calculations of Ga <sub>2</sub> O(g) Partial Pressures.....	12
2.2.1.3. Thermodynamics and Phase Relations in the System Ga-O.....	15
2.2.1.4. Thermodynamics and Phase Relations in the System Pu-O.....	18
2.2.1.5. Thermodynamics and Phase Relations in the System Ce-O.....	24
2.2.1.6. Solubility of Ga <sub>2</sub> O <sub>3</sub> in PuO <sub>2</sub> and the Ga <sub>2</sub> O <sub>3</sub> -PuO <sub>2</sub> Pseudobinary and Ternary Phase Diagrams.....	25
2.2.1.7. Thermodynamics of the Perovskite Phase in PuO <sub>2-x</sub> and CeO <sub>2-x</sub> .....	30
2.2.2. Ga Removal from Surrogate MOX Fuel .....	38
2.2.2.1 CeO <sub>2</sub> -Ga <sub>2</sub> O <sub>3</sub> .....	38
2.2.2.2 Ga Removal in Surrogate Feedstock.....	42
2.2.3. PuO <sub>2</sub> Studies .....	51
2.2.4. Development of a Production-Scale TIGR System.....	51
2.2.4.1. TIGR Overview .....	52
2.2.4.2. Design Parameters.....	54
2.2.4.3. System and Equipment Description.....	56
2.2.4.4. Modeling of the Plutonium and Gallium Separation.....	57
2.2.4.5. Preliminary Cost and Schedule Estimates .....	59
2.2.4.6. Conclusions .....	59
2.2.4.7. Aqueous Separation of Plutonium and Gallium.....	60
3.0. FUEL FABRICATION DEVELOPMENT .....	62
3.1. Fabrication Studies.....	62
3.1.1. PuO <sub>2</sub> Variability.....	63
3.1.2. UO <sub>2</sub> Variability .....	65
3.1.3. Sintering Study.....	65
3.2. Analytical Development.....	67
3.2.1. Homogeneity.....	68
3.2.2. Upgrade TA-55 Analytical Capability.....	69

3.2.3. Trace Analysis Validation .....	69
3.2.4. X-Ray Microfluorescence Gallium Measurement .....	70
3.2.4.1. Elemental Detection.....	71
3.2.4.2. Demonstrate Phase Identification .....	72
3.2.4.3. XRMF of MOX Fuel Surrogates.....	73
3.2.4.3.1. Experimental Parameters.....	73
3.2.4.3.2. Results and Discussion .....	75
3.2.4.3.3. Conclusions .....	84
4.0. SUMMARY OF ACTIVITIES IN FY97.....	85
5.0. REFERENCES.....	89

## List of Tables

TABLE 2.1.1-1	PuO <sub>2</sub> POWDER CHARACTERISTICS .....	6
TABLE 2.2.1-1	SUMMARY OF X-RAY CRYSTALLOGRAPHIC DATA OF PLUTONIUM OXIDES.....	12
TABLE 2.2.1-2	SUMMARY OF REPORTED THERMODYNAMIC VALUES FOR PLUTONIUM OXIDES.....	13
TABLE 2.2.1-3	SUMMARY OF CONSTANTS SHOWN IN EQUATION 1.....	14
TABLE 2.2.1-4	SUMMARY OF X-RAY CRYSTALLOGRAPHIC DATA OF GALLIUM OXIDES.....	17
TABLE 2.2.1-5	SUMMARY OF REPORTED OR ASSESSED $\Delta G_F^O$ EQUATIONS FOR GALLIUM AND ITS OXIDES.....	17
TABLE 2.2.1-6	REGULAR SOLUTION MODEL PARAMETERS USED IN ASSESSING THE Ga <sub>2</sub> O <sub>3</sub> -Ga PSEUDOINARY PHASE DIAGRAM.....	17
TABLE 2.2.1-7	CALCULATED REDUCING AND OXIDIZING OXYGEN PRESSURES, AND $\Delta G_f$ AS FUNCTION OF TEMPERATURE .....	33
TABLE 2.2.1-8	LINEAR LEAST SQUARE FIT OF DATA IN TABLE 2.2.1-7 .....	34
TABLE 2.2.1-9	SUMMARY OF PLUTONIUM PEROVSKITE PREPARATIONS.....	36
TABLE 2.2.1-10	SUMMARY OF PuAlO <sub>3</sub> PREPARATIONS .....	37
TABLE 2.2.2-1	DESCRIPTION OF RAW MATERIALS USED TO FABRICATE SURROGATE FEEDSTOCK POWDERS.....	39
TABLE 2.2.2-2	PROCESSING EQUIPMENT USED TO FABRICATE CeO <sub>2</sub> -2 wt % Ga <sub>2</sub> O <sub>3</sub> POWDERS .....	39
TABLE 2.2.4-1	PRELIMINARY DESIGN PARAMETERS FOR THE TIGR SYSTEM .....	55
TABLE 3.1.1-1	RESULTS OF PELLET MEASUREMENTS FOR PARALLEX MOX FUEL PELLETS .....	63
TABLE 3.2.3-1	RESULTS FROM GALLIUM CONCENTRATION ANALYSES .....	70
TABLE 4.0-1	FISCAL YEAR 1997 R&D MILESTONE SUMMARY.....	85

## List of Figures

Figure 2.1.1-a.	Particle size distribution for 2-Step LLNL PuO <sub>2</sub> .....	7
Figure 2.1.1-b.	Particle size distribution for 3-Step LLNL PuO <sub>2</sub> .....	7
Figure 2.1.1-c.	Particle size distribution for Los Alamos PuO <sub>2</sub> .....	8
Figure 2.1.2-a.	Morphology of LLNL 2-Step PuO <sub>2</sub> powder.....	8
Figure 2.1.2-b.	Morphology of LLNL 3-Step PuO <sub>2</sub> powder.....	9
Figure 2.1.2-c.	Morphology of Los Alamos PuO <sub>2</sub> powder.....	9
Figure 2.2.1-1.	Structure of thermodynamic database management system.....	14
Figure 2.2.1-2.	Calculated equilibrium partial pressures above aGa <sub>2</sub> O <sub>3</sub> = 0.01 in reducing atmospheres and vacuum.....	16
Figure 2.2.1-3	Calculated Ga-Ga <sub>2</sub> O <sub>3</sub> phase diagram.....	18
Figure 2.2.1-4.	The Gibbs free energy of PuO <sub>2-x</sub> in a solid solution of Pu <sub>4/3</sub> O <sub>2</sub> and PuO <sub>2</sub> ...	18
Figure 2.2.1-5.	The calculated Gibbs free energy of γ and a'' phases in Pu-O system at 1000 K. ....	20
Figure 2.2.1-6.	The calculated Gibbs free energy of γ and a'' phases in Pu-O system at 1250 K. ....	21
Figure 2.2.1-7.	The calculated Gibbs free energy of γ and a'' phases in Pu-O system at 1500 K. ....	21
Figure 2.2.1-8.	The calculated Gibbs free energy of γ and a'' phases in Pu-O system at 2000 K. ....	22
Figure 2.2.1-9.	The calculated Gibbs free energy of γ and a'' phases in Pu-O system at 2250 K. ....	22
Figure 2.2.1-10.	The calculated Gibbs free energy of γ and a'' phases in Pu-O system at 2553 K. ....	23
Figure 2.2.1-11.	The calculated Gibbs free energy of γ and a'' phases in Pu-O system at 2633 K. ....	23
Figure 2.2.1-12.	Calculated Pu-O binary phase diagram.....	24
Figure 2.2.1-13.	Assessment of the Ce-O phase diagram .....	24
Figure 2.2.1-14.	Assessment of the composition and temperature dependence of the spinodal decomposition of CeO <sub>2-x</sub> .....	25
Figure 2.2.1-15.	The measured solubility limit of Al <sub>2</sub> O <sub>3</sub> and the estimated solubility limit of Ga <sub>2</sub> O <sub>3</sub> in PuO <sub>2</sub> .....	26
Figure 2.2.1-16.	The calculated Ga <sub>2</sub> O <sub>3</sub> -PuO <sub>2</sub> phase diagram under oxidizing conditions assuming Ga <sub>2</sub> O <sub>3</sub> and PuO <sub>2</sub> are insoluble in one another. ....	27
Figure 2.2.1-17.	The calculated Ga <sub>2</sub> O <sub>3</sub> -PuO <sub>2</sub> phase diagram under oxidizing conditions assuming Ga <sub>2</sub> O <sub>3</sub> and PuO <sub>2</sub> are mutually soluble in one another to 0.1 atom percent.....	27
Figure 2.2.1-18.	Preliminary pseudobinary phase diagram of the Ga <sub>2</sub> O <sub>3</sub> -PuO <sub>2</sub> system under reducing conditions .....	28

Figure 2.2.1-19. Preliminary 1000 K isothermal ternary phase diagram for the system Pu-Ga-O.....	29
Figure 2.2.1-20. Preliminary 2000 K isothermal ternary phase diagram for the system Pu-Ga-O.....	29
Figure 2.2.1-21. The influence of the reducing conditions on the Ga <sub>2</sub> O <sub>3</sub> -PuO <sub>2-x</sub> phase diagram.....	30
Figure 2.2.1-22. Equilibrium phase diagram of $\log P_{O_2} = f\left(\frac{Ga}{Ce+Ga}\right)$ for the Ce-Ga-O system at 1500 K.....	32
Figure 2.2.1-23. Partial Ce-Ga-O phase diagram at 1573 K.....	32
Figure 2.2.1-24. Diagram of $\log(P_{O_2}) = f(1/T)$ defining PuGaO <sub>3</sub> and CeGaO <sub>3</sub> zones of stability.....	33
Figure 2.2.1-25. Equilibrium phase diagram of $\log P_{O_2} = f\left(\frac{Ga}{Pu+Ga}\right)$ for the Pu-Ga system at 1500 K.....	34
Figure 2.2.1-26. Partial Pu-Ga-O phase diagram at 1500 K.....	35
Figure 2.2.2-1. Flow chart illustrating processing steps used to fabricate CeO <sub>2</sub> -2 wt % Ga <sub>2</sub> O <sub>3</sub> powders.....	40
Figure 2.2.2-2. Plot of green and fired densities of CeO <sub>2</sub> -2% Ga <sub>2</sub> O <sub>3</sub> pellets after the steps described in Figure 2.2.2-1.....	41
Figure 2.2.2-3. Fired CeO <sub>2</sub> -2% Ga <sub>2</sub> O <sub>3</sub> pellets.....	41
Figure 2.2.2-4. Microstructure of the sintered CeO <sub>2</sub> -2% Ga <sub>2</sub> O <sub>3</sub> pellets.....	42
Figure 2.2.2-5. Photographs of surrogate pellets and powders shown as they were placed in alumina boats for gallium evolution testing.....	43
Figure 2.2.2-6. Schematic diagram of the apparatus assembled and used for Ga vaporization studies.....	43
Figure 2.2.2-7. Plot of weight change versus temperature for CeO <sub>2</sub> -2% Ga <sub>2</sub> O <sub>3</sub> samples exposed to Ar-6% H <sub>2</sub> and Ar for 30 minutes.....	44
Figure 2.2.2-8. Plot of weight change versus time for CeO <sub>2</sub> -2% Ga <sub>2</sub> O <sub>3</sub> samples exposed to Ar-6% H <sub>2</sub> at 600, 900, and 1200°C.....	45
Figure 2.2.2-9. Plot of weight percent gallium (measured by x-ray microfluorescence) versus temperature for CeO <sub>2</sub> -2% Ga <sub>2</sub> O <sub>3</sub> powder samples exposed to Ar-6% H <sub>2</sub> for 30 minutes.....	46
Figure 2.2.2-10. Histogram of PIXE measurements of relative Ga concentration in surrogate MOX after exposure to Ar-6% H <sub>2</sub> at 1200°C for 30 minutes.....	46
Figure 2.2.2-11. XPS spectra (top) comparing the relative Ga concentration in surrogate MOX after exposure to Ar-6% H <sub>2</sub> at 1200°C for 30 minutes.....	47
Figure 2.2.2-12. Histogram of ICP measurements of Ga concentrations in surrogate MOX after exposure to Ar-6% H <sub>2</sub> at 1200°C for 30 minutes.....	48
Figure 2.2.2-13. Plot of weight change versus temperature for CeO <sub>2</sub> -2% Ga <sub>2</sub> O <sub>3</sub> samples exposed to Ar-6% H <sub>2</sub> at 1.5 and 3.0 cm/sec flow rates.....	49
Figure 2.2.2-14. Plot of weight change versus temperature for CeO <sub>2</sub> -2% Ga <sub>2</sub> O <sub>3</sub> samples doped with varying levels of carbon and exposed to Ar-6% H <sub>2</sub> and subsequently air at 1000°C for 30 minutes.....	50

Figure 2.2.2-15. Photograph of CeO <sub>2</sub> /Ga <sub>2</sub> O <sub>3</sub> /CeO <sub>2</sub> diffusion couples following exposure to air at 1000 and 1200°C for 0.5 and 4 hours.....	50
Figure 2.2.4-1. Preliminary flow chart for TIGR process.....	53
Figure 2.2.4-2. Pits to MOX fuel conversion .....	56
Figure 2.2.4-3. Conceptual TIGR design.....	57
Figure 2.2.4-4. Time dependent nature of TIGR mechanisms.....	58
Figure 2.2.4-5. Solvent extraction flowsheet for separating plutonium and gallium.....	60
Figure 2.2.4-6. Ion exchange flowsheet for separating plutonium and gallium.....	61
Figure 2.2.4-7. Oxalate precipitation flowsheet for separation of plutonium and gallium.....	61
Figure 3.1.1-1. Autoradiograph of a high fired Paralex MOX fuel pellet.....	64
Figure 3.1.1-2. Microstructure of a Paralex MOX fuel pellet.....	64
Figure 3.1.3-1. Particle size distribution of CeO <sub>2</sub> powder.....	66
Figure 3.1.3-2. Particle size distribution of Ga <sub>2</sub> O <sub>3</sub> powder.....	66
Figure 3.1.3-3. Particle size distribution of UO <sub>2</sub> powder .....	67
Figure 3.2.4-1. Interior dynamic mode XRMF gallium images acquired of the surrogate pellets reduced from 600°C–1200°C.....	76
Figure 3.2.4-2. Interior dynamic mode XRMF zirconium image of a surrogate pellet reduced at 600°C .....	76
Figure 3.2.4-3. White light of the internal surface of the surrogate pellet reduced at 1200°C .....	77
Figure 3.2.4-3B Dynamic mode XRMF gallium image of the internal surface of the surrogate pellet reduced at 1200°C.....	78
Figure 3.2.4-4. White light image (A) and microprobe mode XRMF gallium image (B) of the internal surface of the surrogate pellet reduced at 1200°C.....	79
Figure 3.2.4-5. Interior dynamic mode XRMF cerium image of a surrogate pellet reduced at 900°C .....	79
Figure 3.2.4-6. Plot of the gallium XRF intensity ratio vs. reduction temperature .....	81
Figure 3.2.4-7. Typical gallium line scan intensity profile observed from the external skin of the reduced surrogate pellets .....	81
Figure 3.2.4-8. Gallium line scan profiles acquired from the outside of the surrogate pellets reduced at 600°C, 800°C, and 1200°C.....	82
Figure 3.2.4-9. Plot of the average P2 gallium intensity vs. reduction temperature from the external line scans of the reduced surrogate pellets.....	83
Figure 3.2.4-10. Plot of the distance from the pellet bottom to the start of the P2 region vs. reduction temperature.....	83
Figure 3.2.4-11. Plot of the XRF gallium/cerium intensity ratio from the reduced surrogate powders vs. reduction temperature.....	84

## EXECUTIVE SUMMARY

During FY97, a number of research and development (R&D) activities occurred at Los Alamos in support of the Department of Energy (DOE) Office of Fissile Materials Disposition's program for the irradiation of excess weapons-grade plutonium as MOX fuel (i.e. reactor-based disposition). The primary purpose of these activities was to conduct studies involving feed qualification as well as ones supporting fuel fabrication and analytical methods development. Research areas included:

- Obtaining PuO<sub>2</sub> feed for research, development, and testing,
- Starting to establish a database of chemical and physical characteristics of various PuO<sub>2</sub> feed materials,
- Establishing a thermodynamic relationship for the Pu-O-Ga system to support the development and design of the TIGR (Thermally Induced Gallium Removal) system,
- Establishing a thermodynamic relationship for the Pu-U-O-Ga system to support MOX sinterability studies,
- Verifying the feasibility of the TIGR system,
- Establishing the use of a plutonium (Pu) surrogate for assessment of the TIGR processing parameters, including benchmarking with PuO<sub>2</sub>,
- Beginning the optimization of TIGR process parameters,
- Beginning a conceptual layout of TIGR production processes, equipment, and costs,
- Identifying backup, aqueous Ga removal processing options and establishing a baseline process,
- Understanding the impact of variations in PuO<sub>2</sub> feedstock (primarily physical characteristics) on fuel fabrication and fuel quality,
- Understanding the impact of variations in UO<sub>2</sub> feedstock on fuel fabrication and fuel quality,
- Establishing AUC-derived UO<sub>2</sub> as the new baseline UO<sub>2</sub> used in all research, development, and testing activities,
- Understanding the impact of gallium on the fuel sintering process and process equipment,
- Establishing an acceptable technique to measure plutonium homogeneity,

- Establishing an acceptable technique to measure the oxygen-to-metal ratio in feedstocks and fuel pellets,
- Establishing an acceptable technique to measure fuel pellet surface finish,
- Validating current techniques for measuring the concentration of trace amounts of elements in feedstocks and fuel pellets, and
- Developing a technique to measure quickly the spatial distribution of residual gallium in green and sintered MOX fuel pellets.

This report summarizes the progress made in FY97 in each of these areas of research.

## 1.0. INTRODUCTION

This document details results from research and development (R&D) activities that were conducted in fiscal year 1997 (FY97) by the Nuclear Fuels Technologies project team for the Department of Energy (DOE) Office of Fissile Materials Disposition. This work was a continuation and extension of experimental activities that have been conducted in support of the disposition program with regard to using weapons plutonium in the fabrication of mixed-oxide (MOX) nuclear fuel for reactor-based disposition. The purpose of this work was to identify and to resolve technical issues associated with applying the large experience base (existing mainly in Europe) of making MOX fuel with recycled reactor-grade plutonium to the fabrication of MOX using surplus plutonium. Therefore, the projects were designed to fill one or more of three needs: (1) To provide potential fabricators a technical basis upon which to evaluate the uncertainties and technical risks associated with MOX fabrication using weapons-plutonium; (2) To provide the fuel fabricator ultimately selected for the disposition mission with a technical basis upon which to build, thereby reducing the amount of development and time required for implementation of the MOX disposition option; and (3) To identify to DOE technical issues unlikely to be addressed by the fabricator (e.g., gallium removal), and to resolve these issues or provide a clear path forward for doing so. Because of the nature of the disposition program as it transitions into the implementation phase, results of experiments in FY97 were obtained for one of two goals: (1) a summary of the technical results sufficient to hand over to commercial MOX fabricators for their use in planning activities; or (2) an estimate with regard to cost and schedule for follow-on activities to completely resolve the issue as well as sufficient technical supporting information for DOE to make well-informed decisions in this regard.

Although fabrication of MOX fuel using reactor-grade plutonium is a well-developed, industrialized process, several differences exist between reactor-grade and surplus weapon plutonium which generate technical issues that must be resolved. These differences include: variation in powder characteristics because the weapons material is to be converted using a dry pyrochemical process as opposed to the chemical dissolution and precipitation processes used in spent-fuel reprocessing facilities; the presence of gallium in the weapons material; and the variation in plutonium isotopics between the reactor-grade and weapons-grade material. All of the experiments described in this report address the first two of these issues.

The projects are divided into two categories: feed qualification (Section 2.0), which deals with issues involving obtaining and characterizing appropriate  $\text{PuO}_2$  sources and developing a process to remove the gallium from the  $\text{PuO}_2$  feed; and fuel fabrication development (Section 3.0), which includes experimental fabrication activities to evaluate the effects of various feeds and processing parameters on the fabrication process and fuel quality, and development of analytical techniques required because of the unique nature of the material or the necessity of upgrading existing laboratory infrastructure.

This document and the R&D experiments performed in FY97 follow the outline and descriptions provided in the *Nuclear Fuel Technologies Fiscal Year 1997 Research and Development Test Plan*.<sup>\*</sup> Exact parameters and measurements obtained during experiments may not directly match those indicated in the Test Plan, but they are relevant nonetheless.

---

<sup>\*</sup> LA-UR-97-449

## 2.0. FEED QUALIFICATION

The current disposition plan as outlined in the General Requirements Document,<sup>1</sup> calls for the conversion of approximately 35 MT of pit material (plutonium in weapons) into MOX fuel PuO<sub>2</sub> feed using the Advanced Recovery and Integrated Extraction System (ARIES). This process, under development at Los Alamos National Laboratory (Los Alamos) and Lawrence Livermore National Laboratories (LLNL), involves production of PuO<sub>2</sub> via hydride-oxidation (2-step), hydride-nitride-oxidation (3-step), or direct oxidation (DO) of plutonium metal (all of these processes are generically referred to as HYDOX). Characterization of the PuO<sub>2</sub> produced by the 2-step and 3-step processes has shown that the physical characteristics (primarily particle morphology) are quite different than those produced by conventional aqueous conversion processes. In addition, any gallium that is contained in the plutonium metal is also converted to oxide (Ga<sub>2</sub>O<sub>3</sub>) during the conversion process and remains as an impurity in the PuO<sub>2</sub> feed. Consequently, in terms of MOX fuel fabrication, it is necessary (1) to demonstrate that the variation in physical characteristics is acceptable for producing quality fuel, (2) to determine the concentration of gallium in the PuO<sub>2</sub> that is considered acceptable, and (3) to show that the gallium concentration in PuO<sub>2</sub> can be reduced to this amount.

### 2.1. PuO<sub>2</sub> Production

During previous fiscal years, a variety of processes were instigated for the production of PuO<sub>2</sub> powder from weapon pits. These included a hydride-oxidation process and a hydride-dehydride process followed by hydride-oxidation. Subsequently, it has been established that neither of these two processes is likely to be prototypic of what ultimately will be used for the disposition mission. Thus, one of the goals in FY97 was to perform analyses on powder produced by the current prototypic process, which is a hydride-nitride-oxide process.

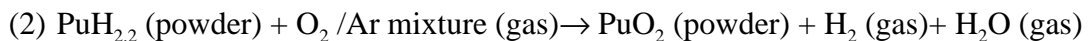
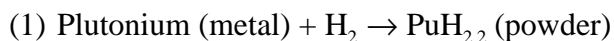
In addition, weapons grade PuO<sub>2</sub> powder that was produced through an aqueous purification method, which is representative of what is used in commercial MOX fuel fabrication, was also obtained, but characterization of this powder has not yet occurred.

Overall, the two main purposes of the research summarized in this section were: (1) to obtain PuO<sub>2</sub> feed for research, development, and testing, and (2) to start establishing a database of chemical and physical characteristics of various PuO<sub>2</sub> feed materials.

#### 2.1.1. HYDOX-Derived PuO<sub>2</sub>

As previously mentioned, there were two variations of the HYDOX process being studied at Lawrence Livermore National Laboratory (LLNL), the "2-Step" and "3-Step." Both of these processes convert metallic plutonium weapon components to PuO<sub>2</sub> ceramic powder using a hydriding step eventually followed by an oxidizing step as shown below:

2-Step:



3-Step:

- (1) Plutonium (metal) + H<sub>2</sub> → PuH<sub>2.2</sub> (powder)
- (2) PuH<sub>2.2</sub> (powder) + N<sub>2</sub> (gas) → PuN (powder) + H<sub>2</sub> (gas)
- (3) PuN (powder) + O<sub>2</sub> /He (gas) → PuO<sub>2</sub> (powder) + He (gas) + N<sub>2</sub>/NO<sub>x</sub> (gas)

The formation of PuH<sub>2.2</sub> destroys the crystalline structure of metallic plutonium, producing a hydride powder which is then oxidized to produce PuO<sub>2</sub>. The 3-Step process consists of an additional step that drives off the hydrogen before oxidation occurs. This step in the 3-Step process avoids the simultaneous presence of the highly combustible oxygen-hydrogen gas mixture necessary in the 2-Step oxidation step.

Six different containers containing plutonium dioxide were received from LLNL during FY97, two of which contained powder from one lot of 2-Step process feed material, one from another lot of 2-Step feed, two more from a lot of 3-Step material, and the remaining one from a separate lot of 3-Step feed material (a lot typically refers to different weapon and/or process types). The 3-Step process samples discussed in this report were taken from this later lot, and the 3-Step material that came from the other two containers has not yet been characterized. The three containers of 2-Step material were blended together before samples were taken, and results from the characterization of this mixture are presented in this report. Table 2.1.1-1 lists final results from the 2-Step and 3-Step powder characterization data from these samples, and it compares them to final results obtained from the PuO<sub>2</sub> powder produced at Los Alamos in FY96. These values do not reflect the powder after any type of thermal treatment for gallium removal.

The gallium content of the LLNL powders on the first line of Table 2.1.1-1 represents the amount measured by LLNL, and the second line is the value as measured by Los Alamos. The gallium content of the Los Alamos-produced powder was slightly larger than that from LLNL, probably because the powders were obtained from different types of weapons. For more information on the methods that were used for gallium detection, see Section 3.2.3. Plutonium and plutonium isotopic concentrations for the two LLNL powders were fairly similar, but they varied slightly for the Los Alamos powder (for example, the weight percent of plutonium in the sample was smaller, the Pu-239 isotopic content was larger, and the Pu-240 isotopic content was smaller). These differences can be attributed either to statistical deviation in chemical analyses or varying compositions of the plutonium from weapon pits.

Figures 2.1.1-a through c are histograms representing the particle size distribution of the three powders that were analyzed. The value listed on the x-axis represents the lower boundary of the range contained in each "bin." These distributions and the mean particle sizes for each of the powders were fairly similar, but the Los Alamos and LLNL 2-Step powders were, on average, slightly larger than the LLNL 3-Step powder. Scanning electron microscopy (SEM) morphology of the three powders indicates that the LLNL powders appear to be more flake-like while the Los Alamos powder is more cake-like. Additionally, Figure 2.1.2-c shows that the Los Alamos powder appears more layered, which may indicate crystal growth of the powder during dehydration. Nonetheless, the morphologies of these powders show that the powders should be acceptable for producing quality fuel.

**TABLE 2.1.1-1**  
**PuO<sub>2</sub> POWDER CHARACTERISTICS**

<b>Characteristic</b>	<b>LLNL 2-Step</b>	<b>LLNL 3-Step</b>	<b>Los Alamos<sup>2</sup></b>
<b>Ga content (weight %)</b>	0.79	0.74 0.88	0.86
<b>Particle size distribution</b>	see Figure 2.1.1-a	see Figure 2.1.1-b	see Figure 2.1.1-c
<b>Mean particle size (μm)</b>	18.40	15.25	17.35
<b>Mean surface area (m<sup>2</sup>/g)</b>	4.01	6.37	6.85
<b>Particle morphology</b>	see Figure 2.1.2-a	see Figure 2.1.2-b	see Figure 2.1.2-c
<b>Plutonium weight percent in sample</b>	86.44	86.37	85.84
<b><u>Isotopic weight %:</u></b>			
<b>Plutonium-238</b>	0.0101	0.0111	0.0124
<b>Plutonium-239</b>	93.8318	93.8044	93.9201
<b>Plutonium-240</b>	6.0008	6.0329	5.8676
<b>Plutonium-241</b>	0.1324	0.1278	0.1406
<b>Plutonium-242</b>	0.0250	0.0238	0.0593
<b>Plutonium-244</b>	0.0000	0.0000	0.0000

Although this limited amount of powder was characterized during FY97, the statistical deviation of the results was fairly small because they only represent a single series of data points. More sample characterization is required in the future to draw definitive conclusions about the 2-Step and 3-Step powders. The Los Alamos-derived PuO<sub>2</sub> powder discussed in this section was used in the fabrication of MOX fuel for the Parallex project,\* and the LLNL powder is currently being used in fabricating MOX fuel for the ATR project.†

---

\* The Parallex project (Parallel Experiment) was performed for DOE's MD program with the intent of placing both MOX fuel fabricated from weapons-grade plutonium here in the United States and in Russia in the AECL-owned test CANDU reactors. Although the logistics of the Parallex program are still being negotiated with Russia and Canada, a number of MOX pellets were produced by Los Alamos for this program.

† After the Parallex project was started for the joint disposition of Russian and U.S. plutonium, it was also desired in the United States to perform sample MOX fuel irradiations in a light water reactor (LWR). The ATR (Advanced Test Reactor) project was then initiated, and it involves the fabrication of MOX fuel from weapons-grade plutonium at Los Alamos and irradiation of the fuel in the ATR reactor at INEEL (Idaho National Engineering and Environmental Laboratory).

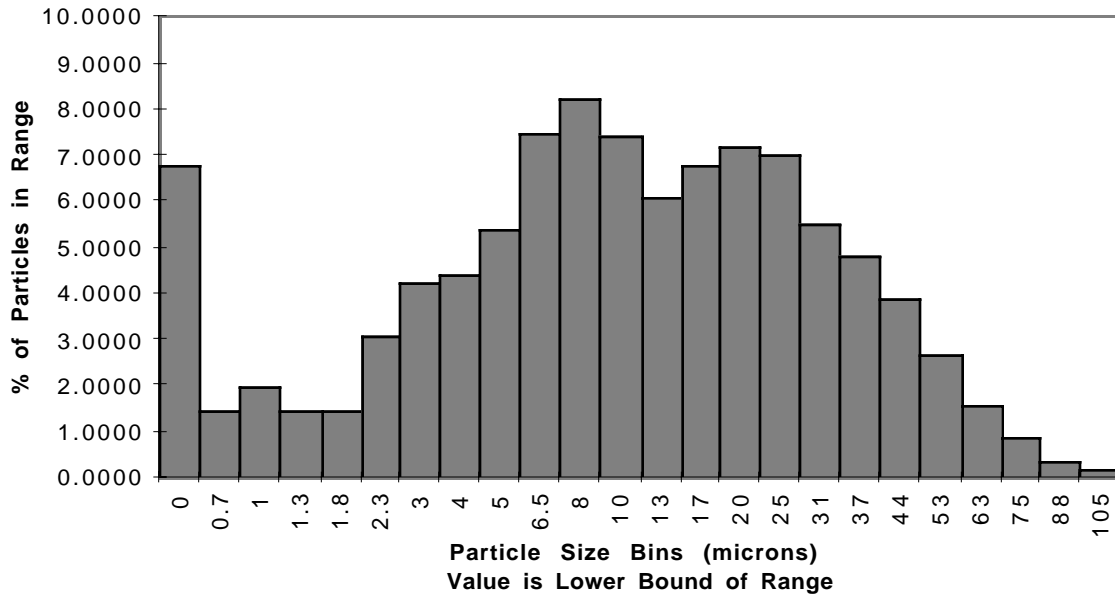


Figure 2.1.1-a. Particle size distribution for 2-Step LLNL PuO<sub>2</sub>.

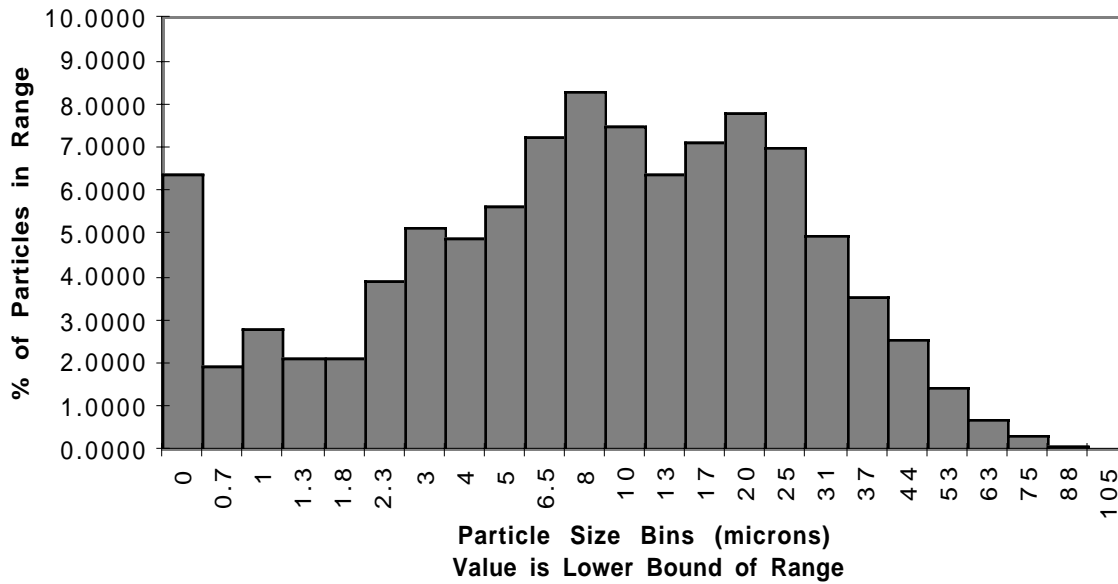


Figure 2.1.1-b. Particle size distribution for 3-Step LLNL PuO<sub>2</sub>.

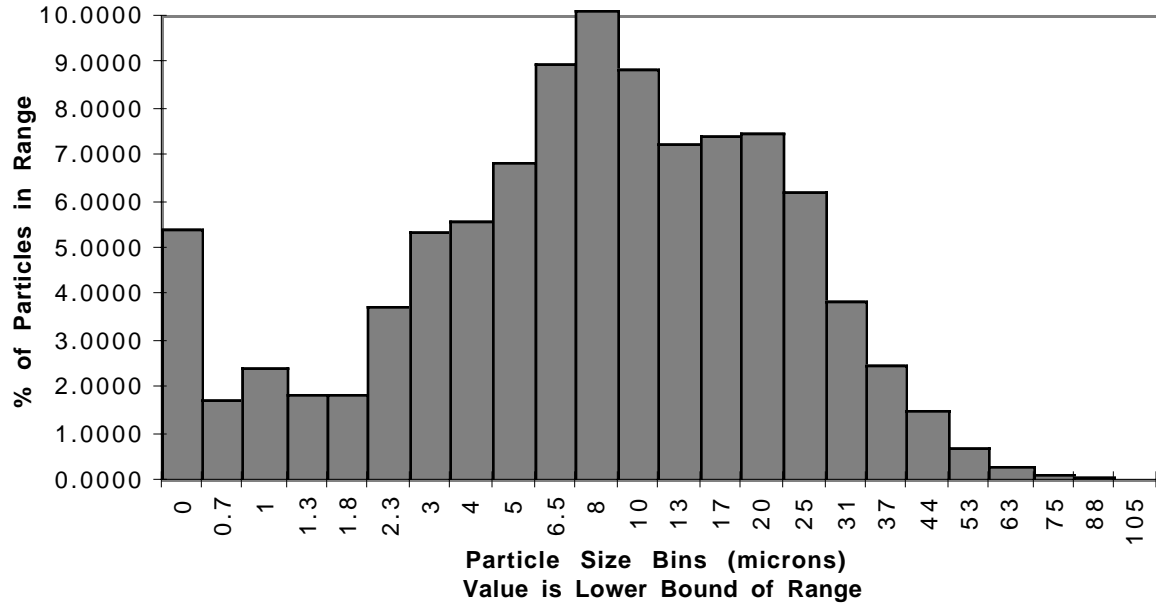


Figure 2.1.1-c. Particle size distribution for Los Alamos PuO<sub>2</sub>.

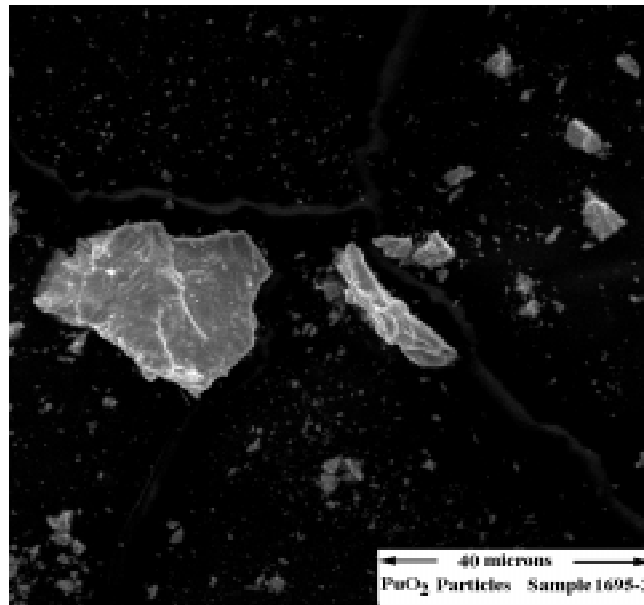


Figure 2.1.2-a. Morphology of LLNL 2-Step PuO<sub>2</sub> powder.

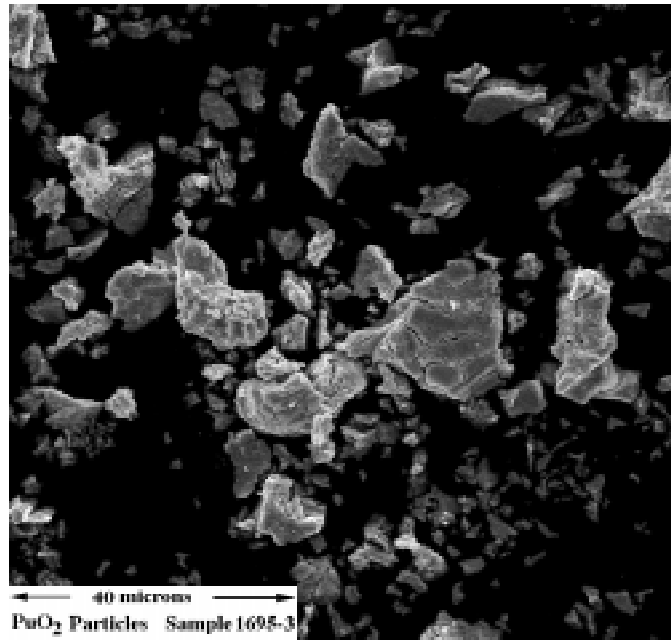


Figure 2.1.2-b. Morphology of LLNL 3-Step PuO<sub>2</sub> powder.

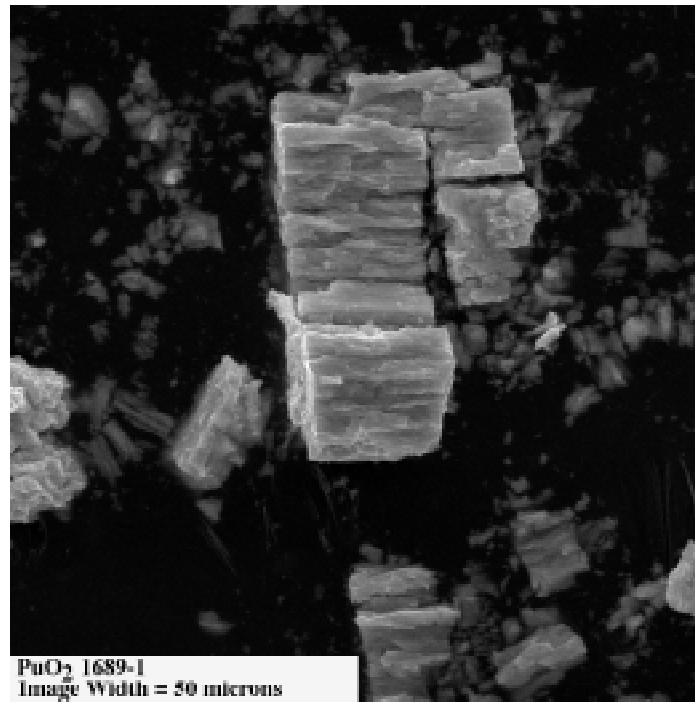


Figure 2.1.2-c. Morphology of Los Alamos PuO<sub>2</sub> powder.

### 2.1.2. Aqueous-Derived PuO<sub>2</sub>

200 g of aqueous-derived PuO<sub>2</sub> feed material were obtained at Los Alamos during FY97. However, due to schedule constraints, characterization has not yet been performed on this material.

## 2.2. Ga Removal

The presence of Ga in weapons material is a key difference between weapons-surplus and reactor-grade plutonium. Experiments have shown that gallium oxide volatilizes under certain thermal conditions, including those encountered during MOX fuel sintering. This can cause problems with regard to the effect that this material has on the sintering furnace because it is corrosive and will deposit on the furnace surfaces. In addition, gallium affects the sintering behavior of the MOX ceramic. This could cause operational difficulties if frequent adjustment to the operational parameters (i.e., time and temperature) is required or this characteristic causes large pellet reject rates following sintering. Accordingly, the current approach for fabricating MOX fuel for the disposition program is to remove most of the Ga prior to fabrication. Studies were initiated in FY96 to learn more about the behavior of Ga in general, including Gallium transport and collection, and how the volatilization of its suboxide state can be used to provide a simple gallium removal mechanism by using a thermal treatment of the PuO<sub>2</sub> powder. This process, referred to as the Thermally-Induced Gallium Removal (TIGR) process, was shown to reduce the residual gallium concentrations to less than 200 ppm in the PuO<sub>2</sub> feed. This results in a less than 10 ppm concentration of gallium in the final MOX fuel.

During FY97, experiments were conducted to further examine the behavior of gallium, particularly with regard to the evolution of Ga under a variety of process parameters. Work was performed on the assessment of Ga phase relations, building on last year's efforts and incorporating the data obtained from this year's experiments. Studies were also performed using surrogate materials to examine the effects that varying the process parameters has on the Ga evolution from the material. A limited amount of similar experiments were performed using PuO<sub>2</sub> powders, and more of these will be conducted in FY98. And finally, an assessment of possible production-level Ga removal systems, including both the TIGR process and a back-up aqueous purification process, was initiated.

Overall, the main purposes of the research presented in this section were to:

- Establish thermodynamic relationships for the Pu-O-Ga system to support the development and design of the TIGR (thermally induced gallium removal) system.
- Establish thermodynamic relationships for the Pu-U-O-Ga system to support MOX sinterability studies
- Verify the feasibility of the TIGR system
- Establish use of a Pu surrogate for assessment of the TIGR processing parameters, including benchmarking with PuO<sub>2</sub>
- Begin optimization of the TIGR process parameters
- Begin a conceptual layout of the TIGR production processes, equipment, and costs

- Identify backup, aqueous Ga removal processing options and establish a baseline process

### 2.2.1. Thermodynamics and Phase Relationships

Understanding the processability and performance of a nuclear fuel and its potential interactions with surrounding cladding requires a thorough understanding of its thermodynamic properties. MOX fabricated from surplus weapons Pu has never been used in a nuclear reactor. Consequently, the literature is lacking pertinent information on, in particular, the thermodynamics of gallium or gallium oxide in either plutonium oxide or in MOX fuel. Consequently, an understanding of the thermodynamics is critical for having a basis from which to interpret and predict gallium removal, gallium collection, fuel sintering, and (depending on the final Ga concentration) fuel and cladding performance.

The following subsections address four important thermodynamic needs:

1. Although the  $\text{PuO}_2\text{-Ga}_2\text{O}_3$  system has never been of significant concern until now, a good understanding of its thermodynamic behavior is an essential part of the design of the TIGR removal process. For example, the optimum thermal and atmospheric conditions for the volatilization of  $\text{Ga}_2\text{O}$  from  $\text{Ga}_2\text{O}_3$  can be estimated by thermodynamics. Also, the formation of stable gallium-oxide species can be predicted and may ultimately limit the removal efficiency of the TIGR process. Section 2.2.1.2 addresses studies involving the partial pressure of  $\text{Ga}_2\text{O}$ , and Sections 2.2.1.3 and 2.2.1.4 present thermodynamics and phase relations in the Ga-O and Pu-O systems respectively. Additionally, Section 2.2.1.6 provides information about the solubility of  $\text{Ga}_2\text{O}_3$  in  $\text{PuO}_2$  as well as  $\text{Ga}_2\text{O}_3\text{-PuO}_2$  pseudobinary and ternary phase diagrams, and Section 2.2.1.7 offers insight into the perovskite phase in  $\text{PuO}_{2-x}$  and  $\text{CeO}_{2-x}$ .
2. Because of the cost of using  $\text{PuO}_2$  in experiments, the use of the  $\text{PuO}_2$  surrogate  $\text{CeO}_2$  is being pursued. Understanding and comparing the phase relations of the real and surrogate systems are necessary to fully utilize the surrogate. Section 2.2.1.5 describes thermodynamics and phase relations in the system Ce-O, which can be compared to information in Section 2.2.1.4 for the Pu-O system. Again, Section 2.2.1.7 offers insight into the perovskite phase in  $\text{PuO}_{2-x}$  and  $\text{CeO}_{2-x}$ .
3. Residual levels of gallium in the  $\text{PuO}_2$  feedstock, and consequently in the unsintered MOX fuel pellets, may have a significant impact on the sintering process. For example, studies performed by Arthur and Scott showed that a concentration of only 2000 ppm  $\text{Ga}_2\text{O}_3$  in  $\text{UO}_2$  greatly inhibited sintering.<sup>3</sup> Although they did not explain the effect, it is believed that the  $\text{Ga}_2\text{O}_3$  likely increased surface diffusivity, perhaps by liquid formation and subsequent solution-precipitation, thus enhancing grain growth at the expense of densification. Their result can not be interpreted without knowledge of the  $\text{UO}_2\text{-Ga}_2\text{O}_3$  pseudobinary phase diagram. Unfortunately, there was insufficient resources during FY97 to fully pursue this research, and it is proposed to continue this activity in FY98.
4. It is widely believed that even minor levels of gallium in fabricated MOX fuel may have a fuel performance impact. Understanding the thermodynamics of the  $\text{PuO}_2\text{-UO}_2\text{-Ga}_2\text{O}_3$  system may lead to a better understanding of acceptable levels of gallium in fresh MOX fuel. This activity will also be further developed during FY98.

Thus, the purpose of the work presented in the following subsections is to establish a variety of types of thermodynamic data using information available in the literature and, where appropriate, estimates of thermodynamic values in the systems Pu-Ga-O and Ce-Ga-O under oxidizing as well as reducing conditions where ternary compounds are thought to be stable.

**2.2.1.1. Development of a Relational Thermodynamic Database.** To assess phase relations more easily, Los Alamos developed a relational thermodynamic database. The thermodynamic information is currently updated in an interconnected system of databases that include information such as the physical properties of the components (for example, Table 2.2.1-1), compounds and their phases, the solution and lattice parameters, heat capacities, energies used in the phase diagram computations (for example, Table 2.2.1-2), as well as a large collection of references. The database management system (DMS) is a collection of interrelated files and sets of programs that allows users to access and modify these files. The system is divided into various levels which make it relatively user friendly. The database is essentially a collection of tables into which data can be entered or extracted by another program. The overall structure of the program is illustrated in Figure 2.2.1-1. At this date, the program is being used by a small group of investigators. However, as the program becomes better developed it could be distributed to other users.

**2.2.1.2. Calculations of Ga<sub>2</sub>O(g) Partial Pressures.** It is useful to begin looking at the thermodynamics of Ga in PuO<sub>2</sub> by determining Ga<sub>2</sub>O(g) partial pressures. The partial pressure is important to both Ga removal and Ga transport from the fuel to the cladding interface. Thus, thermodynamic data were collected and free energies of formation were fit, using stepwise multiple linear regression, to the equation:

$$\Delta G_f = a + bT + cT^{-1} + dT^2 + eT^3 + fT \ln T \quad (1)$$

where  $a$ - $f$  are constants and  $T$  is temperature in Kelvin. Table 2.2.1-3 shows some of the data relevant to this brief summary of results.

**TABLE 2.2.1-1  
SUMMARY OF X-RAY CRYSTALLOGRAPHIC  
DATA OF PLUTONIUM OXIDES<sup>4</sup>**

Phase	x	Symmetry	Space group	a <sub>0</sub> , Å	c <sub>0</sub> , Å
γ-PuO <sub>2-x</sub>	0 - 0.28	fcc	Fm3m	5.396	-
α''-PuO <sub>1.61+x</sub>	0-0.10	bcc	Ia3	11.046	-
α'-PuO <sub>1.515</sub>	-	bcc	Ia3	11.04	-
β-PuO <sub>1.500</sub>	-	hex	P3̄ m1	3.841	5.958

**TABLE 2.2.1-2**  
**SUMMARY OF REPORTED THERMODYNAMIC VALUES**  
**FOR PLUTONIUM OXIDES**

			$\Delta G_f = A + B \cdot T$						
Compound	O/Pu	$X_0$	A (kJ/g- atom)	B (kJ/g- atom-T)	Range K	Mp <sup>a</sup> (K)	$\Delta H_{fus}$ (kJ/g- atom)	$\Delta S_{fus}$ (kJ/g- atom)	Ref.
< $\gamma$ -PuO <sub>2</sub> >	2.00	0.6667	-349.75	0.05630	298-2675	2675	-	-	5
< $\gamma$ -PuO <sub>2</sub> >	2.00	0.6667	-348.89	0.06010	298-2716	2716	25.10	0.009242	6
< $\gamma$ -PuO <sub>2</sub> >	2.00	0.6667	-349.27	0.06257	-	-	-	-	7
< $\gamma$ -PuO <sub>2</sub> >	2.00	0.6667	-351.74	0.05788	298-2100	-	-	-	8
< $\gamma$ -PuO <sub>2</sub> >	2.00	0.6667	-347.97	0.05621	1600-2150	-	-	-	9
{liq-PuO <sub>2</sub> }	2.00	0.6667	-347.97	0.05620	2716-3000	2716	25.10	0.003081	6
< $\beta$ -PuO <sub>1.98</sub> >	1.98	0.6644	-346.37	0.05476	1600-2150	-	-	-	9
< $\beta$ -PuO <sub>1.95</sub> >	1.95	0.6610	-344.79	0.05333	1600-2150	-	-	-	9
< $\beta$ -PuO <sub>1.92</sub> >	1.92	0.6575	-343.46	0.05216	1600-2150	-	-	-	9
$\beta$ -PuO <sub>1.90</sub> >	1.90	0.6552	-340.74	0.05189	1600-2150	-	-	-	9
< $\beta$ -PuO <sub>1.85</sub> >	1.85	0.6491	-370.74	0.05066	1600-2150	-	-	-	9
< $\beta$ -PuO <sub>1.80</sub> >	1.80	0.6429	-339.35	0.04927	1600-2150	-	-	-	9
< $\beta$ -PuO <sub>1.75</sub> >	1.75	0.6364	-338.52	0.04884	1600-2150	-	-	-	9
< $\beta$ -PuO <sub>1.70</sub> >	1.70	0.6296	-337.82	0.04881	1600-2150	-	-	-	9
<a''-PuO <sub>1.70</sub> >	1.70	0.6296	-337.82	0.04881	1600-2150	-	-	-	9
<a''-PuO <sub>1.70</sub> >	1.70	0.6296	-337.48	0.05444	1600-1400	-	-	-	7
<a''-PuO <sub>1.65</sub> >	1.65	0.6226	-337.25	0.04889	1600-2150	-	-	-	9
<a''-PuO <sub>1.61</sub> >	1.61	0.6169	-336.74	0.04905	1600-2150	-	-	-	9
<a''-PuO <sub>1.61</sub> >	1.61	0.6169	-341.45	0.05114	298-2000	-	-	-	8
<a''-PuO <sub>1.61</sub> >	1.61	0.6169	-	-	-	2633 ±20	-	-	4
< $\alpha'$ -PuO <sub>1.52</sub> >	1.515	0.6024	-354.97	0.04664	298-2000	-	-	-	6
< $\alpha'$ -PuO <sub>1.52</sub> >	1.515	0.6024	-351.58	0.0450	298-2000	-	-	-	5
< $\beta$ -PuO <sub>1.50</sub> >	1.50	0.60000	-340.36	0.05041	298-2000	-	-	-	6
< $\beta$ -PuO <sub>1.50</sub> >	1.50	0.60000	-331.20	0.0538	800-2100	-	-	-	7
< $\beta$ -PuO <sub>1.50</sub> >	1.50	0.60000	-339.74	0.05138	298-2000	-	-	-	8
< $\beta$ -PuO <sub>1.50</sub> >	1.50	0.60000	-338.51	0.04994	298-2358	-	-	-	5
< $\beta$ -PuO <sub>1.50</sub> >	1.50	0.60000	-	-	-	2358 ±30	-	-	4
<Pu>		0.00000				911 ±2	2.90	0.003183	5

<sup>a</sup>Congruent melting points.

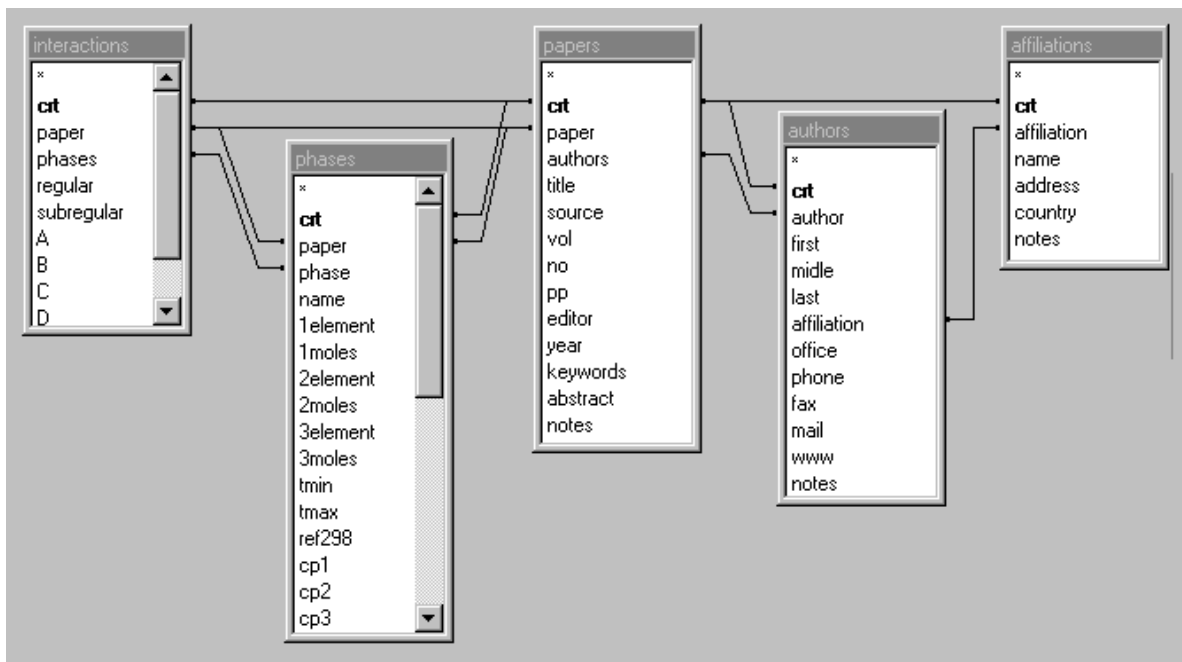
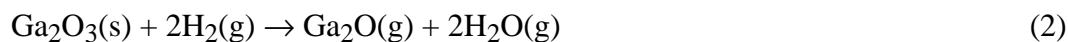


Figure 2.2.1-1. Structure of thermodynamic database management system.

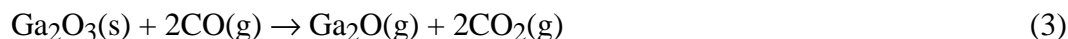
**TABLE 2.2.1-3**  
**SUMMARY OF CONSTANTS SHOWN IN EQUATION 1**

<b>Compound</b>	<b><i>a</i></b>	<b><i>b</i></b>	<b><i>c</i></b>	<b><i>d</i></b>	<b><i>e</i></b>	<b><i>f</i></b>
Ga <sub>2</sub> O <sub>3</sub> (s)	-1123572.	574.0020	2267569.	5.3080E-03	-6.8814E-07	-31.7864
Ga <sub>2</sub> O(g)	-117031.	-55.3176	1295110.	8.3901E-03	-8.9622E-07	0
H <sub>2</sub> O(g)	-236296.	-65.1431	-169071.	-6.2395E-03	4.2670E-07	16.6059
CO <sub>2</sub> (g)	-391347.	-26.6122	-191047.	-4.0186E-04	0	3.2924
CO(g)	-104977.	-123.5504	-642559.	2.4364E-03	-2.8001E-07	3.8731

These data were used to calculate temperature dependent expressions for the vaporization behavior of gallium oxide from doped PuO<sub>2</sub>. Practical, reducing atmospheres of interest are Ar-H<sub>2</sub> and CO/CO<sub>2</sub>. Thus, temperature dependent expressions were determined from the mass action equations:



and



Using the data shown in Table 2.2.1-3, the following equations were derived, from which Ga<sub>2</sub>O(g) partial pressures can be calculated:

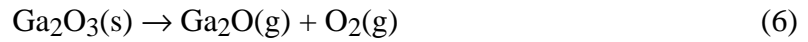
$$p_{Ga_2O} = \frac{a_{Ga_2O_3} p_{H_2}^2}{p_{H_2O}^2} \exp \left[ 91.3647 + 1.1203 \cdot 10^{-3} T \right. \\ \left. - 7.761944 \cdot 10^{-8} T^2 - \frac{64223}{T} + \frac{157638}{T^2} - 7.8179 \ln T \right] \quad (4)$$

and

$$p_{Ga_2O} = \frac{a_{Ga_2O_3} p_{CO}^2}{p_{CO_2}^2} \exp \left[ 52.3747 + 3.1205 \cdot 10^{-4} T \right. \\ \left. - 4.2332 \cdot 10^{-8} T^2 - \frac{52177.2}{T} + \frac{8351.7}{T^2} - 3.68355 \ln T \right] \quad (5)$$

Where  $a$  and  $p$  represent activity and equilibrium partial pressure respectively.

In addition, the vaporization of  $Ga_2O(g)$  may be assessed using the mass action equation:



where the partial pressure of  $Ga_2O(g)$  may be calculated using the equation:

$$p_{Ga_2O} = \frac{a_{Ga_2O_3}}{p_{O_2}} \exp \left[ 75.69396 - 3.7071 \cdot 10^{-4} T \right. \\ \left. + 2.50277 \cdot 10^{-8} T^2 - \frac{121066}{T} + \frac{117327}{T^2} - 3.82324 \ln T \right] \quad (7)$$

Equations (6) and (7) may be substituted for equations (2) through (5) by considering how the partial pressure of oxygen is controlled by either the  $H_2/H_2O$  or  $CO/CO_2$  ratio according to buffer reactions  $H_2(g) + 1/2O_2(g) \rightarrow H_2O(g)$ , or  $CO(g) + 1/2O_2(g) \rightarrow CO_2(g)$ .

The equations described above can be used to calculate the equilibrium partial pressures of  $Ga_2O$  above various  $PuO_2$ - $Ga_2O_3$  solid solutions (i.e., assuming various  $Ga_2O_3$  activities) in inert atmospheres or  $H_2$ - or  $CO$ -bearing gases. Figure 2.2.1-2 shows how the vaporization behavior varies with environment at a  $Ga_2O_3$  activity of 0.01, which is near the expected activity for a typical  $PuO_2$ - $Ga_2O_3$  feedstock. It is apparent from this figure that the vaporization rate in the reducing gases  $H_2$  and  $CO$  is significantly higher than that in vacuum. Section 2.2.2 showed that this has been confirmed experimentally in studies of  $Ga_2O(g)$  vaporization from surrogate feedstock materials.

**2.2.1.3. Thermodynamics and Phase Relations in the System Ga-O.** Data for assessing the Ga-O system were collected and analyzed much like that described for the Pu-O system. For reference, selected physical properties of  $Ga_2O_3$  and Ga are summarized in Table 2.2.1-4. In evaluating the  $Ga_2O_3$ -Ga pseudobinary phase diagram, it was assumed that  $Ga_2O_3$  and Ga were mixed according to the following regular solution model:

$$\Delta G_f^0 \{mix\} = X_B \Delta G_f^0 \{Ga_2O_3\} + X_A RT \ln(X_A) + X_B RT \ln(X_B) + \Delta E X_A X_B \quad (8)$$

where  $X_A$  and  $X_B$  are mole fractions of Ga and  $\text{Ga}_2\text{O}_3$ , respectively,  $\Delta G_f^0 \{ \text{Ga}_2\text{O}_3 \}$  is the free energy of formation of liquid  $\text{Ga}_2\text{O}_3$  (kJ/g-atom), and  $\Delta E$  is the excess energy of mixing (kJ/gm•atom). The liquid phase boundaries were determined from the equation

$$\Delta G_f^0 \{ \text{mix} \} / X_B = 0 \quad (9)$$

The temperature dependence of  $\Delta E$  was determined from  $\langle \text{Ga}_2\text{O}_3 \rangle$  solubility in liq-Ga data.<sup>10</sup> Then the functional form of  $\Delta E$  was incorporated into Eqn. 20, and the phase boundaries for the miscibility gap were calculated as a function of temperature. The liquidus from  $\text{Ga}_2\text{O}_3$  to the eutectic point was estimated using the equation:

$$\ln(X_B) = -\frac{-L_f}{RT} \cdot \frac{T_0 - T}{T_0} \quad (10)$$

where  $L_f$  is the heat of fusion (kJ/g-atom) of  $\text{Ga}_2\text{O}_3$ ,  $T_0$  is its melting temperature in K, and  $RT$  has its usual meaning. The intersection of the composition curves determined from Eqns. 20 and 21 at large values of  $X_B$  gave the eutectic temperature and composition. Tables 2.2.1-5 and 2.2.1-6 summarize the basic thermodynamic values and parameters used in assessing the  $\text{Ga}_2\text{O}_3$ -Ga pseudobinary phase diagram. The phase diagram is shown in Figure 2.2.1-3.

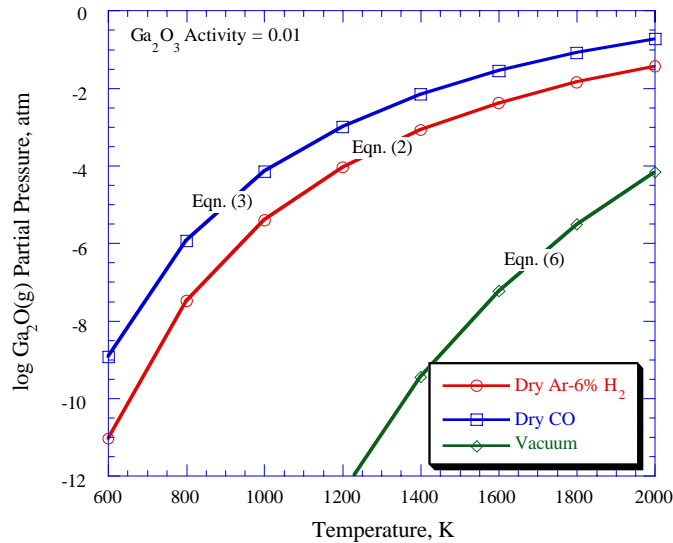


Figure 2.2.1-2. Calculated equilibrium partial pressures above  $a_{\text{Ga}_2\text{O}_3} = 0.01$  in reducing atmospheres and vacuum.

**TABLE 2.2.1-4**  
**SUMMARY OF X-RAY CRYSTALLOGRAPHIC**  
**DATA OF GALLIUM OXIDES<sup>11</sup>**

Phase	Symmetry	Space group	a <sub>0</sub> , Å	b <sub>0</sub> , Å	c <sub>0</sub> , Å	b
β-GaO <sub>1.500</sub>	monoclinic	A <sup>2</sup> /m	5.80	3.04	12.23	103°42'
GaO <sub>0.500</sub>	amorphous	-	-	-	-	-

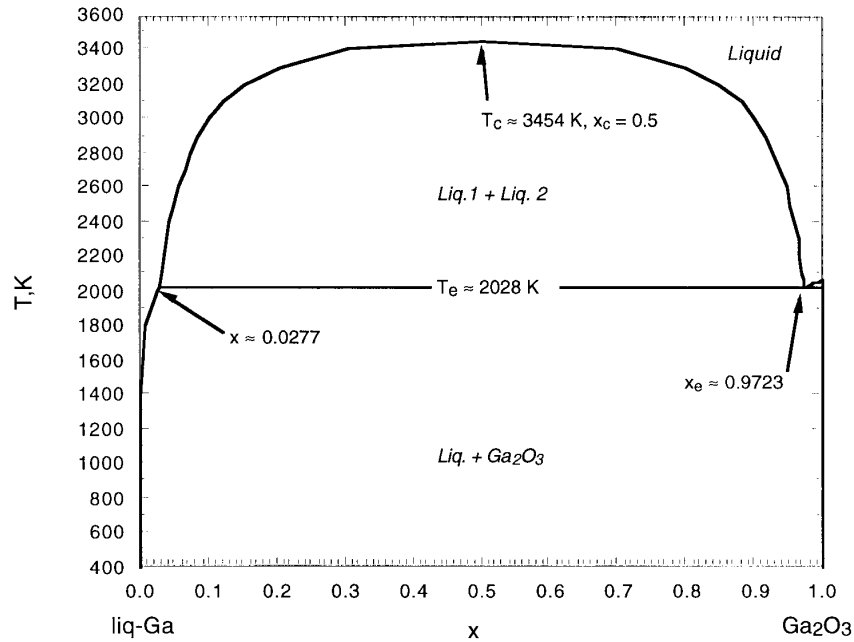
**TABLE 2.2.1-5**  
**SUMMARY OF REPORTED OR ASSESSED  $\Delta G_f^0$  EQUATIONS FOR**  
**GALLIUM AND ITS OXIDES**

$\Delta G_f^0 = A + B \cdot T$									
Comp.	O/Ga	X <sub>0</sub>	A (kJ/g- atom)	B (kJ/g- atom-T)	Range (K)	Mp <sup>a</sup> (K)	$\Delta H_{fus.}$ (kJ/g- atom)	$\Delta S_{fus.}$ (kJ/g- atom)	Ref.
β-GaO <sub>1.50</sub>	1.50	0.60000	-217.72	0.06487	298-2073	2073	-	-	6
β-GaO <sub>1.50</sub>	1.50	0.60000	-189.81	0.05113	2073-2300	2073	21.77	0.01050	12
α-GaO <sub>0.5</sub>	0.50	0.33333	-137.74	0.08491	298-925	925	1.185	0.001281	12
α-GaO <sub>0.5</sub>	0.50	0.33333	-134.06	0.08174	298-2100	-	-	-	12
Ga	0	0	-	-	-	303	5.58	0.01841	12

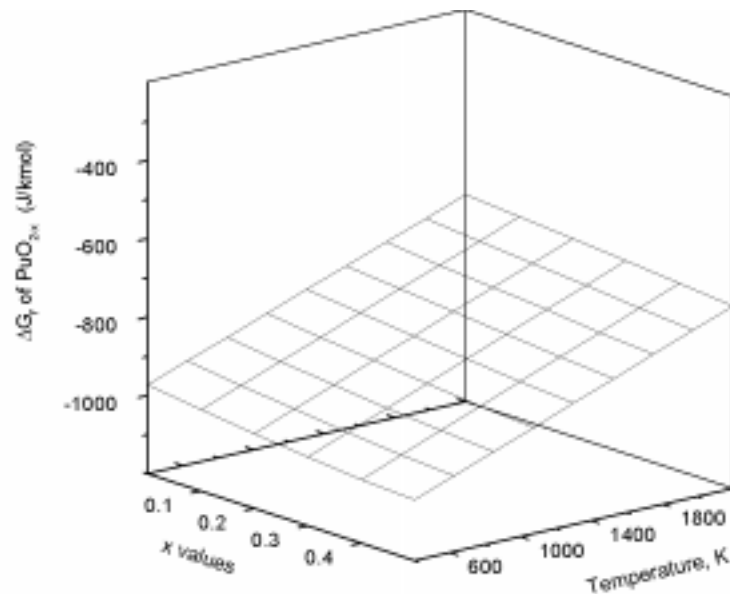
<sup>a</sup>Congruent melting points.

**TABLE 2.2.1-6**  
**REGULAR SOLUTION MODEL PARAMETERS USED IN ASSESSING THE**  
**GA<sub>2</sub>O<sub>3</sub>-GA PSEUDOINARY PHASE DIAGRAM**

Description	X <sub>B</sub> (mole fraction)	$\Delta G_f^0 = A + B \cdot T$		EXS Energy of Mixing		$X_B = A \cdot \exp(B/T)$		Ref.
		A	B	A	B	A	B	
		(kJ/g- atom)	(kJ/g- atom-T)	(kJ/g- atom)	(kJ/g- atom-T)	(mol fraction)	(K)	
{Ga <sub>2</sub> O <sub>3</sub> }	1	-189.81	0.05113	-	-	-	-	12
{Ga-Ga <sub>2</sub> O <sub>3</sub> }	0 - 1	-	-	338.87	-0.089804	-	-	-
<Ga <sub>2</sub> O <sub>3</sub> >	0 - 0.03	-	-	-	-	744.86	-20687	10

Figure 2.2.1-3 Calculated Ga-Ga<sub>2</sub>O<sub>3</sub> phase diagram.

**2.2.1.4. Thermodynamics and Phase Relations in the System Pu-O.** Besmann and Lindemer proposed a model for PuO<sub>2-x</sub><sup>7</sup> assuming there is a solid solution of PuO<sub>2</sub> and a hypotetic compound PuO<sub>4/3</sub>O<sub>2</sub><sup>7</sup>. The solution may be assumed to be regular with an interaction parameter  $E = -63470 + 49.3T$  (J/mol). Figure 2.2.1-4 shows the Gibbs free energy of PuO<sub>2-x</sub> as a function of  $x$  and temperature. The oxygen potential is derived from:

Figure 2.2.1-4. The Gibbs free energy of PuO<sub>2-x</sub> in a solid solution of Pu<sub>4/3</sub>O<sub>2</sub> and PuO<sub>2</sub>.

With this model and by transforming Busmann's relationship for  $\Delta G$  in kJ/gm•atom, the Gibbs free energy of the substoichiometric oxide  $\text{PuO}_{2-x}$  [fcc  $\gamma$ -phase] can be written as:

$$\begin{aligned} \Delta G_f [\text{Pu}_{x_{\text{Pu}}} \text{O}_{x_{\text{O}}}] &= 33556.945 - 149841.901 \cdot X_{\text{O}} + 183286.581 \cdot X_{\text{O}}^2 - \\ &223761.988 \cdot X_{\text{O}}^5 + 159403.744 \cdot X_{\text{O}}^6 + (-423.49228 + 15555.938 \cdot X_{\text{O}}^2 - \\ &64947.727 \cdot X_{\text{O}}^3 + 114444.372 \cdot X_{\text{O}}^4 - 95645.301 \cdot X_{\text{O}}^5 + 31239.311 \cdot X_{\text{O}}^6) \cdot \\ &T \quad (\text{kJ/gm} \cdot \text{atom}) \end{aligned} \quad (12)$$

where the  $\text{PuO}_2$  congruent melting point = 2673 K,

for  $\text{PuO}_{1.61-1.70}$  [bcc  $\alpha''$ -phase]:

$$\Delta G_f [\text{Pu}_{0.0.3831} \text{O}_{0.6169}] = -877.13 + 0.13892 \cdot T \quad (\text{kJ/g-atom}) \quad (13)$$

$$\Delta G_f [\text{Pu}_{0.0.3704} \text{O}_{0.6296}] = \text{needs to be re-evaluated} \quad (14)$$

where the  $\text{PuO}_{1.61}$  congruent melting point = 2633 K,

$\alpha'' + \gamma$  eutectic temperature = 2553 K,

$\alpha'' + \gamma$  eutectic point composition, O/Pu = 1.62,

for  $\text{PuO}_{1.515}$  [bcc  $\alpha'$ -phase]:

$$\Delta G_f [\text{Pu}_{0.0.3796} \text{O}_{0.6204}] = -846.27 + 0.141272 \cdot T \quad (\text{kJ/g-atom}) \quad (15)$$

where the  $\text{PuO}_{1.515}$  peritectic decomposition temperature = 760 K,

and for  $\text{PuO}_{1.500}$  [hex  $\beta$ -phase]:

$$\Delta G_f [\text{Pu}_{0.4000} \text{O}_{0.6000}] = -334.372 + 0.0538 \cdot T \quad (\text{kJ/g-atom}) \quad (16)$$

where the  $\text{PuO}_{1.500}$  congruent melting point = 2358 K,

$\alpha'' + \beta$  eutectic temperature  $\approx$  2330 K,

$\alpha'' + \beta$  eutectic composition, O/Pu  $\approx$  1.54.

The following defines the various reactions in the Pu-O system:

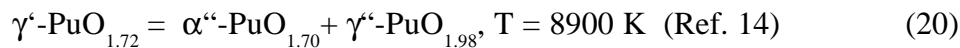
the eutectic reactions:

$$\text{liq-PuO}_{1.53} = \beta\text{-PuO}_{1.50} + \alpha''\text{-PuO}_{1.61}, T \approx 2303 \text{ K (Ref. 4)} \quad (17)$$

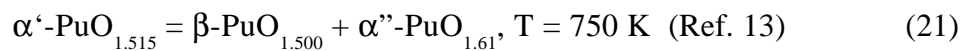
$$\text{liq-PuO}_{1.62} = \alpha''\text{-PuO}_{1.61} + \gamma\text{-PuO}_{\approx 1.75}, T = 2553 \text{ K (Ref. 4)} \quad (18)$$

the eutectoid reactions:

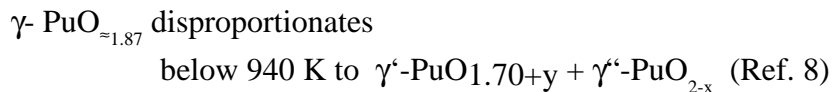
$$\alpha''\text{-PuO}_{1.625} = \alpha'\text{-PuO}_{1.515} + \gamma\text{-PuO}_{1.99}, T = 600 \text{ K (Ref. 13)} \quad (19)$$



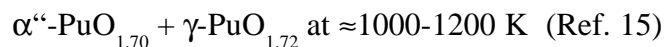
the peritectoid reactions:



the disproportionation reaction:



and the two-phase equilibria:



Examples of calculated free energy curves, used in optimizing the Pu-O binary phase diagram, are shown for each phase in Figures 2.2.1-5 through 2.2.1-11. The resulting assessment of the Pu-O phase diagram is shown in Figure 2.2.1-12.

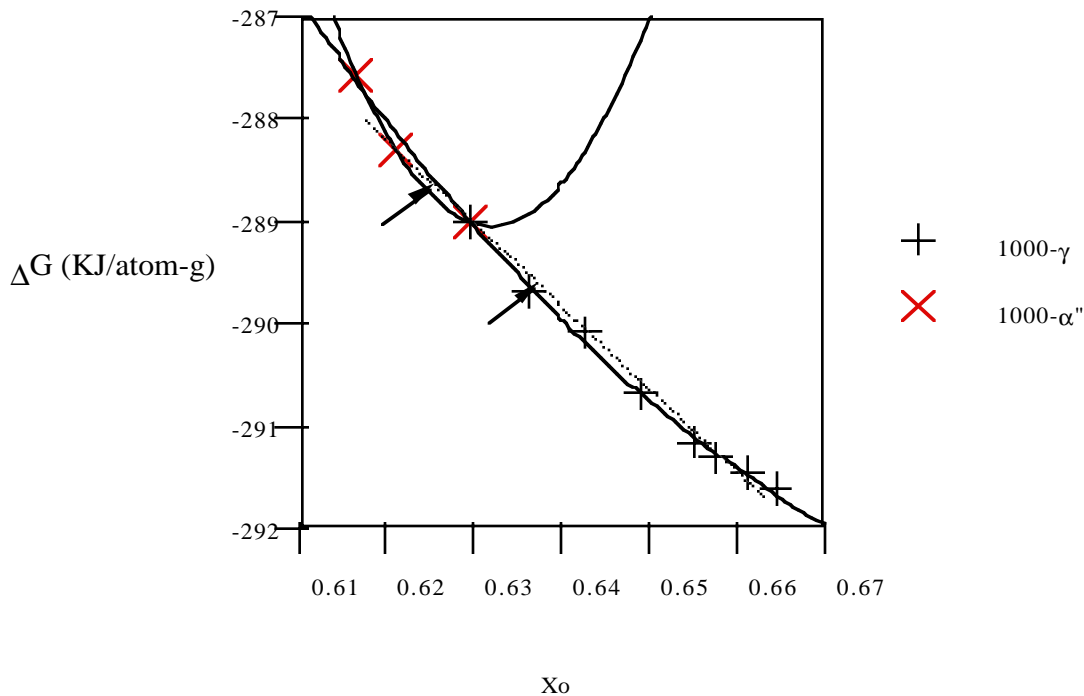


Figure 2.2.1-5. The calculated Gibbs free energy of  $\gamma$  and  $\alpha''$  phases in Pu-O system at 1000 K.

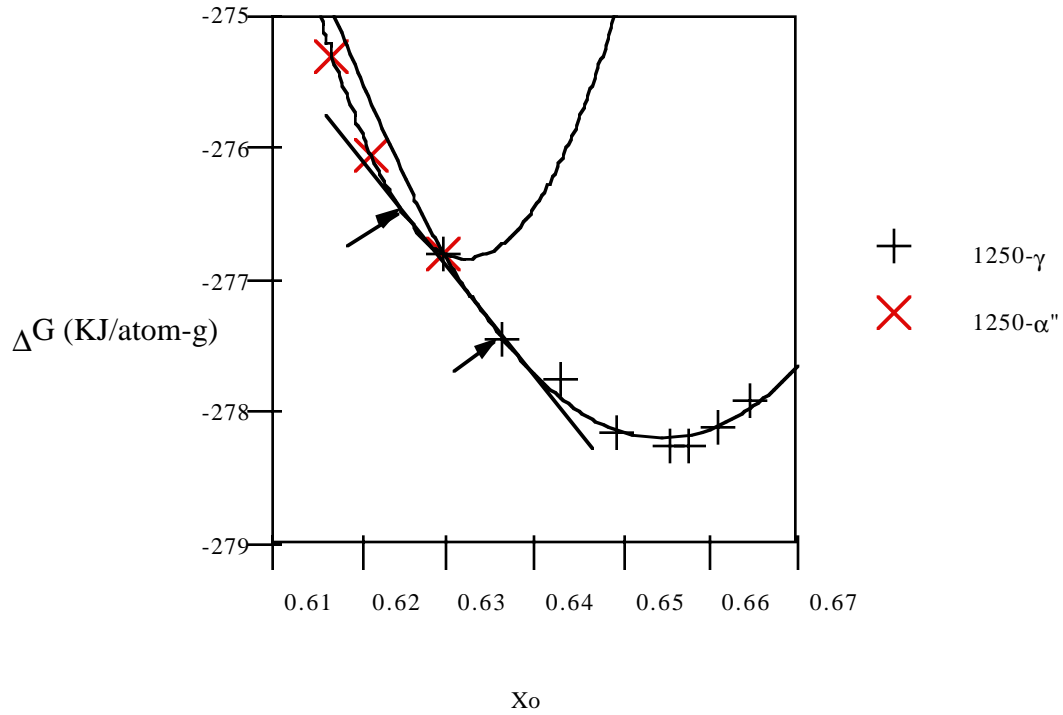


Figure 2.2.1-6. The calculated Gibbs free energy of  $\gamma$  and  $\alpha''$  phases in Pu-O system at 1250 K.

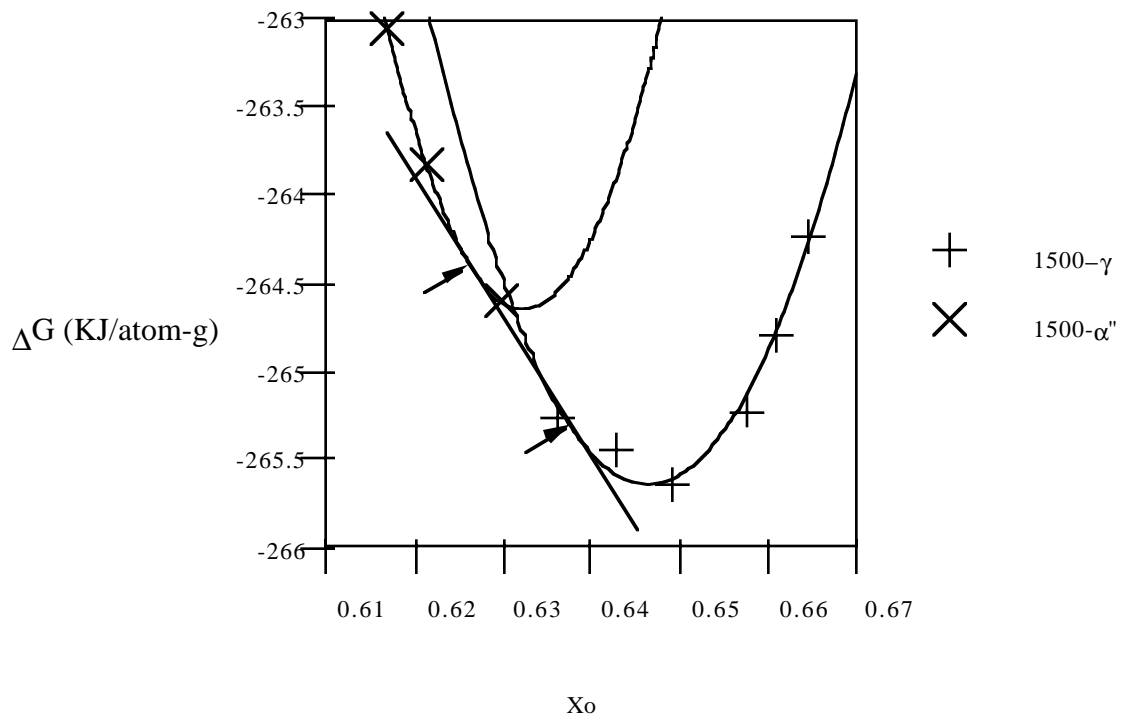


Figure 2.2.1-7. The calculated Gibbs free energy of  $\gamma$  and  $\alpha''$  phases in Pu-O system at 1500 K.

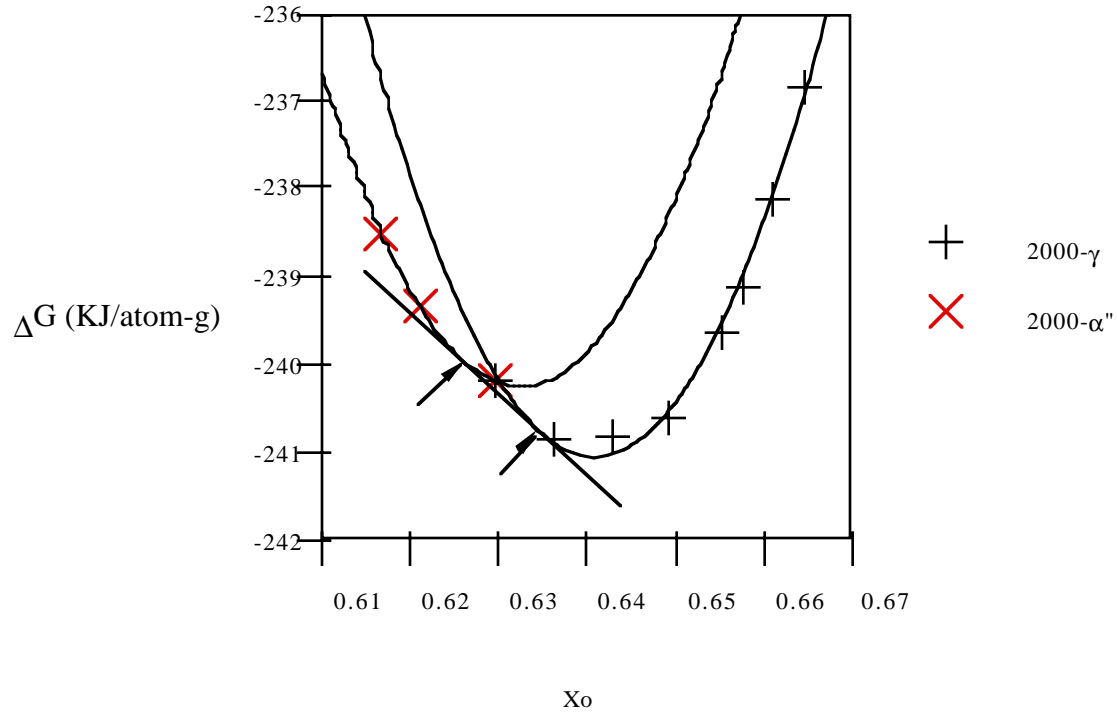


Figure 2.2.1-8. The calculated Gibbs free energy of  $\gamma$  and  $\alpha''$  phases in Pu-O system at 2000 K.

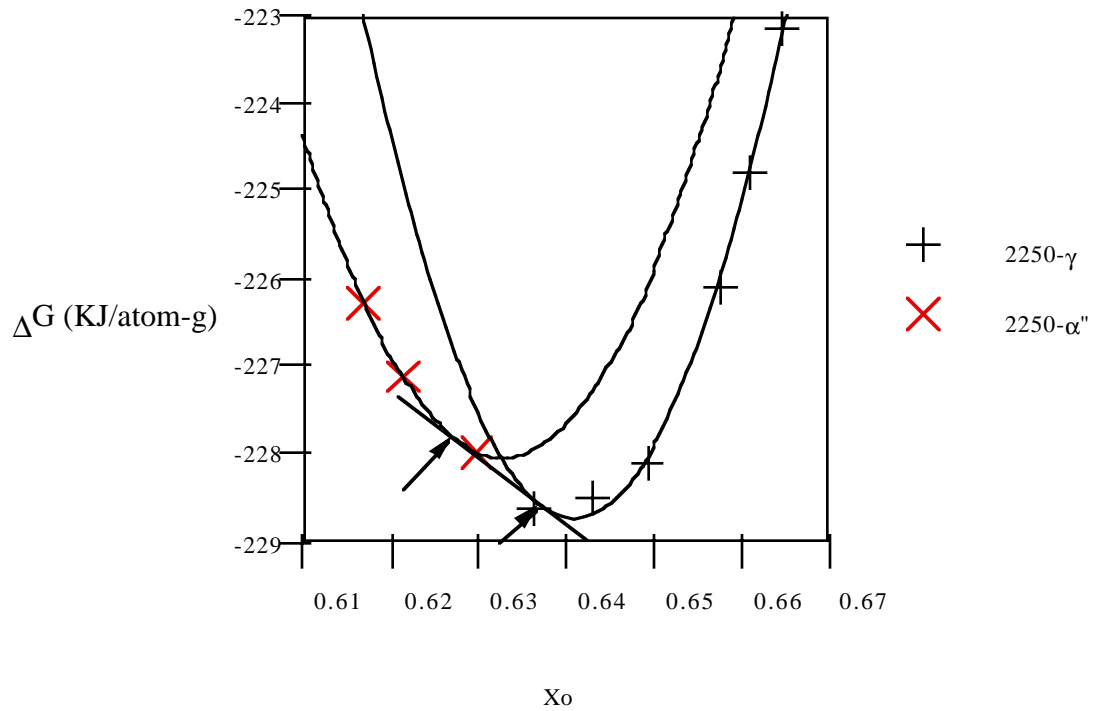


Figure 2.2.1-9. The calculated Gibbs free energy of  $\gamma$  and  $\alpha''$  phases in Pu-O system at 2250 K.

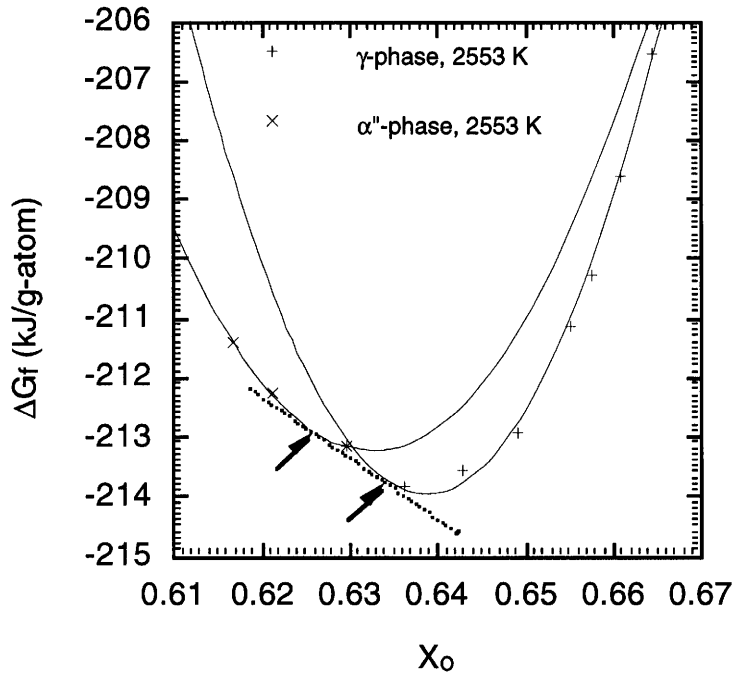


Figure 2.2.1-10. The calculated Gibbs free energy of  $\gamma$  and  $\alpha''$  phases in Pu-O system at 2553 K.

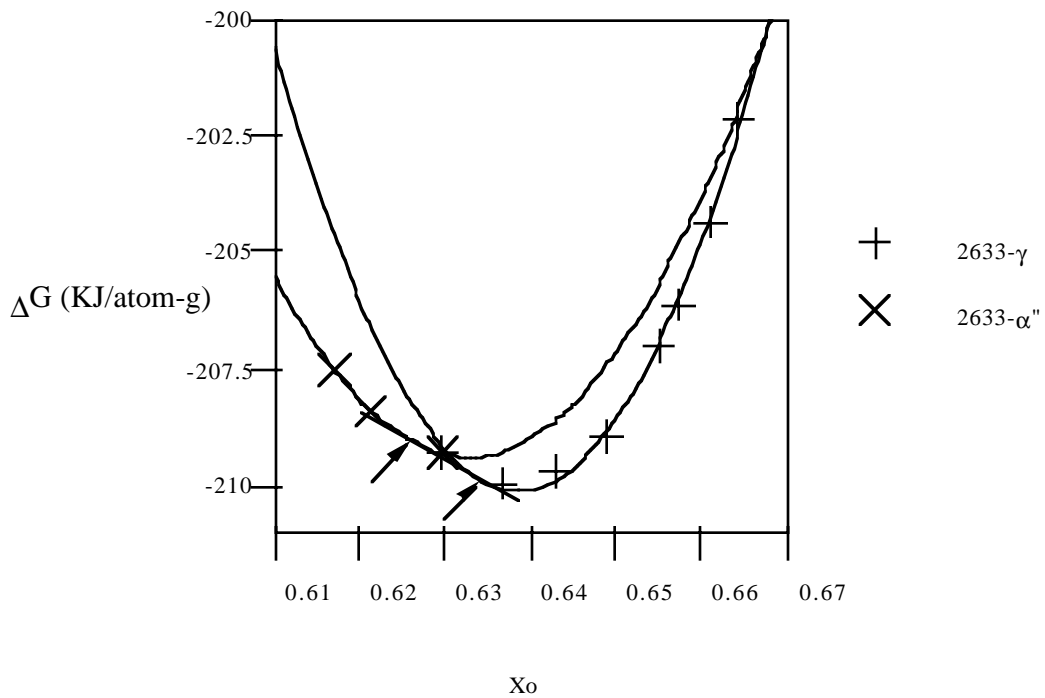


Figure 2.2.1-11. The calculated Gibbs free energy of  $\gamma$  and  $\alpha''$  phases in Pu-O system at 2633 K.

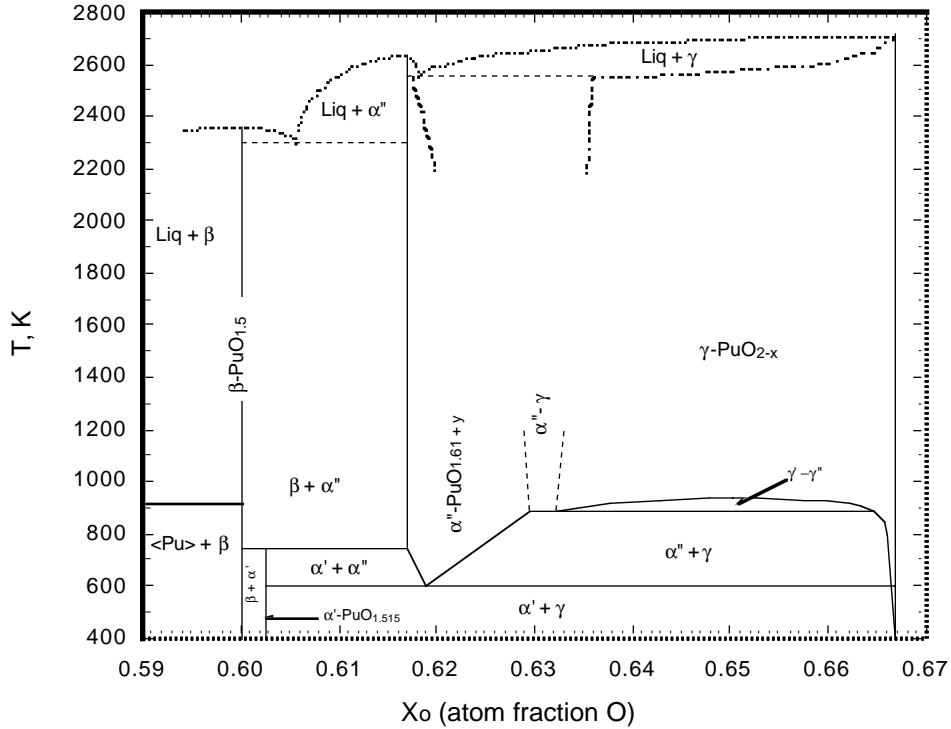


Figure 2.2.1-12. Calculated Pu-O binary phase diagram.

**2.2.1.5. Thermodynamics and Phase Relations in the System Ce-O.** The Ce-O phase diagrams were analyzed in a manner very similar to that described for the Pu-O system. Therefore, details of the methods and thermodynamic data will not be reported. The basics of the assessments of the Ce-O system are presented in Figures 2.2.1-13 and 2.2.1-14.

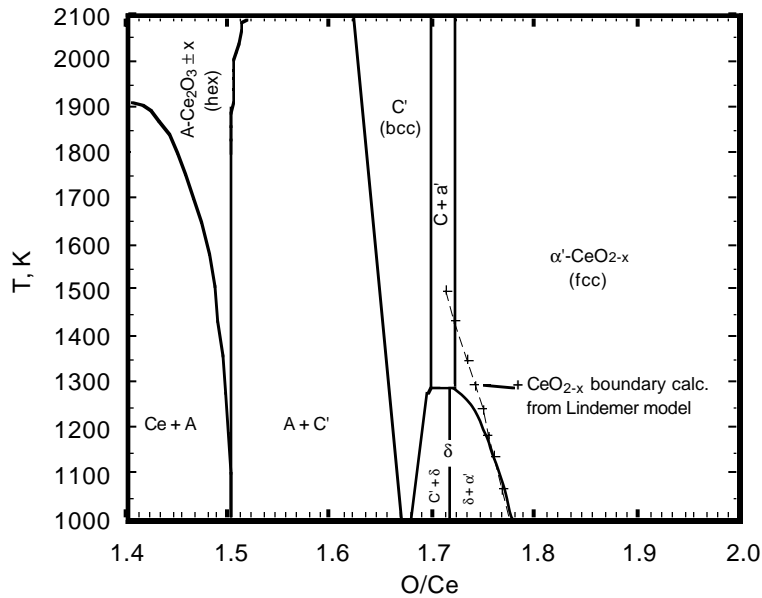


Figure 2.2.1-13. Assessment of the Ce-O phase diagram.

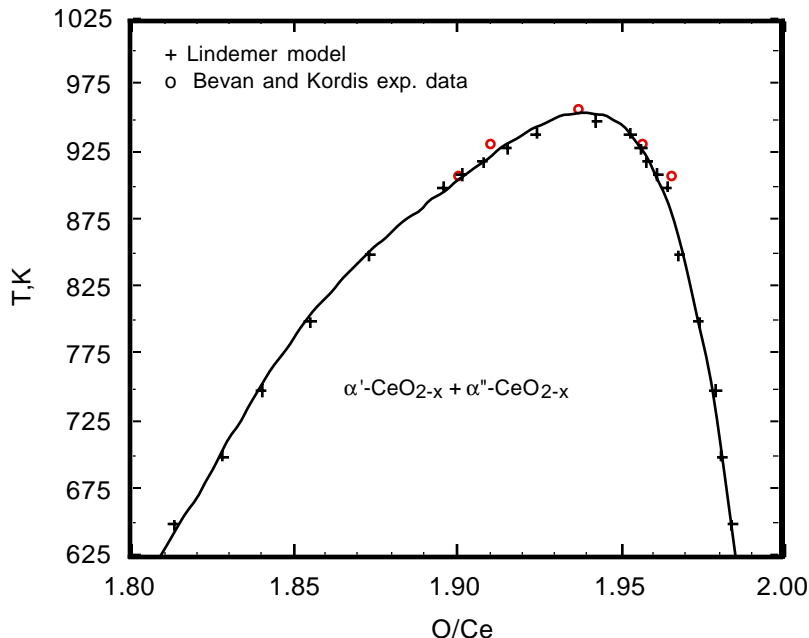


Figure 2.2.1-14. Assessment of the composition and temperature dependence of the spinodal decomposition of  $\text{CeO}_{2-x}$ .

**2.2.1.6. Solubility of  $\text{Ga}_2\text{O}_3$  in  $\text{PuO}_2$  and the  $\text{Ga}_2\text{O}_3$ - $\text{PuO}_2$  Pseudobinary and Ternary Phase Diagrams.** One of the most important thermodynamic values in assessing phenomena such as Ga evolution from  $\text{PuO}_2$  and the behavior of Ga in MOX fuel is the solubility of gallium oxide in  $\text{PuO}_{2-x}$ . This solubility has never been measured. However, there has been one study performed on the solubility of  $\text{Al}_2\text{O}_3$  in  $\text{PuO}_2$ .<sup>16</sup>  $\text{Al}_2\text{O}_3$  is a relatively good surrogate for  $\text{Ga}_2\text{O}_3$  under oxidizing conditions due to its similar bonding and hexagonal crystal structure. By making certain assumptions about the effect of ionic radii on solubility, one can arrive at a rational estimate of the solubility of  $\text{Ga}_2\text{O}_3$  in  $\text{PuO}_2$ .

The effective ionic radius of  $\text{Pu}^{4+}$  with a coordination number of 6 is  $0.86\text{\AA}$ , and the ionic radius for oxygen is  $1.212\text{\AA}$ . For  $\text{Al}^{3+}$  the value of the ionic radius is  $0.546\text{\AA}$  while the value for  $\text{Ga}^{3+}$  is  $0.658\text{\AA}$ . A crude assumption is that the solubility limit might depend on the compound "volume," related to the ionic radii of the metal. Figure 2.2.1-15 shows a comparison between the measured solubility of  $\text{Al}_2\text{O}_3$  and the estimated solubility of  $\text{Ga}_2\text{O}_3$  in  $\text{PuO}_2$ . As this figure suggests, the solubility of  $\text{Ga}_2\text{O}_3$  in  $\text{PuO}_2$  is quite low, in the ppm range. Thus, one can expect that  $\text{Ga}_2\text{O}_3$  will precipitate out as fine particles in  $\text{PuO}_2$ , perhaps as perovskite if the oxygen potential is right. As described elsewhere in this report, this is precisely what has been observed in surrogate studies. It has yet to be confirmed that the  $\text{Ga}_2\text{O}_3$  (or the perovskite) does precipitate out as discrete phases in  $\text{PuO}_2$ . One should also be cautioned that the solubility of  $\text{Al}_2\text{O}_3$  has only been determined in  $\text{PuO}_2$ , not in  $\text{PuO}_{2-x}$ . Thus, the solubility could be altered substantially with decreasing oxygen content.

With knowledge of the solubility of  $\text{Ga}_2\text{O}_3$  in  $\text{PuO}_2$ , sufficient thermodynamic data for the binary system (described in part above), and making assumptions about ternary interaction parameters (to be described in detail in future publications), theoretical pseudobinary and ternary phase diagrams can begin to be mapped out. Figures 2.2.1-16 and 2.2.1-17 show calculated pseudobinary phase diagrams for the  $\text{Ga}_2\text{O}_3$ - $\text{PuO}_2$  system assuming negligible and finite solubility limits for  $\text{Ga}_2\text{O}_3$  under oxidizing conditions. As illustrated in Figure 2.2.1-18, under reducing conditions where the perovskite phase may be stable, the phase diagram becomes more complicated. The effect of the oxygen potential is illustrated further in the calculated ternary phase diagrams presented in Figures 2.2.1-19, 2.2.1-20, and 2.2.1-21. Further characterization of these phase diagrams will continue in FY98. A limited number of experiments will be performed to valid areas of the phase diagram that are critical to the MOX program.

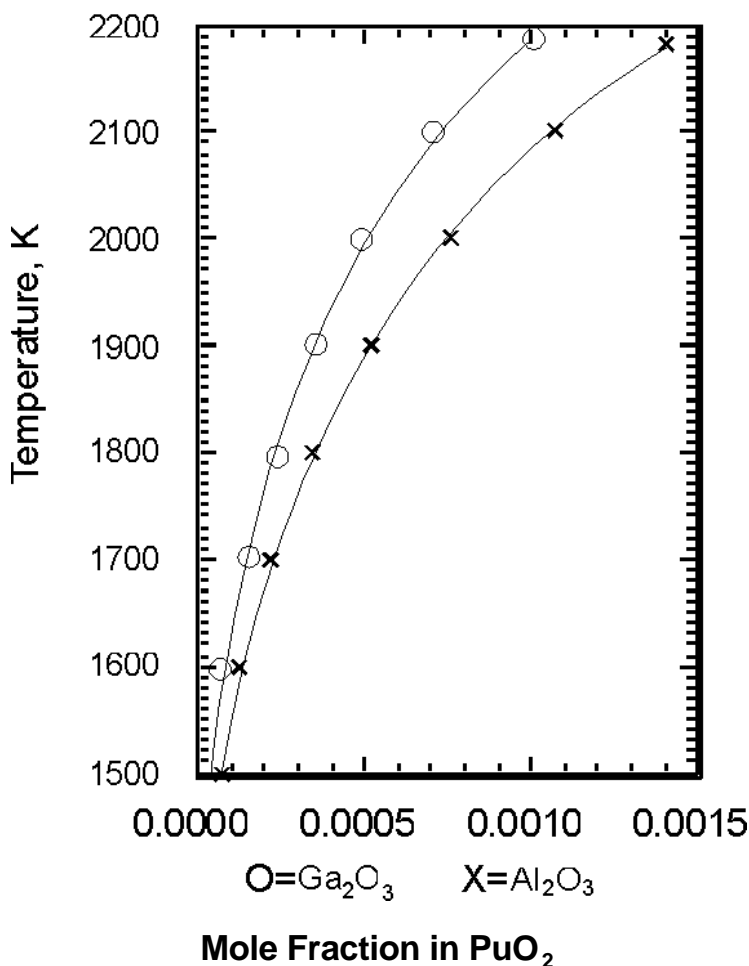


Figure 2.2.1-15. The measured solubility limit of  $\text{Al}_2\text{O}_3$  and the estimated solubility limit of  $\text{Ga}_2\text{O}_3$  in  $\text{PuO}_2$ .

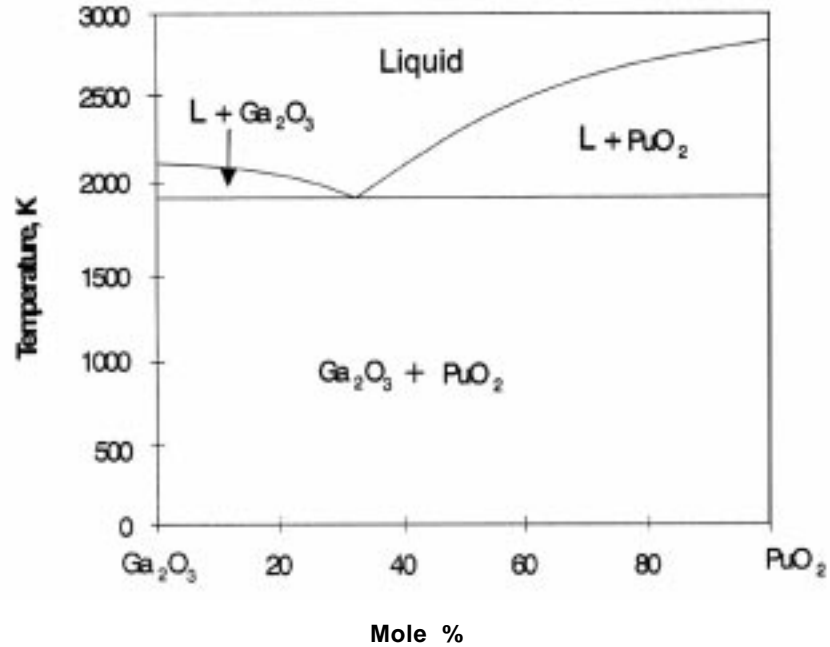


Figure 2.2.1-16. The calculated Ga<sub>2</sub>O<sub>3</sub>-PuO<sub>2</sub> phase diagram under oxidizing conditions assuming Ga<sub>2</sub>O<sub>3</sub> and PuO<sub>2</sub> are insoluble in one another.

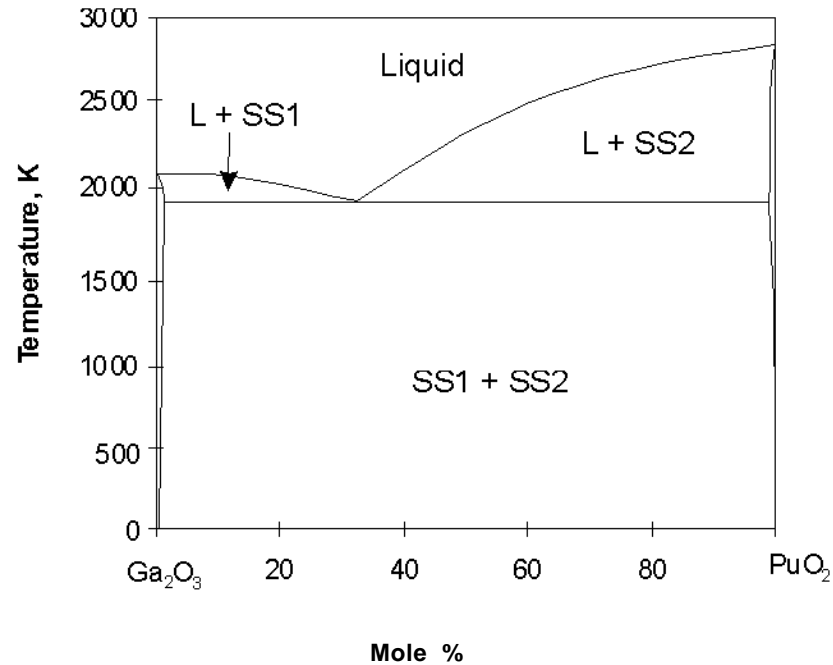


Figure 2.2.1-17. The calculated Ga<sub>2</sub>O<sub>3</sub>-PuO<sub>2</sub> phase diagram under oxidizing conditions assuming Ga<sub>2</sub>O<sub>3</sub> and PuO<sub>2</sub> are mutually soluble in one another to 0.1 atom percent.

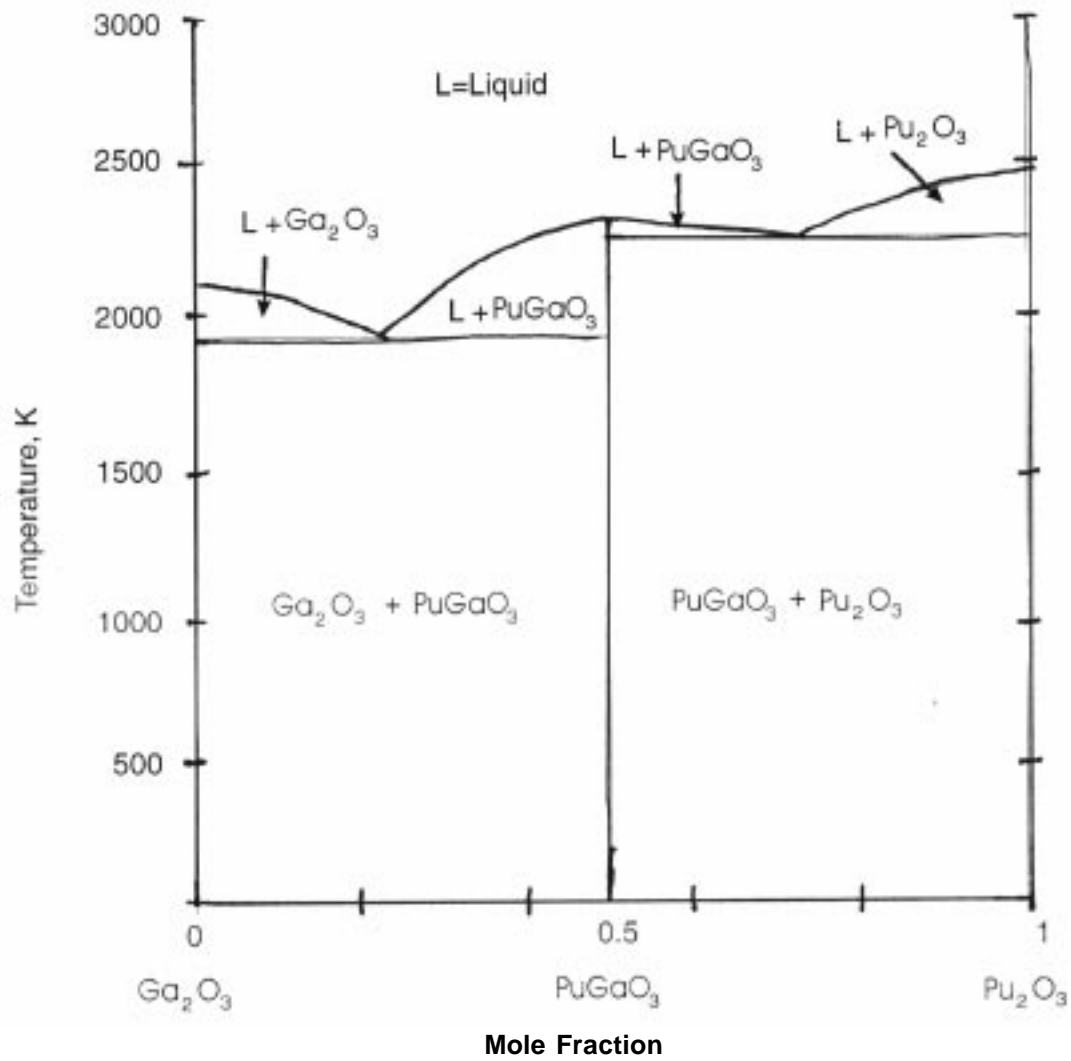


Figure 2.2.1-18. Preliminary pseudobinary phase diagram of the  $\text{Ga}_2\text{O}_3$ - $\text{PuO}_2$  system under reducing conditions.

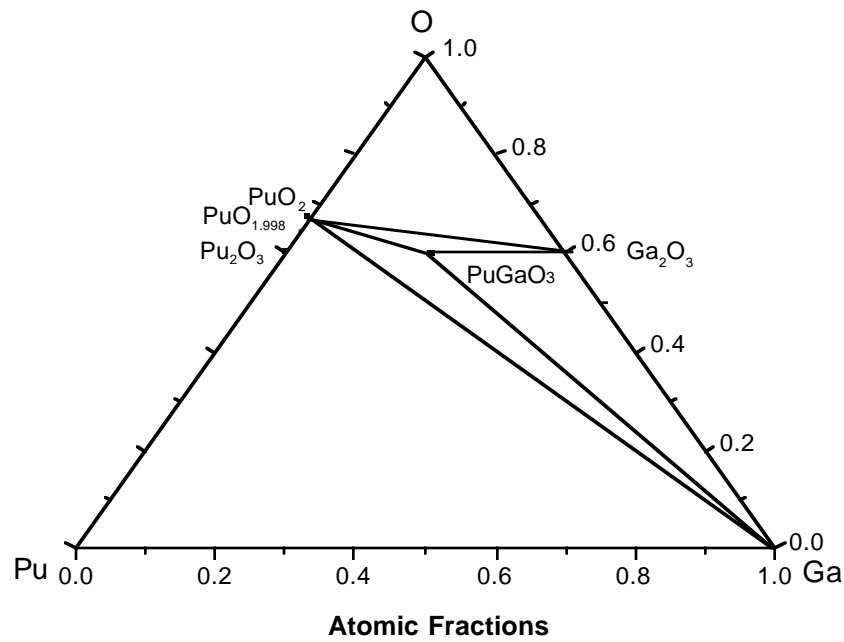


Figure 2.2.1-19. Preliminary 1000 K isothermal ternary phase diagram for the system Pu-Ga-O.

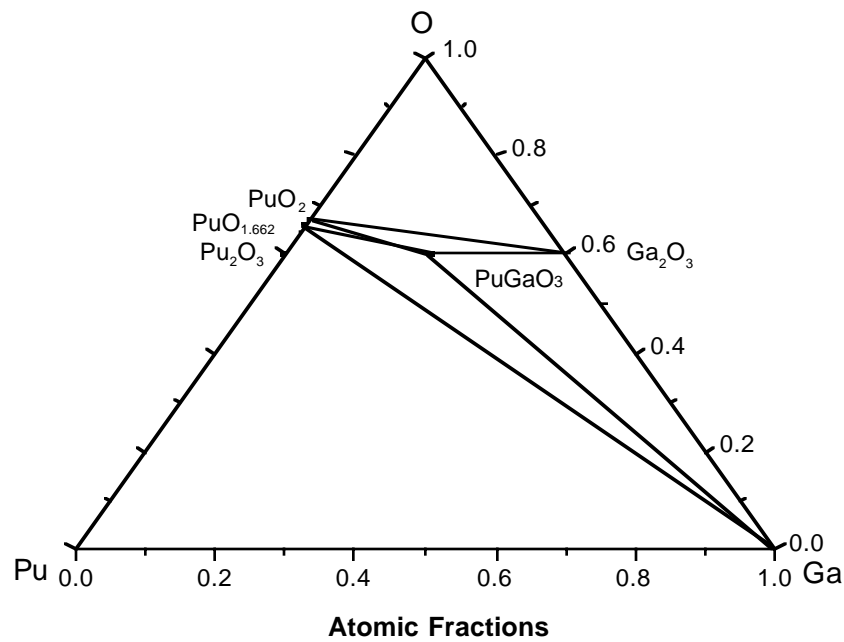


Figure 2.2.1-20. Preliminary 2000 K isothermal ternary phase diagram for the system Pu-Ga-O.

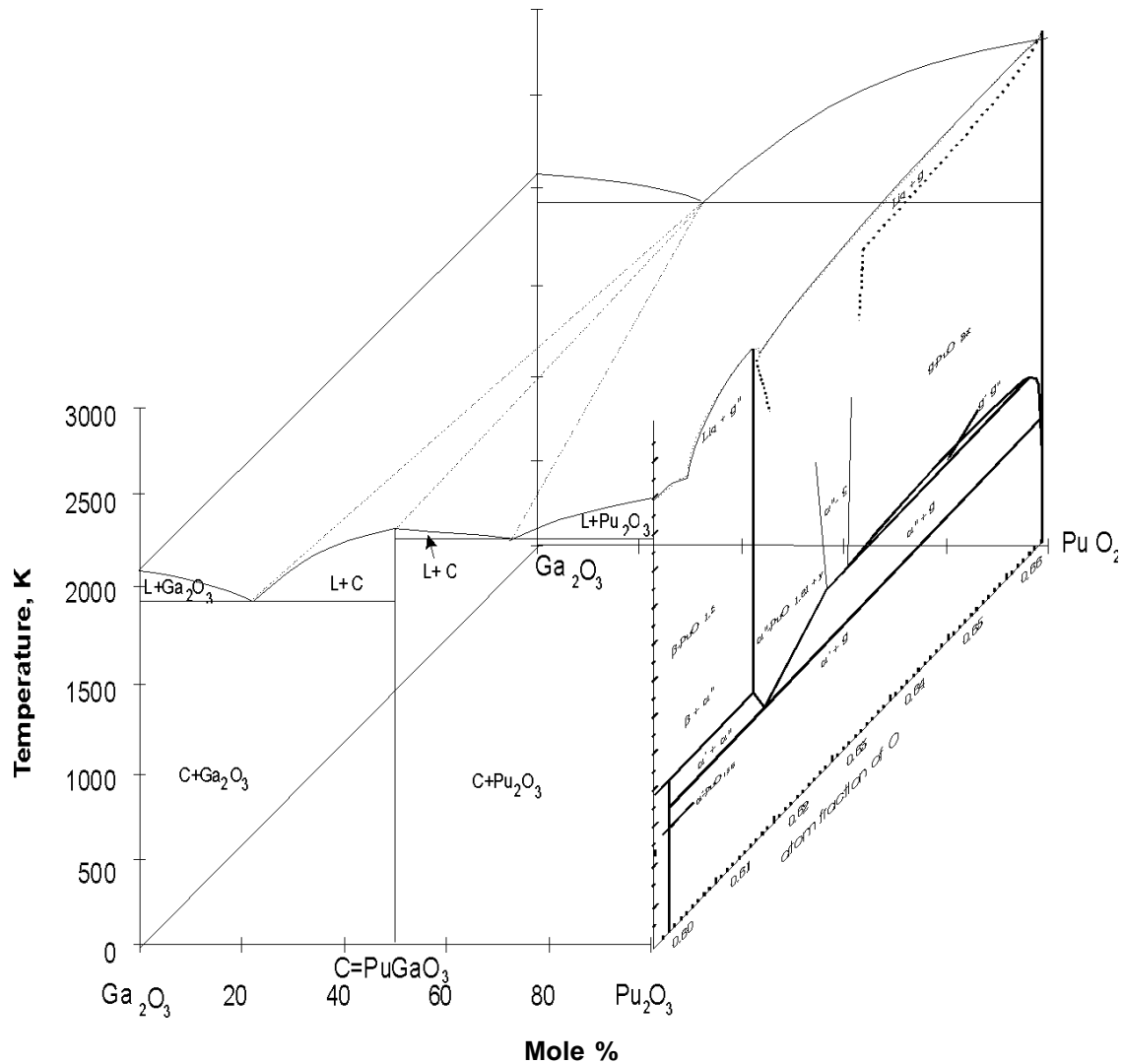
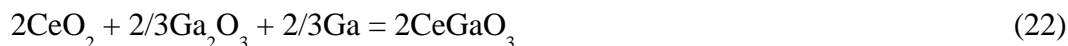


Figure 2.2.1-21. The influence of the reducing conditions on the Ga<sub>2</sub>O<sub>3</sub>-PuO<sub>2-x</sub> phase diagram.

**2.2.1.7. Thermodynamics of the Perovskite Phase in PuO<sub>2-x</sub> and CeO<sub>2-x</sub>.** The possibility exists for the formation of a relatively stable PuGaO<sub>3</sub> perovskite phase in MOX fuel, particularly under reducing conditions. Based on qualitative judgments, it is possible that the perovskite may form during Ga removal, making it more difficult to reach low Ga levels without atmospheric cycling, and alternatively, that the perovskite may not be present in MOX fuel. This is because in MOX, the oxide will be close to stoichiometry, allowing Ga to be more easily vaporized. These statements are purely speculative at this point due to the lack of much detailed thermodynamic data. However, based on the availability of limited data for similar perovskites, such as CeGaO<sub>3</sub>, some qualitative and, in some cases, quantitative inferences can be made about the stability of this gallate under various conditions.

Leonov et al.<sup>17</sup> attempted to synthesize CeGaO<sub>3</sub> from molar ratios of Ce<sub>2</sub>O<sub>3</sub>/Ga<sub>2</sub>O<sub>3</sub> equal to 1:1, 3:5, and 1:11. The synthesis was conducted in oxidizing and inert gas environments at

temperatures from 1273 to 1973 K. No ternary compounds of defined structure or solid solutions were formed. When the synthesis was conducted in  $H_2$  or  $NH_3$  at 1273 K,  $CeGaO_3$  was formed. However, the reaction did not go to completion even in the case of repeated heating with intermediate grinding. Synthesis at 1573, 1673, and 1773 K indicated that gallium oxide is volatilized, which complicated fabrication in a furnace of relatively large volume. Subsequently, Leonov et al. synthesized  $CeGaO_3$  in an evacuated and sealed quartz tube at 1573 K by the following reaction:



Examination of the isothermal  $\Delta G(O_2)$  changes with composition for the Ce-O and Ga-O binaries suggests that  $CeGaO_3$  undergoes a reducing disproportionation process by the reaction:



at  $\log(P_{O_2}) = -12.77$ . Solving the  $\Delta G_{rxn}$  equation yields  $\Delta G_f < CeGaO_3 > = -96.3$  kJ/mole. Further examination of  $\Delta G(O_2)$  change with composition suggests that  $CeGaO_3$  undergoes an oxidizing disproportionation by the following reaction:



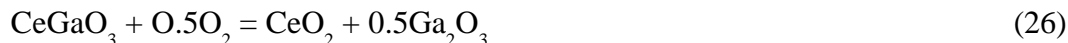
Using the estimated value for  $\Delta G_f < CeGaO_3 >$  yields a  $\log(P_{O_2})$  value equal -4.91. The thermodynamics and effects of oxygen partial pressure on perovskite stability are summarized in Figures 2.2.1-22 through 2.2.1-24. Table 2.2.1-7 gives values of reducing and oxidizing oxygen decomposition pressures, and values of  $\Delta G_f < CeGaO_3 >$  calculated at 1573, 1000, and 500 K. Table 2.2.1-8 summarizes the least squares fit of the data presented in Table 2.2.1-7.

Examination of isothermal  $\Delta G(O_2)$  change with composition for the Pu-O and Ga-O binaries suggest that  $PuGaO_3$  undergoes a reducing disproportionation similar to that in the Ce-Ga-O system at 1500 K according to the following reaction:



at  $\log(P_{O_2}) = -13.93$ . Solving the  $\Delta G_{rxn}$  equation yields  $\Delta G_f < PuGaO_3 >$  equal to -96.6 kJ/mole.

Further examination of  $\Delta G(O_2)$  change with composition suggests that  $PuGaO_3$  undergoes an oxidizing disproportionation by the following reaction:



Using the value for  $\Delta G_f < PuGaO_3 >$  yields  $\log(P_{O_2}) = -6.89$ . The results are summarized in Figures 2.2.1-25 and 2.2.1-26 and Tables 2.2.1-7 and 2.2.1-8. Further information on other comparable plutonium based perovskites is summarized in Tables 2.2.1-9 and 2.2.1-10.

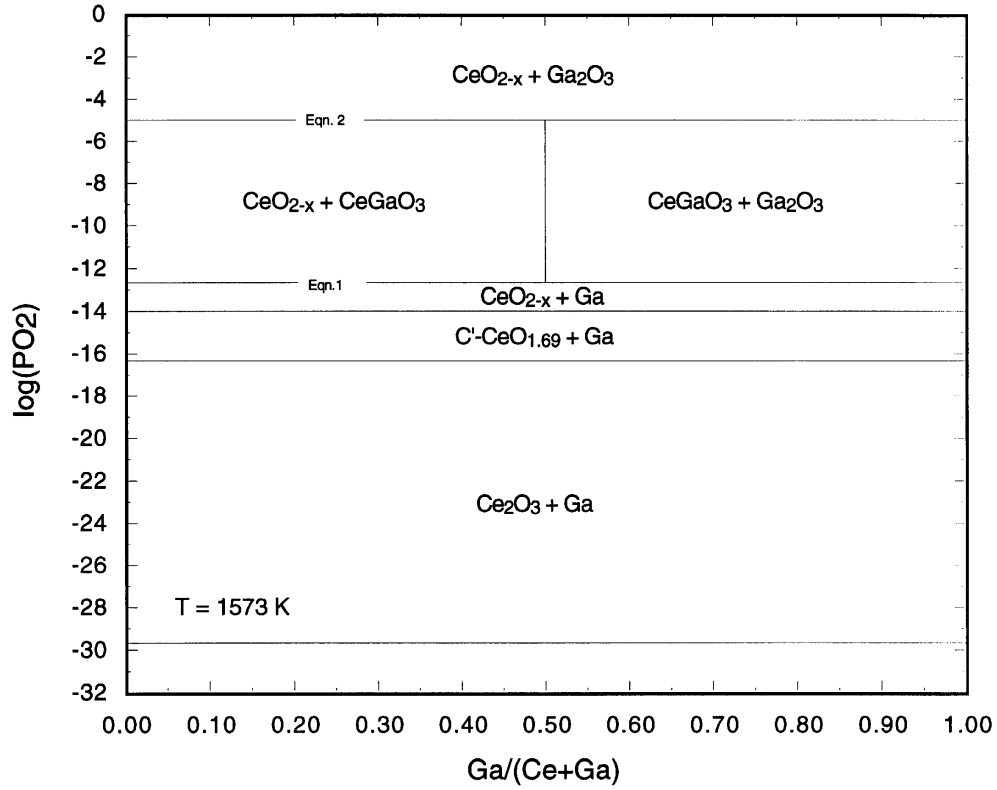


Figure 2.2.1-22. Equilibrium phase diagram of  $\log P_{O_2} = f\left(\frac{Ga}{Ce+Ga}\right)$  for the Ce-Ga-O system at 1500 K.

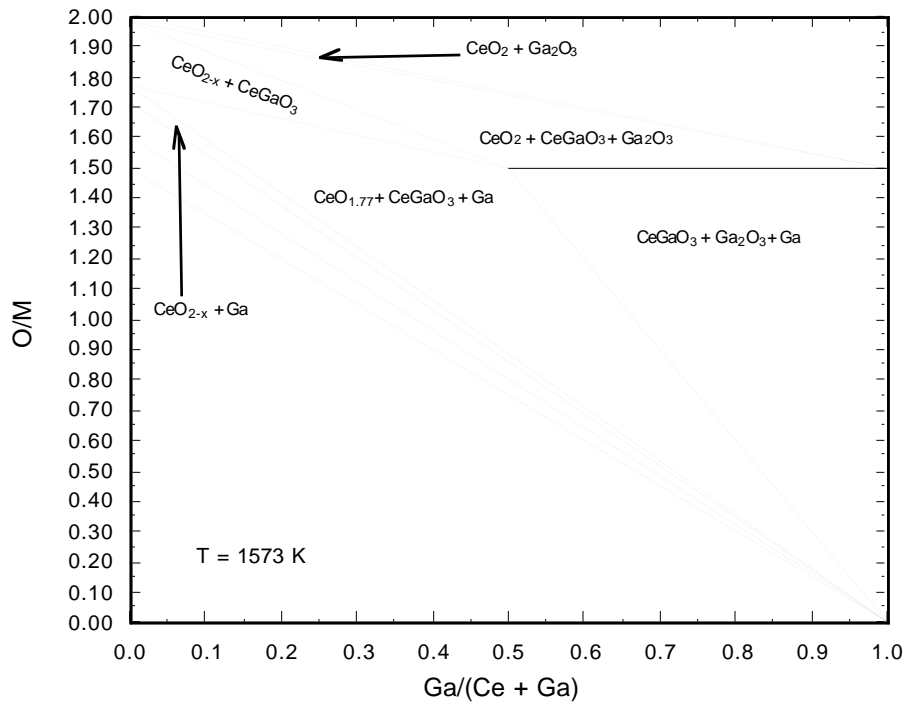


Figure 2.2.1-23. Partial Ce-Ga-O phase diagram at 1573 K.

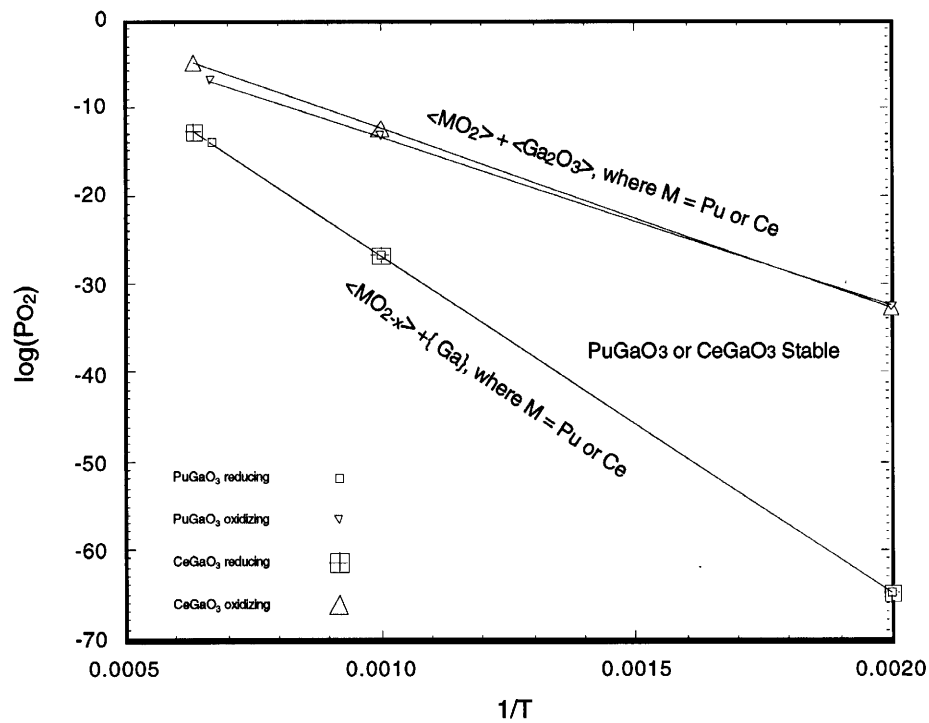


Figure 2.2.1-24. Diagram of  $\log(P_{O_2}) = f(1/T)$  defining  $\text{PuGaO}_3$  and  $\text{CeGaO}_3$  zones of stability.

**TABLE 2.2.1-7**  
**CALCULATED REDUCING AND OXIDIZING OXYGEN PRESSURES, AND**  
 **$\Delta G_f$  AS FUNCTION OF TEMPERATURE**

T, K	CeGaO <sub>3</sub>			PuGaO <sub>3</sub>		
	Reducing log(P <sub>O<sub>2</sub>)</sub>	Oxidizing log(P <sub>O<sub>2</sub>)</sub>	$\Delta G_f$ (kJ/mol)	Reducing log(P <sub>O<sub>2</sub>)</sub>	Oxidizing log(P <sub>O<sub>2</sub>)</sub>	$\Delta G_f$ (kJ/mol)
500	-64.74	-32.61	-129.2	-64.74	-32.36	-126.4
1000	-26.54	-12.66	-113.8	-25.54	-13.24	-111.4
1500				-13.93	-6.89	-96.6
1573	-12.77	-4.91	-96.3			

**TABLE 2.2.1-8**  
**LINEAR LEAST SQUARE FIT OF DATA IN TABLE 2.2.1-7**

Perovskite	$\Delta G_f$ (kJ/mole) = $A + B \cdot T$		Environ-ment	$\log(\text{PO}_2) = C + D/T$	
	A	B		C	D
PuGaO <sub>3</sub>	-141.19	0.029725	-	-	-
CeGaO <sub>3</sub>	-144.47	0.030641	-	-	-
PuGaO <sub>3</sub>	-	-	reducing	11.532	-38128.8
PuGaO <sub>3</sub>	-	-	oxidizing	5.856	-19106.5
CeGaO <sub>3</sub>	-	-	reducing	11.510	-38116.2
CeGaO <sub>3</sub>	-	-	oxidizing	7.824	-20241.5

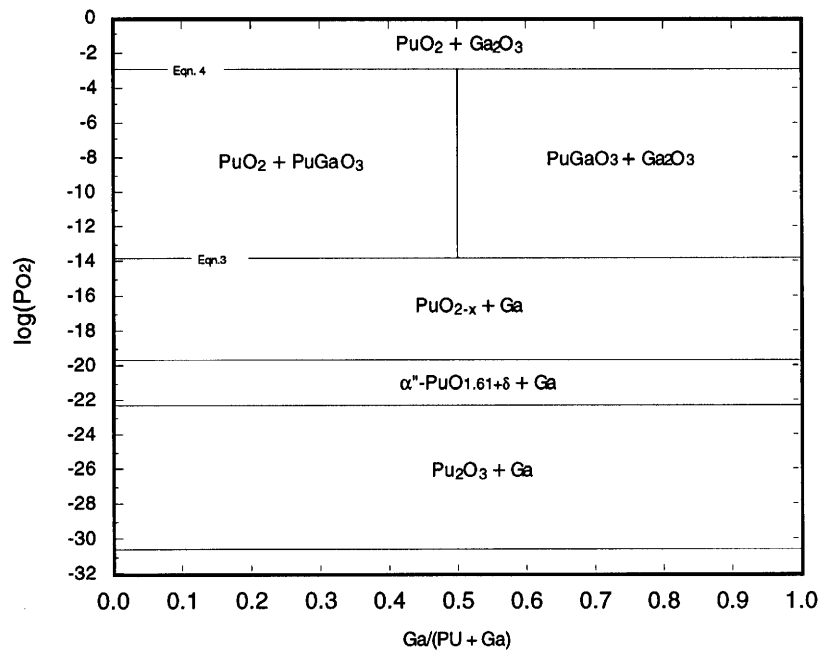


Figure 2.2.1-25. Equilibrium phase diagram of  $\log P_{\text{O}_2} = f\left(\frac{\text{Ga}}{\text{Pu}+\text{Ga}}\right)$  for the Pu-Ga system at 1500 K.

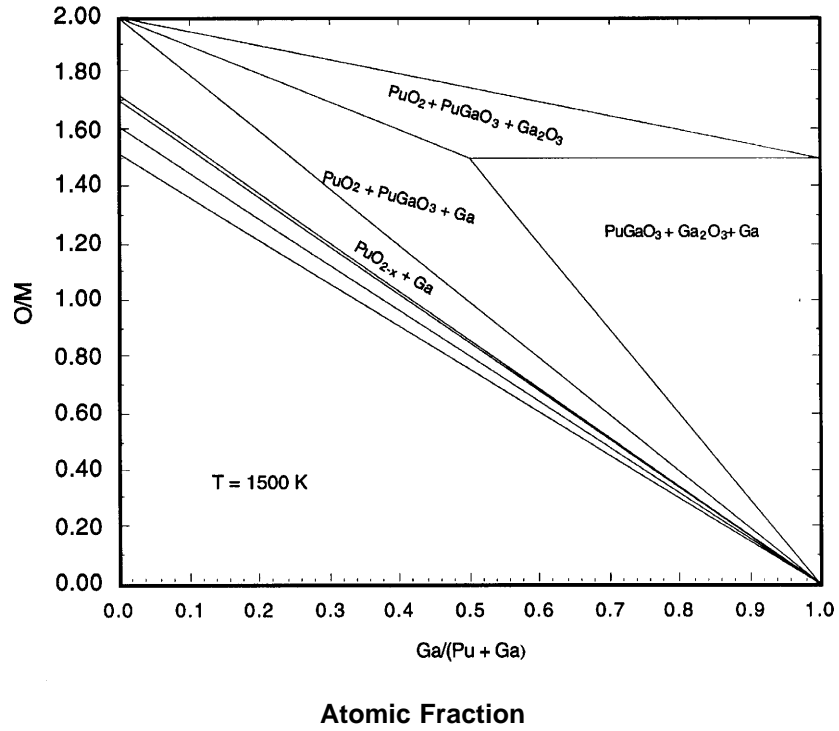


Figure 2.2.1-26. Partial Pu-Ga-O phase diagram at 1500 K.

**TABLE 2.2.1-9  
SUMMARY OF PLUTONIUM PEROVSKITE PREPARATIONS\***

Perovskite	Reactants	Preparation Method	Firing Conditions			X-ray Examination
			Temp. (K)	Time (h)	Atmosphere	
PuAlO <sub>3</sub>	PuO <sub>2</sub> + Al <sub>2</sub> O <sub>3</sub> + C	C	1773	2	Argon	(PuAlO <sub>3</sub> ) Cubic pattern with line splitting.
	PuO <sub>2</sub> + Al(OH) <sub>3</sub>	B	1773	2	Air	PuO <sub>2</sub> only.
	PuO <sub>2</sub> + Al(OH) <sub>3</sub>	A	1773	2	Hydrogen	PuO <sub>2</sub> + cubic pattern (PuAlO <sub>3</sub> ).
	PuO <sub>2</sub> + Al(OH) <sub>3</sub> (10% excess)	B	1773	2	Hydrogen	Cubic pattern (PuAlO <sub>3</sub> ) with line splitting.
	PuO <sub>2</sub> + Al(OH) <sub>3</sub> (10% excess)	-	Arc melted		Argon	PuO <sub>2</sub> + Pu <sub>2</sub> O <sub>3</sub> + cubic pattern (PuAlO <sub>3</sub> ).
PuCrO <sub>3</sub>	PuO <sub>2</sub> + CrO <sub>3</sub>	A	1773	2	Hydrogen	PuAlO <sub>3</sub> from reaction with alumina crucible.
	PuO <sub>2</sub> + CrO <sub>3</sub>	B	1773	2	Hydrogen	Orthorhombic pattern only (PuCrO <sub>3</sub> ).
	PuO <sub>2</sub> + Pu <sub>2</sub> O <sub>3</sub> + CrO <sub>3</sub>	D	1573	2	Hydrogen	PuO <sub>2</sub> + orthorhombic pattern (PuCrO <sub>3</sub> ).
PuFeO <sub>3</sub>	PuO <sub>2</sub> + Fe <sub>2</sub> (C <sub>2</sub> O <sub>4</sub> ) <sub>3</sub> •5H <sub>2</sub> O	A	1773	2	Hydrogen	PuO <sub>2</sub> + other weak lines.
	PuO <sub>2</sub> + Fe <sub>2</sub> (C <sub>2</sub> O <sub>4</sub> ) <sub>3</sub> •5H <sub>2</sub> O	B	1773	2	Hydrogen	PuO <sub>2</sub> + other weak lines.
	PuO <sub>2</sub> + Pu <sub>2</sub> O <sub>3</sub> + Fe <sub>2</sub> (C <sub>2</sub> O <sub>4</sub> ) <sub>3</sub> •5H <sub>2</sub> O	D	1573	2	Hydrogen	PuO <sub>2</sub> + other weak lines.
PuGaO <sub>3</sub>	PuO <sub>2</sub> + Ga <sub>2</sub> O <sub>3</sub>	B	1873	3	Hydrogen	PuO <sub>2</sub> + Pu <sub>2</sub> O <sub>3</sub>

A. Mixed powders fired in hydrogen;

B. Mixed powders compacted to 0.6 cm (0.25 in) right cylinders at 300 kg/cm<sup>2</sup> (40,000 psi) - sintered in hydrogen;

C. Mixed powders with excess graphite above that needed to reduce PuO<sub>2</sub> to Pu<sub>2</sub>O<sub>3</sub> - compacted into 0.6 cm right cylinders - sintered in Ar; and

D. PuO<sub>2</sub> previously reduced in hydrogen to about 50 % α-Pu<sub>2</sub>O<sub>3</sub> used instead of PuO<sub>2</sub> - compacted to 0.6 cm right cylinders - sintered in hydrogen.

\*Observations:

- PuAlO<sub>3</sub> does not form from mixtures of PuO<sub>2</sub> and Al<sub>2</sub>O<sub>3</sub> in air at 1773 K.
- PuAlO<sub>3</sub>, and PuCrO<sub>3</sub> do form from mixtures of PuO<sub>2</sub> and Al<sub>2</sub>O<sub>3</sub>, and CrO<sub>3</sub>, respectively, in hydrogen at 1773 K. PuCrO<sub>3</sub> also forms from mixtures of 50/50 mixtures of Pu<sub>2</sub>O<sub>3</sub>/PuO<sub>2</sub> + CrO<sub>3</sub> in hydrogen at 1573 and 1773 K.
- PuFeO<sub>3</sub> did not form from heating mixtures of the oxides in hydrogen at 1773 and 1573 K although the tolerance factor, *t*, is favorable.
- PuGaO<sub>3</sub> did not form from heating mixtures of the oxides in hydrogen at 1873 K.

**TABLE 2.2.1-10**  
**SUMMARY OF PuAlO<sub>3</sub> PREPARATIONS\***

Perovskite	Reactants	Preparation Method	Firing Conditions			X-ray Examination
			Temp. (K)	Time (h)	Atmosphere	
PuAlO <sub>2</sub>	PuO <sub>2</sub> + Al <sub>2</sub> O <sub>3</sub> 40 mol % PuO <sub>2</sub>	E	2195	0.01	O <sub>2</sub>	PuO <sub>2</sub> + Al <sub>2</sub> O <sub>3</sub>
	PuO <sub>2</sub> + Al <sub>2</sub> O <sub>3</sub> 50 mol % PuO <sub>2</sub>	E	2171	0.01	O <sub>2</sub>	PuO <sub>2</sub> + Al <sub>2</sub> O <sub>3</sub>
	PuO <sub>2</sub> + Al <sub>2</sub> O <sub>3</sub> 60 mol % PuO <sub>2</sub>	E	2180	0.01	O <sub>2</sub>	PuO <sub>2</sub> + Al <sub>2</sub> O <sub>3</sub>
	PuO <sub>2</sub> + Al <sub>2</sub> O <sub>3</sub> 35 mol % PuO <sub>2</sub>	E	2085	0.01	O <sub>2</sub>	PuO <sub>2</sub> + Al <sub>2</sub> O <sub>3</sub>
	PuO <sub>2</sub> + Al <sub>2</sub> O <sub>3</sub> 45 mol % PuO <sub>2</sub>	E	2073	0.01	O <sub>2</sub>	PuO <sub>2</sub> + Al <sub>2</sub> O <sub>3</sub>

E. These sample were prepared for a pseudo-binary phase diagram study. Mixed powders were finely ground in an agate mortar then compacted to 0.6 cm (0.25 in) or 0.95 cm (0.375 in) right cylinders at 120,000 and 160,000 psi, respectively - sintered in an oxygen atmosphere at 1523 K for 2 hrs.

\*Observations:

- PuAlO<sub>3</sub> does not form in the PuO<sub>2</sub>-Al<sub>2</sub>O<sub>3</sub> pseudo-binary system in O<sub>2</sub> or Ar within the temperature range 2195 to 2073 K.
- In O<sub>2</sub> the pseudo-binary eutectic temperature is 2183 ± 15 K, and in Ar the value is 2088 ± 7 K. The pseudo-binary eutectic composition is 42 mole % PuO<sub>2</sub>.
- The terminal solid solubility of PuO<sub>2</sub> in Al<sub>2</sub>O<sub>3</sub> is 0.28 ± 0.2 mol % (0.75 ± 0.04 wt. %).
- The terminal solid solubility of Al<sub>2</sub>O<sub>3</sub> in PuO<sub>2</sub> is 0.14 ± 0.14 mol % (0.05 ± 0.05 wt. %).

### 2.2.2. Ga Removal from Surrogate MOX Fuel

A variety of studies were performed on surrogate feedstock materials to assess the kinetics of gallium evolution. Due to the similarities between oxygen diffusion, thermodynamics, crystal structure, melting point, non-stoichiometric characteristics, and d-orbital bonding,  $\text{CeO}_{2-x}$  was considered a relatively good surrogate for  $\text{PuO}_{2-x}$ . The primary surrogate investigated was a  $\text{CeO}_2$ -2 wt %  $\text{Ga}_2\text{O}_3$  powder. Studying surrogates provides a relatively safe and rapid means for understanding the kinetics of Ga removal as well as means for collecting the evolved Ga. In addition, a well characterized surrogate aides in evaluations of pilot or full scale production equipment outside of a glovebox environment, thus preventing unnecessary radiation dose to personnel, reduced levels of radioactive waste, and costly errors that could be associated with setting up large scale systems in a glovebox without the advantage of prior operational checks.

**2.2.2.1  $\text{CeO}_2$ - $\text{Ga}_2\text{O}_3$ .** First, it was necessary to develop an inexpensive and consistent method for producing  $\text{CeO}_2$ -2 wt %  $\text{Ga}_2\text{O}_3$  powder. Several methods were, and still are, under consideration for producing a feedstock consisting of both  $\text{CeO}_2$  and  $\text{Ga}_2\text{O}_3$  powders, which have been co-precipitated from solution, metallic hydride-oxidation, and cold-press and sintering. Each process has its own peculiarities, including process complexity, cost, and final product form. It is believed that in the worst case (for Ga removal), the  $\text{Ga}_2\text{O}_3$  will be in solid solution with  $\text{PuO}_2$  in the prototypic feed. Because a cold-press and sintering capability already exists in the surrogate lab, this process was pursued. Other possibilities are being examined in addition to determination of the prototypic feed form resulting from the HYDOX process.

Table 2.2.2-1 shows the raw materials that were used, Table 2.2.2-2 shows the list of processing equipment, and Figure 2.2.2-1 shows a flow diagram of the final process that was developed. As illustrated in Figure 2.2.2-2 where  $n$  represents the number of specimens on which measurements were made, the method gave relatively consistent pellets (see Figure 2.2.2-3 for more information) with fired densities near 95% of theoretical. The pellets are typically ground and classified after this stage in processing. As shown in Figure 2.2.2-4, the sintered surrogate pellets had an average grain size of approximately 50  $\mu\text{m}$ . Also, as can be seen in the dark regions in Figure 2.2.2-4, not all of the  $\text{Ga}_2\text{O}_3$  was in solution with the  $\text{CeO}_2$ . The dark spots within grains are area enriched in Ga. As was discussed in Section 2.2.1 of this report, this is what is predicted by thermodynamic modeling and is expected to be true of  $\text{Ga}_2\text{O}_3$  in  $\text{PuO}_2$ . Following sintering, the pellets were re-crushed and passed through various screens, providing surrogate feedstock powders of several particle sizes, typically below 45  $\mu\text{m}$ .

**TABLE 2.2.2-1.  
DESCRIPTION OF RAW MATERIALS USED TO FABRICATE  
SURROGATE FEEDSTOCK POWDERS**

<b>Description</b>	<b>Materials</b>	<b>Supplier</b>	<b>Description</b>
Powder	Gallium (III) oxide Ga <sub>2</sub> O <sub>3</sub>	Johnson Matthey	99.999% -325 mesh
Powder	Cerium (IV) oxide CeO <sub>2</sub>	Johnson Matthey	99.99% 5 micron
Binder	Polyethylene Glycol (PEG)	J.T. Baker	PEG 8000 (U222-08)
	Stearic Acid	E.M. Science	EM-SX0947-1
Lubricant	Liqui Moly	Lockery Company	Moly Grade NV regular

**TABLE 2.2.2-2.  
PROCESSING EQUIPMENT USED TO FABRICATE  
CeO<sub>2</sub>-2 WT % Ga<sub>2</sub>O<sub>3</sub> POWDERS**

<b>Processing</b>	<b>Name</b>	<b>Maker / Description</b>
Weighing	Balance	Denver Instrument Co., A-160, accuracy: 0.0001 g
Milling	Spex mill	SPEX mixer 8000
Pressing	Pressing / Die	Carver model-6, range: 0-24000 lbs
Sieving	Screen	Dual MFG. Co. 40, 60, 80, 100 mesh
Sintering	Furnace	DelTec Inc. < 1750°C
Reduction	Furnace	Thermolyne 59300 Thermox CG1000: Oxygen Analyzer

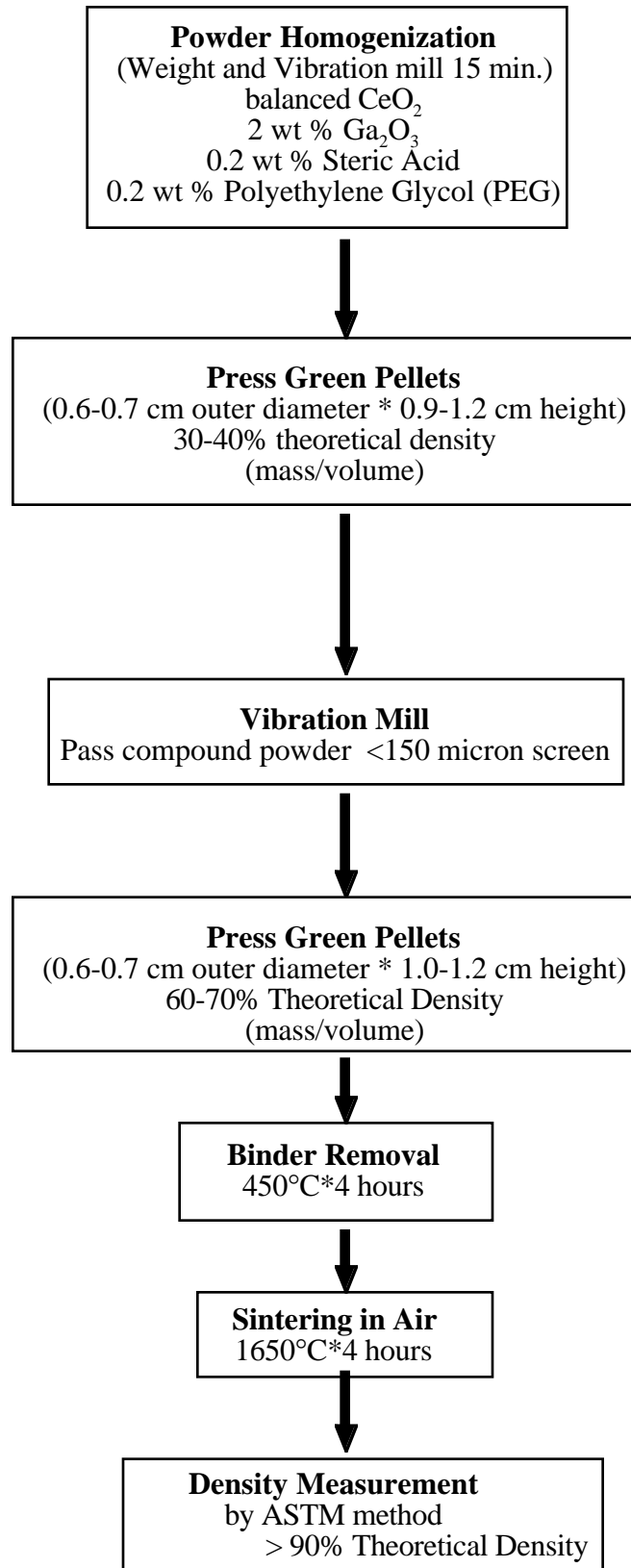


Figure 2.2.2-1. Flow chart illustrating processing steps used to fabricate CeO<sub>2</sub>-2 wt % Ga<sub>2</sub>O<sub>3</sub> powders.

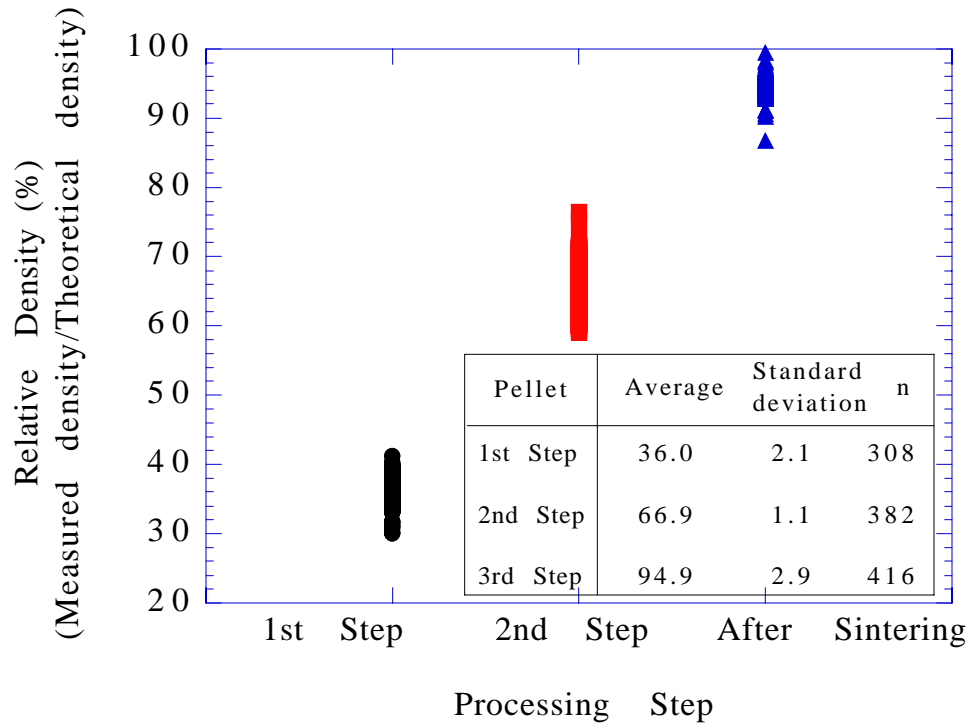


Figure 2.2.2-2. Plot of green and fired densities of  $CeO_2$ -2 wt %  $Ga_2O_3$  pellets after the steps described in Figure 2.2.2-1.



Figure 2.2.2-3. Fired  $CeO_2$ -2%  $Ga_2O_3$  pellets.

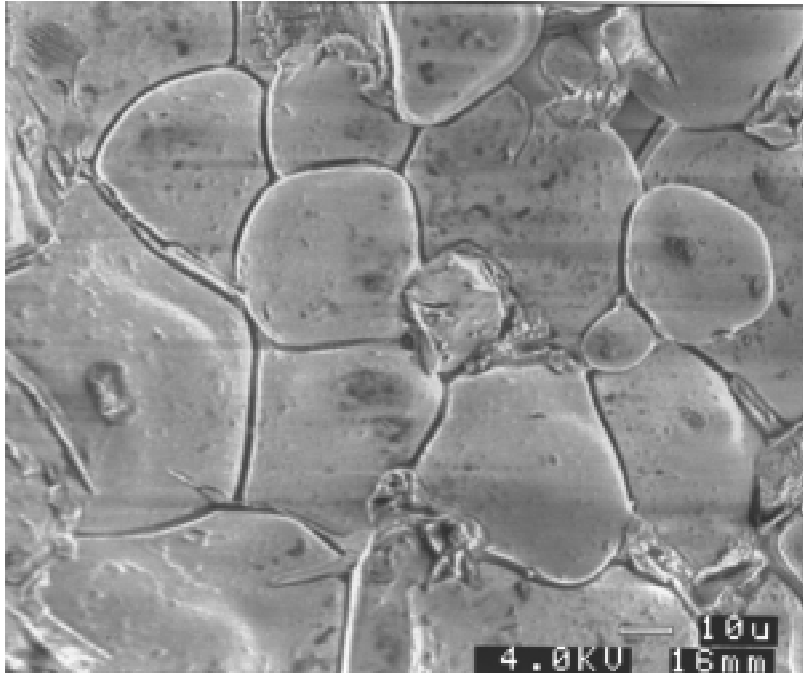


Figure 2.2.2-4. Microstructure of the sintered CeO<sub>2</sub>-2% Ga<sub>2</sub>O<sub>3</sub> pellets.

**2.2.2.2 Ga Removal in Surrogate Feedstock.** The prepared surrogate feedstock materials were subsequently heat treated in various environments to assess the rate and efficacy of Ga removal. The majority of these studies were done in Ar-6% H<sub>2</sub> under slow flowing conditions. For comparison, samples were also exposed to pure argon. Four sample loading morphologies were used as illustrated in Figure 2.2.2-5 which included a single, uncrushed pellet and flat boats filled with 0.3, 0.9, and 2.5 grams of powder. The photos on the left-hand side of the page show the materials before exposure, and the ones on the right show the materials after exposure. In the top picture, materials were exposed to a Ar-6% H<sub>2</sub> environment, and in the bottom one, they were exposed to a pure Ar environment, both at 1100°C for 30 minutes. Three powder lot sizes were used for most tests: 0.3, 0.9, and 2.5 grams.

The samples were placed side-by-side into a controlled atmosphere tube furnace as illustrated in Figure 2.2.2-6. The furnace was thoroughly purged with Ar-6% H<sub>2</sub> for 12 hours by pumping the system to low vacuum, filling with purified gas, pumping, and so on. The oxygen levels were constantly monitored using zirconia oxygen cells. The oxygen partial pressure was always at or well below 10<sup>-21</sup> atm. Surrogate powder and pellet samples were heated to the desired temperature (600-1200°C) at 20°C/min and held for 0.5-12 hours. Following exposure, the samples were cooled to room temperature at 20°C/min.

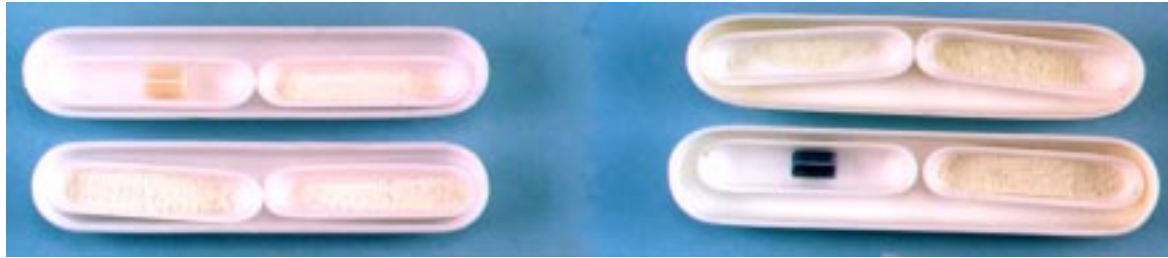
As discussed in Section 2.2.1 of this report, it is possible to remove Ga from MOX through the reaction:





Starting Feedstock

After 1100°C, 0.5 hr in Ar-6% H<sub>2</sub>



Starting Feedstock

After 1100°C, 0.5 hr in pure Ar

Figure 2.2.2-5. Photographs of surrogate pellets and powders shown as they were placed in alumina boats for gallium evolution testing.

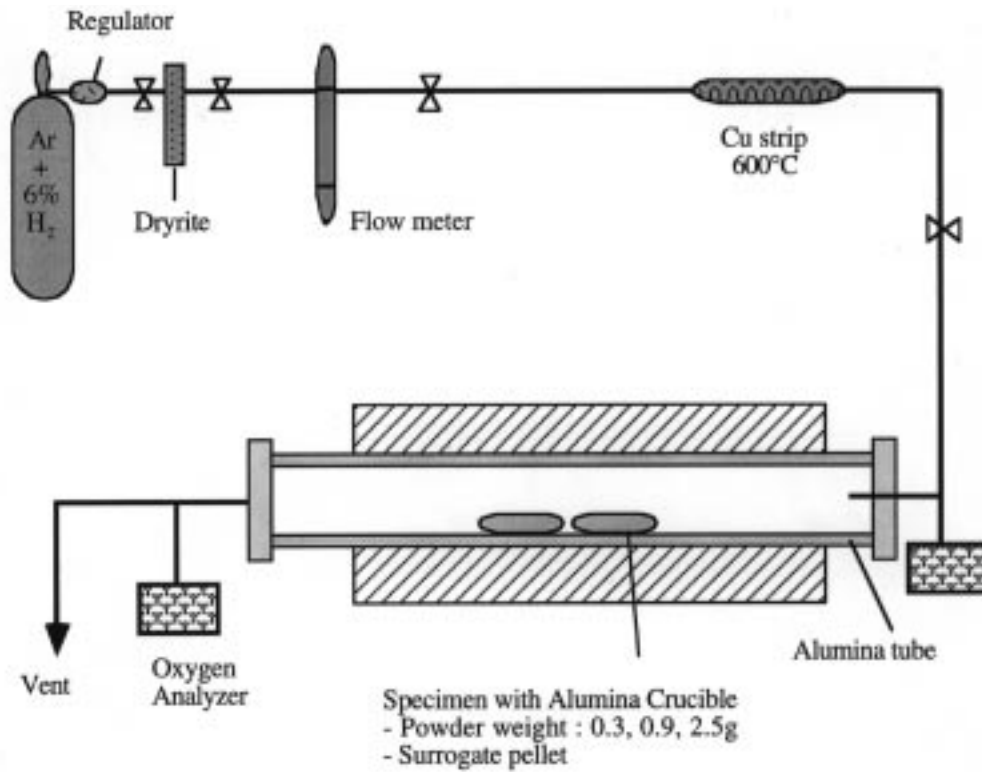


Figure 2.2.2-6. Schematic diagram of the apparatus assembled and used for Ga vaporization studies.

The partial pressure of  $\text{Ga}_2\text{O}(\text{g})$  in  $\text{H}_2$  is orders of magnitude higher than in an inert atmosphere or vacuum where Ga can only be removed through the sublimation reaction:



Figure 2.2.2-7 shows the effect of temperature on the weight loss of the surrogate material in both Ar-6%  $\text{H}_2$  and pure Ar after 30 minutes of exposure as a function of sample geometry. It must be kept in mind that the measured weight loss is the combined effect of loss of Ga and O associated with the two mass action equations described above as well as loss of oxygen from cerium oxide, i.e., cerium oxide becomes more substoichiometric under reducing conditions. Thus, weight loss alone is only a qualitative measure of Ga loss. Chemical analyses and determination of oxygen to metal ratio (O/M) are required to more fully elucidate the kinetics of Ga removal. However, as Figure 2.2.2-7 suggests, there appears to be negligible Ga loss in Ar, but significant loss in  $\text{H}_2$ , as predicted by thermodynamics. Schedule and resource limitations for performing quantitative chemical analyses on the surrogate materials preclude a comprehensive study of the kinetics at this stage. However, as will be discussed below, Los Alamos initiated an effort to assess a variety of types (of methods) and sources (personnel) for doing these analyses. As a consequence, 50 samples have been sent to a private laboratory for chemical and O/M analysis, and approximately 50 more samples are being prepared. The first 50 analyses should be complete by mid-November 1997.

Time is a critical parameter in assessing the kinetics of a process. Figure 2.2.2-8 shows the effect of time on the weight loss of the surrogate material in Ar-6%  $\text{H}_2$  at 600, 900, and 1200°C exposed for 0.5 to 12 hours. Although further data are needed, it appears that the kinetics of Ga removal are nonlinear, perhaps parabolic, with most of the loss occurring in the first 30 minutes to an hour.

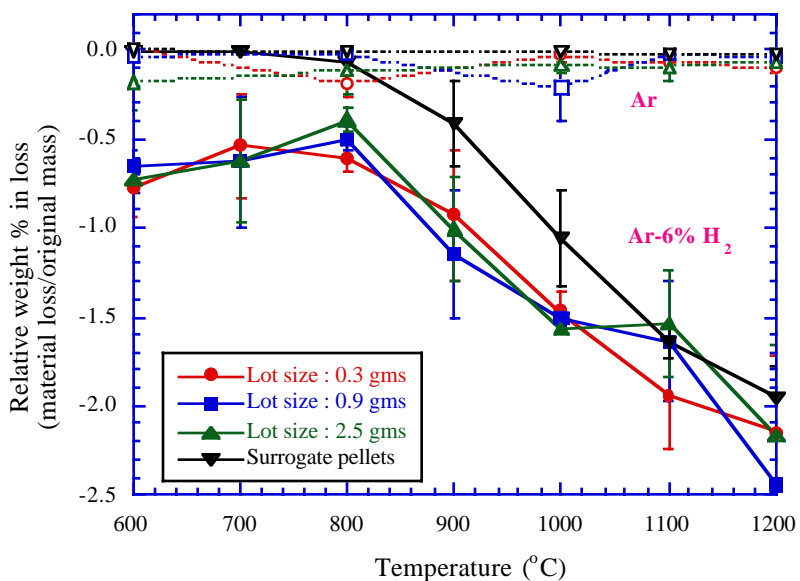


Figure 2.2.2-7. Plot of weight change versus temperature for  $\text{CeO}_2$ -2%  $\text{Ga}_2\text{O}_3$  samples exposed to Ar-6%  $\text{H}_2$  and Ar for 30 minutes.

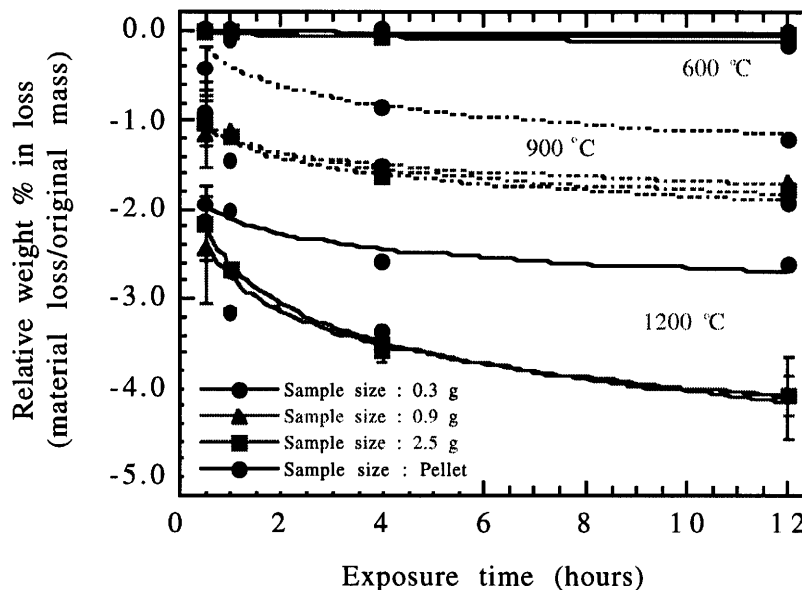


Figure 2.2.2-8. Plot of weight change versus time for  $\text{CeO}_2$ -2%  $\text{Ga}_2\text{O}_3$  samples exposed to Ar-6%  $\text{H}_2$  at 600, 900, and 1200°C.

A limited number of chemical analyses were performed in FY97 on the surrogate materials. A primary purpose of these measurements was to assess whether sample size affected Ga removal. These data are summarized in Figures 2.2.2-9 to 2.2.2-12, which display results for x-ray microfluorescence (XRMF), proton induced x-ray emission (PIXE), x-ray photoelectron spectroscopy (XPS), and inductively coupled plasma emission (ICP) analyses, respectively. As shown in Figure 2.2.2-9, XRMF demonstrated that the kinetics of Ga removal are strongly affected by temperature, i.e., the rate is faster at higher temperatures, which is in agreement with the weight loss measurements shown in Figure 2.2.2-7. However, due to the scatter in data at these low Ga concentrations, XRMF did not provide a clear indication of whether lot size influenced the kinetics. PIXE (Figure 2.2.2-10), XPS (Figure 2.2.2-11), and ICP (Figure 2.2.2-12) gave consistent results (although semiquantitative in the first two cases), which indicated overall that the efficacy of Ga removal improved with decreasing sample size. In particular, in Figure 2.2.2-10, the data indicate that the efficacy of Ga removal improves with decreasing lot size, in Figure 2.2.2-11, the efficacy of Ga removal appears to improve with decreasing lot size and the spectra for the cerium peaks are shown, and Figure 2.2.2-12 indicates that the efficacy of Ga removal improves with decreasing lot size. The numbers at the right of this figure are the corresponding O/M ratios. Additionally, further analyses have been submitted to confirm these results. However, the results suggest that gas diffusion may be rate limiting (most likely by diffusion of  $\text{Ga}_2\text{O}(\text{g})$  from the bed).

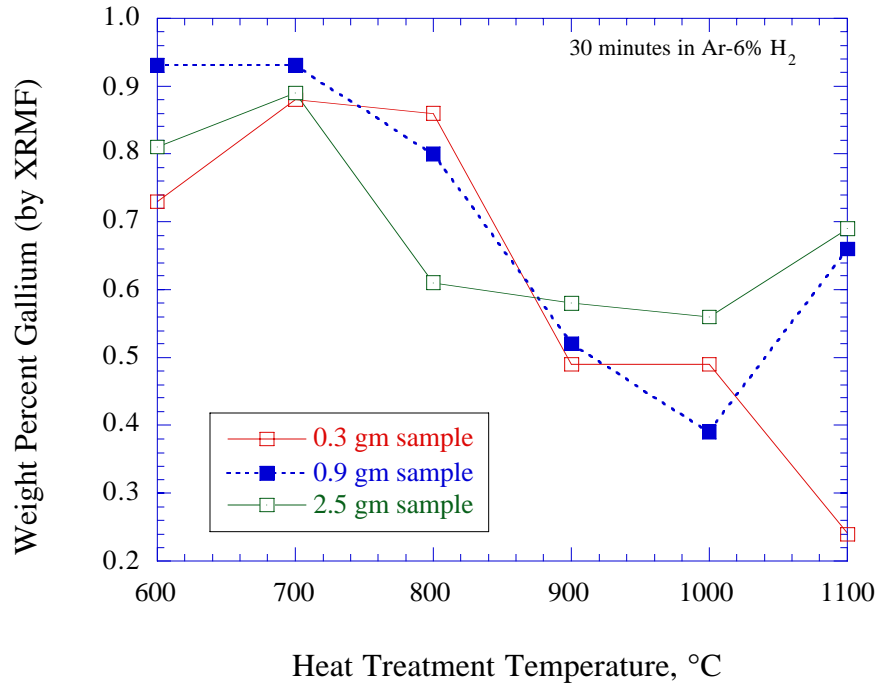


Figure 2.2.2-9. Plot of weight percent gallium (measured by x-ray microfluorescence) versus temperature for CeO<sub>2</sub>-2% Ga<sub>2</sub>O<sub>3</sub> powder samples exposed to Ar-6% H<sub>2</sub> for 30 minutes.

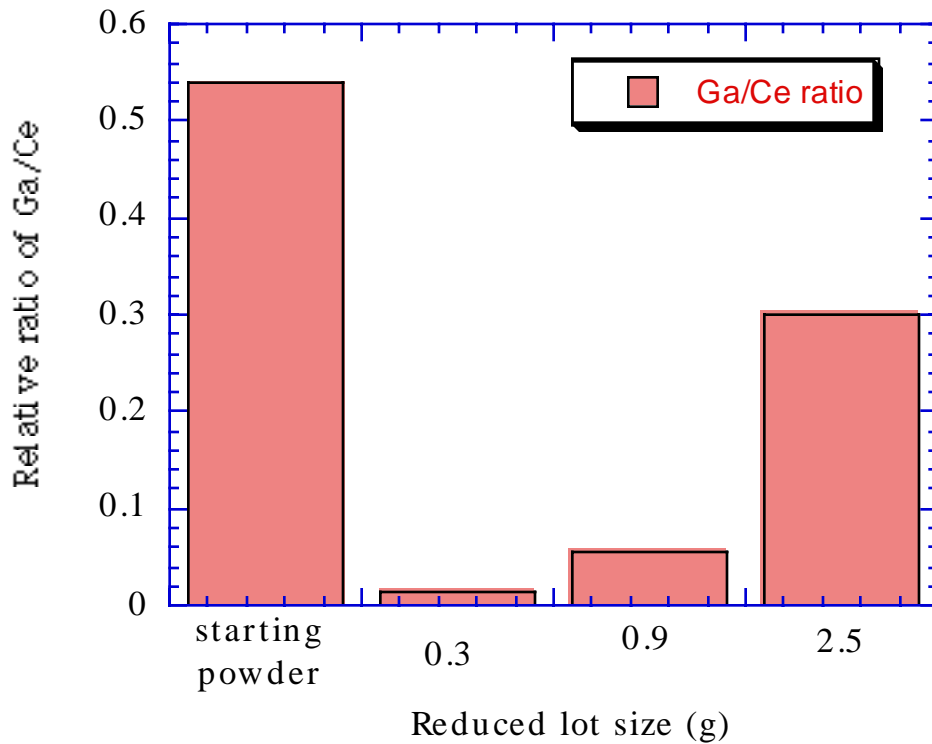


Figure 2.2.2-10. Histogram of PIXE measurements of relative Ga concentration in surrogate MOX after exposure to Ar-6% H<sub>2</sub> at 1200°C for 30 minutes.

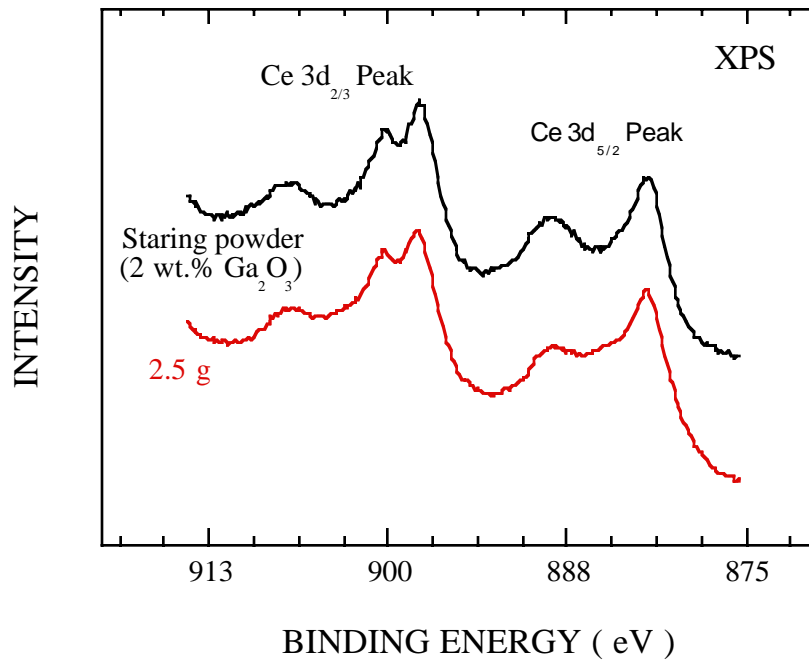
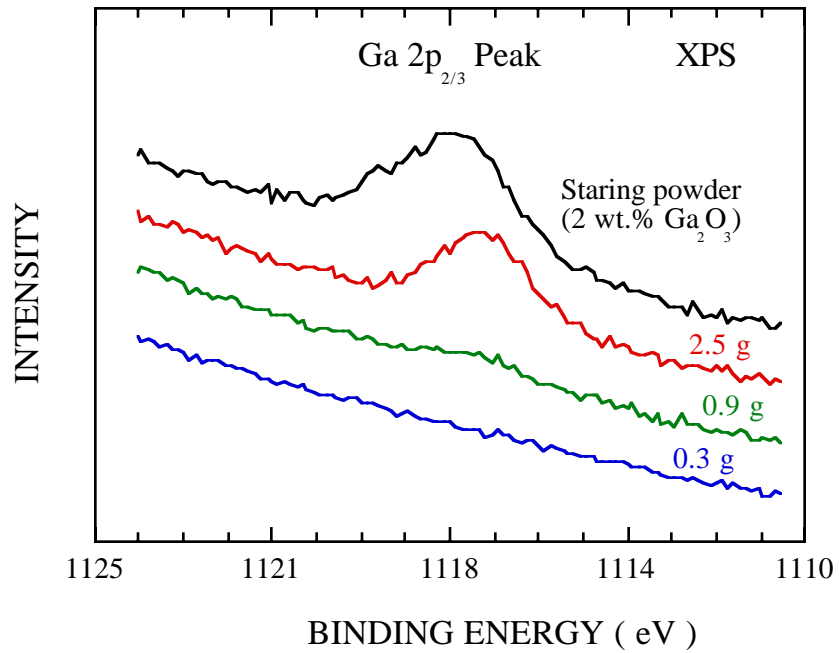


Figure 2.2.2-11. XPS spectra (top) comparing the relative Ga concentration in surrogate MOX after exposure to Ar-6% H<sub>2</sub> at 1200°C for 30 minutes.

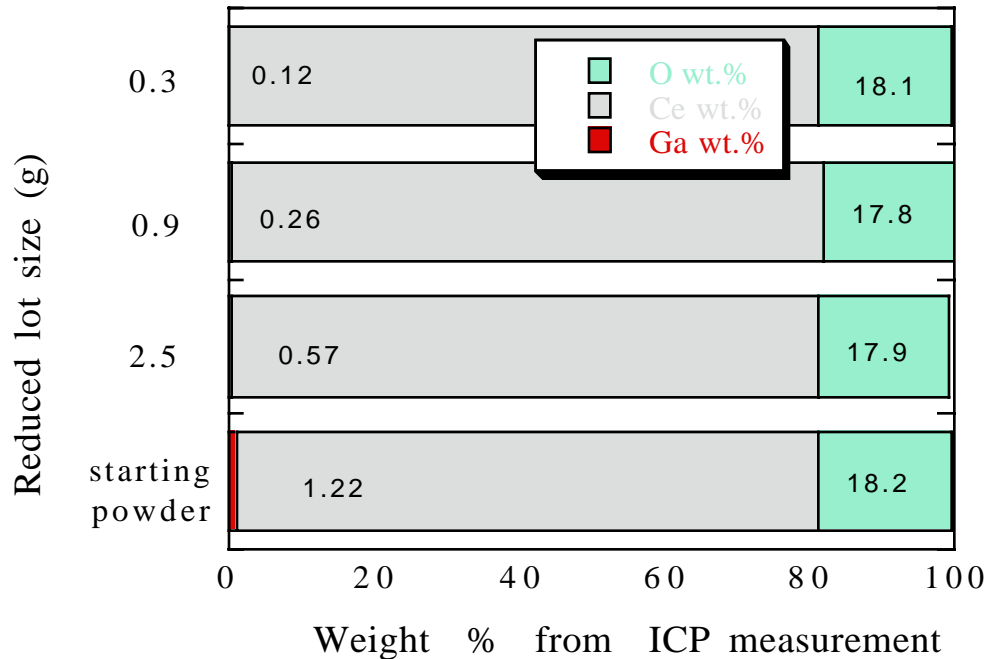


Figure 2.2.2-12. Histogram of ICP measurements of Ga concentrations in surrogate MOX after exposure to Ar-6% H<sub>2</sub> at 1200°C for 30 minutes.

In addition to the techniques described above, Los Alamos also recently conducted a series of experiments with the University of Florida Training Reactor (UFTR) Neutron Activation Analysis (NAA) facility in order to determine if NAA could be used for the rapid quantitative trace analysis for Ga, in particular. This set of experiments was an unqualified success. The lower level of detection for Ga using NAA was well below 1 ppm. Los Alamos successfully analyzed 6 specimens in a period of a few hours and determined that the UFTR could offer analysis services at a very reasonable fee with a turnaround time of 1 week or less.

Figure 2.2.2-13 shows some preliminary results illustrating the effect of the gas flow rate of Ga removal. The shaded regions show the predicted mass loss for samples exposed at 3.0 cm/sec, assuming the Ga and O fluxes increase as the square root of gas velocity. Specimens were placed in boats as shown in Figure 2.2.2-5, and the gas flow rate was doubled from 1.5 cm/sec to 3.0 cm/sec. The shaded regions in Figure 2.2.2-13 show the predicted average weight loss for the pellets or the composite of powders, assuming the flux is proportional to the square root of gas velocity. As the figure indicates, gas flow rate apparently had minimal effect on Ga removal under these conditions. This implies the kinetics are not rate limited by H<sub>2</sub> transport, but it does negate the possibility that loss is rate limited by Ga<sub>2</sub>O(g) transport. Further studies are planned to elucidate the exact rate limiting mechanism.

Experiments involving the effects of particle size on Ga removal were initiated in FY97, but they are incomplete at this date and will therefore be further studied and reported in FY98. In addition to studying the effects of H<sub>2</sub> on Ga removal, the use of carbon as a reducing

agent was also investigated. If carbon could be used effectively, it might be possible to reduce the surrogate material in a vacuum where gas transport issues would be less significant. Figure 2.2.2-14 shows the weight loss of  $\text{CeO}_2$ -2%  $\text{Ga}_2\text{O}_3$  doped with zero to 9.25% carbon after heat treatment in Ar-6%  $\text{H}_2$  and subsequently in air. The air treatment was done to remove carbon. Careful study of this figure reveals that most of the mass loss was associated loss of carbon. These measurements are also currently being performed in pure Ar.

In addition to the vaporization studies, the diffusion of Ga in  $\text{CeO}_2$  and the reactions between  $\text{Ga}_2\text{O}_3$  and  $\text{CeO}_2$  was also investigated in FY97. These studies have included mapping the Ga distribution in sintered pellets using XRMF (see Section 3.2.1.2) and by studying  $\text{CeO}_2/x\text{Ga}_2\text{O}_3/\text{CeO}_2$  couples. Figure 2.2.2-15 shows a photograph of a number of these diffusion couples following sintering at 1650°C and after exposure to Ar-6%  $\text{H}_2$  at 1000 and 1200°C for 0.5 and 4 hours. The  $\text{Ga}_2\text{O}_3$  interlayer consisted of  $\text{CeO}_2$ -x%  $\text{Ga}_2\text{O}_3$  with x equal to 2, 5, or 50 as indicated at the left of the photograph. In addition, as the photograph indicates, there can be a rather significant and somewhat catastrophic reaction (as may be true of  $\text{PuO}_2$ ) between the layers. These data are being used to assist in validating diffusion data as well as phase diagram information. The specimens have been further prepared for analyses which will include mapping diffusion profiles and identifying crystal phases.

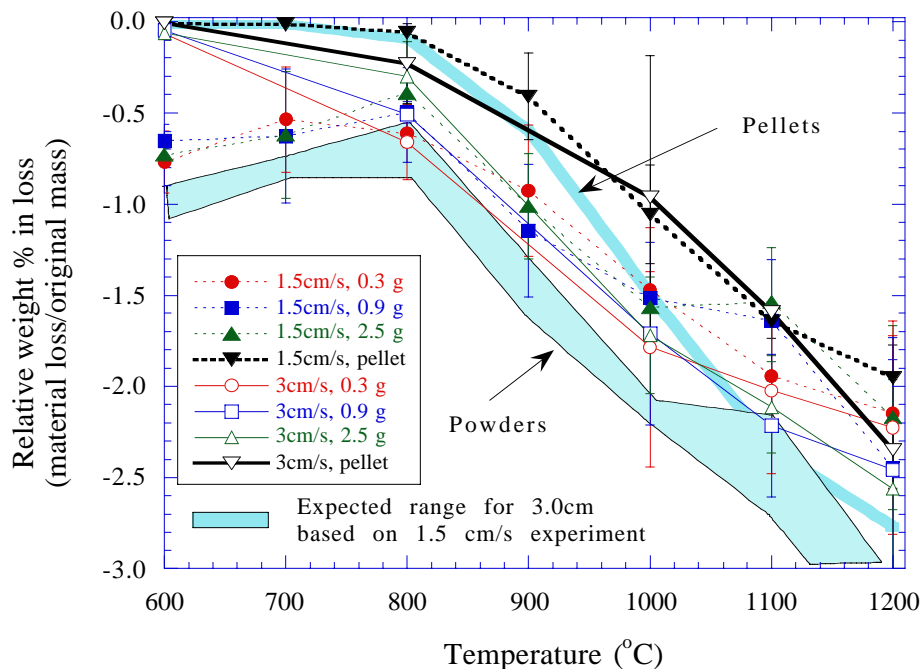


Figure 2.2.2-13. Plot of weight change versus temperature for  $\text{CeO}_2$ -2%  $\text{Ga}_2\text{O}_3$  samples exposed to Ar-6%  $\text{H}_2$  at 1.5 and 3.0 cm/sec flow rates.

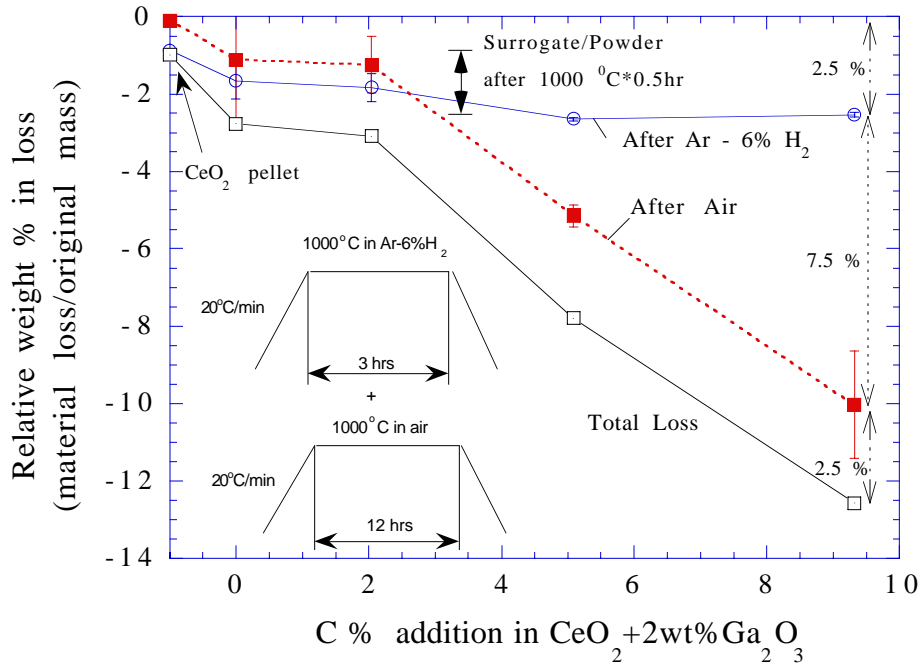


Figure 2.2.2-14. Plot of weight change versus temperature for CeO<sub>2</sub>-2% Ga<sub>2</sub>O<sub>3</sub> samples doped with varying levels of carbon and exposed to Ar-6% H<sub>2</sub> and subsequently air at 1000°C for 30 minutes.

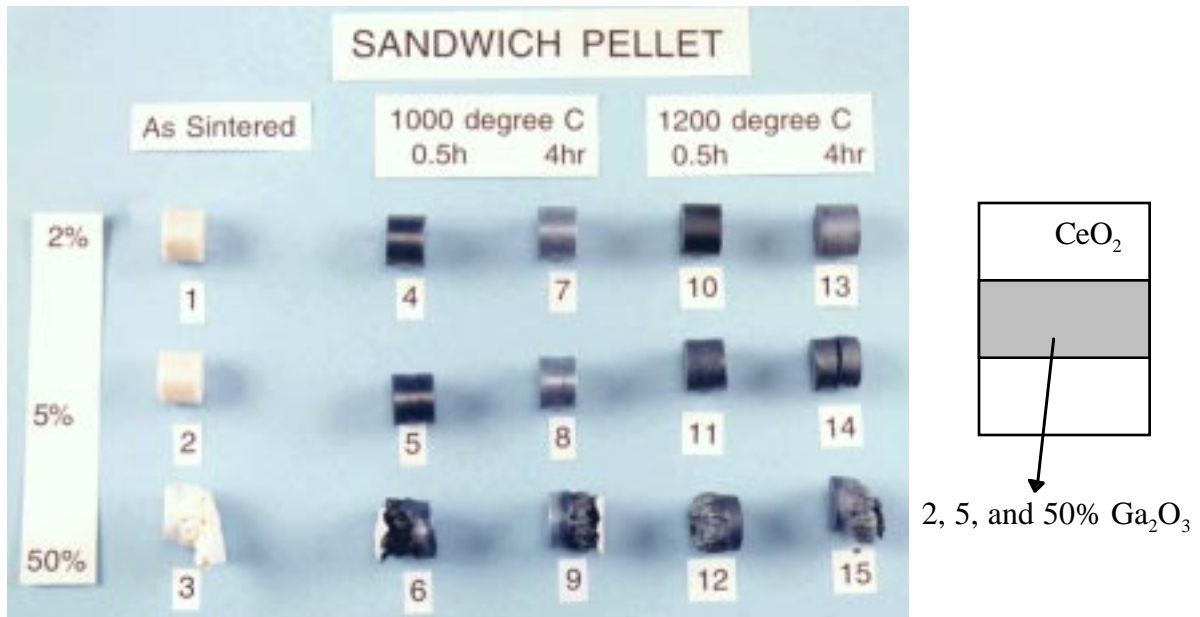


Figure 2.2.2-15. Photograph of CeO<sub>2</sub>/Ga<sub>2</sub>O<sub>3</sub>/CeO<sub>2</sub> diffusion couples following exposure to air at 1000 and 1200°C for 0.5 and 4 hours.

### **2.2.3. PuO<sub>2</sub> Studies**

Work in the area of PuO<sub>2</sub> studies was initiated in July 1997. The aim of the limited FY97 effort was to lay some groundwork for the thermally-induced gallium removal (TIGR) design effort beginning in FY98. The FY98 studies are comprised of two distinct research areas (1) process development for TIGR and (2) on-line gallium analysis. Both of these areas seek to develop processes to be integrated into the pit disassembly and conversion process. To integrate these two tasks into the overall MOX fuel research plan, three days were devoted to a product realization workshop for planning TIGR activities. The scope of work, responsibilities for portions of that work, and budgeting were determined during the workshop. Because resources were limited, no experiments involving the evolution of Ga from PuO<sub>2</sub> were conducted in FY97. However, A range of thermal treatment parameters is proposed to be tested in FY98.

#### TIGR Process Development

The objective of this portion of the TIGR program is to determine the optimal processing conditions for removing gallium from PuO<sub>2</sub> via thermal evolution. Optimization requires analysis of the effects of time, temperature, mass transport, etc., on the rate of gallium removal from PuO<sub>2</sub>. FY97 efforts focused on acquisition of equipment, space, personnel, and required approvals as a precursor to the FY98 studies.

Two parallel paths were undertaken for the appropriation of equipment and space. The first path is the preferred path of the two. It involves the purchase and setup of a furnace in an available glovebox. Because the acquisition of, approval for use of, and setup of a furnace in a glovebox is a relatively slow process and can take many months, a second path comprising the identification and acquisition of an existing glovebox/furnace combination that would be suitable for use in the intervening period was pursued. Suitable space and equipment was identified. Negotiations with facility management for their use are underway.

An experimental plan under an existing standard operating procedure for performing furnace work in PF-4 has been authored and reviewed by facility management. The plan is currently awaiting facility management approval.

#### On-Line Gallium Concentration Analysis Development

The objective of this portion of the TIGR program is to develop an on-line method for determining trace gallium concentration in PuO<sub>2</sub> in real time, as the product is treated for Ga removal. Initially, the suitability of a variety of techniques for on-line trace analysis was explored, and a preliminary literature search was performed. Preliminary discussions suggested that laser induced breakdown spectroscopy (LIBS) was the best candidate for on-line analysis because (1) critical LIBS components can remain external to the glovebox, and (2) the technique was already in the early stages of setup in the plutonium facility. Initial tests to determine the LIBS signature of gallium have been performed in a cold laboratory at TA-55. A LIBS spectrum on pure Ga metal has been collected and is currently being analyzed.

### **2.2.4. Development of a Production-Scale TIGR System**

The purpose of this task was to start the design of a TIGR system that could be built and tested during FY98 and FY99. The system design is based on the requirements for the production-scale TIGR system that will be designed, fabricated and integrated into the pit disassembly and conversion facility (PDCF). The gallium removal system will directly integrate with the HYDOX system and must meet mixed-oxide (MOX) fuel fabrication requirements.

Work on the thermal gallium removal system design was limited in part due to the delays imposed upon research and development (R&D) of the surrogate fuel and the MOX fuel fabrication studies. Much of the required data was not available until the end of FY97, so the information presented in this section is limited to preliminary results of some of the research. The rest of the research and analysis will not be completed until later in FY98. Therefore, there are several parameters that cannot be established until additional work in this area is completed.

The purpose of this section is to provide a preliminary overview of the thermal gallium removal process, including how it will be integrated into PDCF, what the primary design parameters and material considerations are, geometry considerations, and analytical modeling of the gallium/plutonium separation process.

Many of the key inputs for the design have not yet been established from the on-going gallium removal R&D effort. These input parameters will be identified and their potential impacts discussed. A preliminary cost and schedule estimate for the development of the TIGR laboratory-scale system has been included with the assumption that the system can be used for the integrated system test of the PDCF.

**2.2.4.1. TIGR Overview.** One of the critical steps in preparing the weapons plutonium for use as MOX fuel in the plutonium disposition project is the removal of the gallium. In fabricating MOX fuel it is important to have consistent feed material so the sintering parameters that produce acceptable fuel pellets can be established. At high concentrations, gallium affects the sintering behavior of the ceramic. Therefore, to ensure consistent feed and processing parameters for sintering of the pellets, it is important to reduce the levels of gallium in the powder.

In addition, MOX fuel that still contains the original levels of gallium from the weapons plutonium may also cause fuel pin failure by chemical attack of the zirconium clad material by the gallium. This issue is currently being studied.<sup>18</sup>

Thus, it has been decided programmatically that the removal of gallium to levels as low as reasonably achievable will be undertaken. Two different processes for the removal have been examined: (1) thermally induced gallium removal (TIGR) and (2) aqueous processing.<sup>19, 20</sup> The TIGR system is a simple, low-cost method for removing the gallium from the PuO<sub>2</sub> powder derived from pit plutonium processed through the HYDOX system. It has a low environmental impact and should have few waste management activities associated with it.

The TIGR design must integrate with the existing HYDOX system and meet the plutonium-oxide powder specifications. In addition, it must fit within the feed requirements and plans for the PDCF. The gallium removal R&D program was reviewed, and information gaps required for the system were identified.

Based upon this information, the preliminary input and output parameters for the TIGR process were defined (see Figure 2.2.4-1). Several of the design parameters cannot be established until the additional R&D has been completed. This includes defining additional process steps that may be required as part of the TIGR system, such as grinding and blending of the powder after thermal processing. These steps have been identified and included in the baseline until additional data is provided.

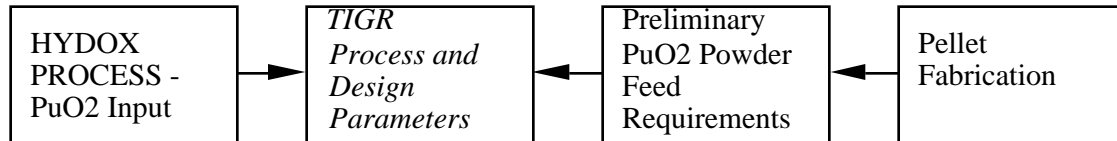


Figure 2.2.4-1. Preliminary flow chart for TIGR process.

#### Definition of the Plant Design Requirements

The establishment of the TIGR process and design requirements, as well as demonstration of the TIGR unit, is currently planned to run concurrent with the HYDOX Phase I demonstration at Los Alamos. It is proposed that the Phase I demonstration will begin in November 1997 and run for two years providing operational data on a number of pit types. During this phase, plutonium metal will be removed from the pit using the HYDOX unit and will be converted into oxide. The output from the Phase I demonstration HYDOX will be used to support the design of the TIGR system and, likewise, during the design of the TIGR system, there may be operational changes proposed for the HYDOX unit. These are discussed further in Section 2.2.4.2.

The completion of the TIGR system will be concurrent with the initiation of the ARIES Phase II demonstration at Los Alamos. TIGR and HYDOX will be integrated into a single operational unit. This is an important step in ensuring that the HYDOX/TIGR unit is developed to the level at which it can be transferred to the full-scale PDCF. The ARIES Phase II demonstration is planned to begin operation in early FY99 and will operate for a two-year period. Currently, it is planned to process a total of 200 pits through the integrated unit converting plutonium metal pits into  $\text{PuO}_2$ , which will then be used for MOX fuel fabrication.

The purpose of the Phase I and II demonstrations of the HYDOX system and the integration of the TIGR unit into Phase II is to provide a functional system for the PDCF. The preliminary design of the PDCF consists of two conversion lines with 3 HYDOX modules per line and 2 HYDOX reactors per module. Therefore, there will be a total of 12 HYDOX reactors within the plant. According to the preliminary design, there will be a single canning and NDA station for the plant. The PDCF is to begin initial operation in mid-2005.

Preliminary estimates show that the processing time in the TIGR system is approximately half of that for the HYDOX reactors, and, therefore, a single TIGR unit is proposed for each HYDOX module. This proposed arrangement will integrate well with the proposed glovebox arrangement for the PDCF.

Preliminary results from fuel fabrication R&D show that the powder may require post-gallium removal mechanical treatment (grinding) to reduce the particle size after gallium removal. This would require an additional step and equipment in the plant. As a preliminary estimate, a single grinder or ball mill is proposed for each HYDOX module. In addition, if specific impurities require down-blending to disassociate them from specific pit material and to reduce the concentrations, then a general-area blending step that will blend the powder from several batches may be required in the plant design. The powder may also require sieving to ensure the particle size specification has been met prior to packaging and shipping to the MOX fuel fabrication vendor.

The proposed schedule for the design, fabrication and operation of the laboratory-scale TIGR system is to begin the design work in early FY98 and have the unit operational by mid-FY99. Testing will be completed by the end of FY99, and the final unit will be

integrated into the HYDOX Phase II testing by early FY00. The above assumptions are based upon a specific funding level for the supporting R&D activities and for the TIGR project.

#### Impact of Plutonium Inventory Characteristics

The source of the excess plutonium that will be dispositioned is primarily from nuclear weapons pits, although a percentage will also be provided from other sources. The critical factors in the as-delivered plutonium relate to the impurities: (1) do they include classified information pertaining to the production of nuclear weapons, and (2) do they exceed impurity levels as defined by general PuO<sub>2</sub> ASTM and industrial powder specifications?

If a small fraction of the pits have impurities that are classified, it may be feasible to process these using existing facilities within the United States, including the Savannah River Site (SRS) or TA-55 at Los Alamos. Currently there is an on-going analysis at Los Alamos to address this issue, and the results of the study will be available during FY98.

If the level of impurities is low, the powder can be blended within the plant with other plutonium-dioxide powder to dilute the level of the impurities. It still must be determined through a plutonium material review if there is an excess of impurities within the fuel that are not considered to be classified but exceed acceptable values for PuO<sub>2</sub> powder and MOX fuel specifications. The pit sampling project that will begin in FY98 will address this critical issue.

**2.2.4.2. Design Parameters.** A review of the existing data was completed to determine the approximate operating range for the TIGR system. It was clear, after reviewing the information, that results from the surrogate studies (see Section 2.2.2) were required before the design parameters could be finally established.

The surrogate studies have provided data on different gas mixtures, gas flow-rate, effects of particle size, temperature and time studies, and the fundamental release mechanism of the gallium from the base material. The final analysis and results from the surrogate studies have not yet been completed, but the preliminary data provide a starting point for the TIGR design. It may be required that the design parameters be revised during early FY98 as the analyses are completed. In addition, data are available from the gallium removal work completed by the fuel fabrication team as part of the Parallex and ATR fuel fabrication work.

Based upon the results of the surrogate fuel studies and the gallium removal work completed by the fuel teams, the preliminary design of the TIGR system is to use Ar 5-6% H<sub>2</sub> mixture at 1000 to 1100°C for run times of two to four hours (Table 2.2.4-1). The minimum level of gallium in the PuO<sub>2</sub> powder that can reasonably be achieved by this system has not yet been ascertained. It is reasonable to anticipate levels of 100 ppm, but it is desired to reach lower levels if possible. The system will be designed such that lower levels of residual Ga can be obtained by further processing. The effects of which will be understood through the TIGR R&D tasks. The gallium levels within the PuO<sub>2</sub> affect the amount of gallium that will be released during sintering of the MOX fuel pellet in a furnace.

In the baseline process each module will process 5 to 6 kgs of PuO<sub>2</sub> powder per operating cycle. After the completion of the thermal treatment, it is assumed that the powder will be processed through a grinder or ball mill to ensure that the particle size will meet the fuel specifications and then through a particle sieve prior to packaging. Some of the powder may require blending prior to packaging to meet specific impurities specifications.

**TABLE 2.2.4-1  
PRELIMINARY DESIGN PARAMETERS FOR THE TIGR SYSTEM**

Temperature	1000 to 1100°C
Gas Mixture	Ar 5-6% H <sub>2</sub>
System Configuration	Flowing over beds of PuO <sub>2</sub> powder or through a rotating cylinder
Batch size	5-6 kgs
Batch Time	2 - 4 hours @ temperature
Gallium levels	50 - 100 ppm post processing

There are a number of open issues associated with the preliminary design assumptions, including

- Powder thermally treated in the 1000 to 1100°C temperature range may not meet the mean surface area requirements as specified in ASTM standards\* for PuO<sub>2</sub> powder. For this reason, results need to be well characterized and the effect(s) quantified.
- If the TIGR system operates at 1000 - 1100°C for gallium removal, then it is possible to raise the temperature within the PDCF HYDOX unit for the oxidation step. Currently the PuN is oxidized at 600°C to reduce the thermal effect on the particle mean surface area. If the temperature were allowed to increase to 900 - 1000°C during this step, the processing time could be significantly reduced without affecting the equipment design.
- Grinding of the powder has been completed on batches of fuel fabricated at Los Alamos both for the Parallex and ATR projects upon the removal of gallium. The technical need for this step has not been verified. Therefore, additional work should be completed in this area before it is established as a requirement for the TIGR system.
- Impurities data derived from weapons plutonium must be obtained prior to assuming that blending in the processing line will be required to dilute such impurities or if aqueous processing of a subset of material will be needed.
- The level of gallium in the feed PuO<sub>2</sub> powder and the estimated release during sintering will be an important input parameter for the fuel vendors. An understanding of this process is planned for FY98.
- Gallium is a highly corrosive material and is highly reactive with most structural materials at higher temperatures (>900°C). Material compatibility studies will be initiated during FY98, and the results will not be available until late in the fiscal year. These studies will provide input into the final system design prior to fabrication in FY99.

---

\* American Society for Testing and Materials (ASTM), Standard Specification for Nuclear-Grade Plutonium Dioxide Powder, Sinterable, Designation C757-90.

**2.2.4.3. System and Equipment Description.** The TIGR process is shown in context of the entire “Pits to MOX fuel conversion” by Figure 2.2.4-2. The gallium concentration in the PDCF  $\text{PuO}_2$  feed will be less than or equal to approximately 1wt%. The preliminary design goal for TIGR shall be to reduce this gallium concentration to 50 to 100 ppm for eventual MOX fuel fabrication. Therefore, TIGR must achieve a gallium concentration reduction of approximately 100 to 200. However, the reduction of gallium is not the only constraint placed on the TIGR process; the  $\text{PuO}_2$  physical or ceramic characteristics should also meet the requirements for MOX fuel as well as O/M ratio. Because TIGR may affect these characteristics, an integrated TIGR process must be robust enough to provide for modification of particle size distribution and or O/M ratio following gallium removal until it is proven to be required or not.

The conceptual TIGR design presented here relies on existing off-the-shelf equipment as much as possible. Indirect-heat calciners have been traditionally used for TIGR type processes such as (1) reduction of metal oxides, and (2) removal of volatile organic impurities from metal oxides.<sup>21</sup> Figure 2.2.4-3 shows a potential conceptual TIGR design which includes a replaceable copper getter to chemically trap gallium, and a finishing mill and/or sintering step to adjust particle morphology and O/M ratio. It is anticipated that gallium, which collects on the surface of the calciner, might be removed by heating beyond the operating temperature without  $\text{PuO}_2$  present.

There exists at least two different calciner designs which have been used often for  $\text{PuO}_2$ , in particular, for conversion of plutonium oxalate from aqueous processing. These two designs are (1) an oven calciner and (2) a rotary calciner. Each calciner type has advantages and disadvantages:

Oven calciner - can be operated at higher temperatures than rotary due to lack of moving parts (in particular bearings); however it must be operated in batch mode.

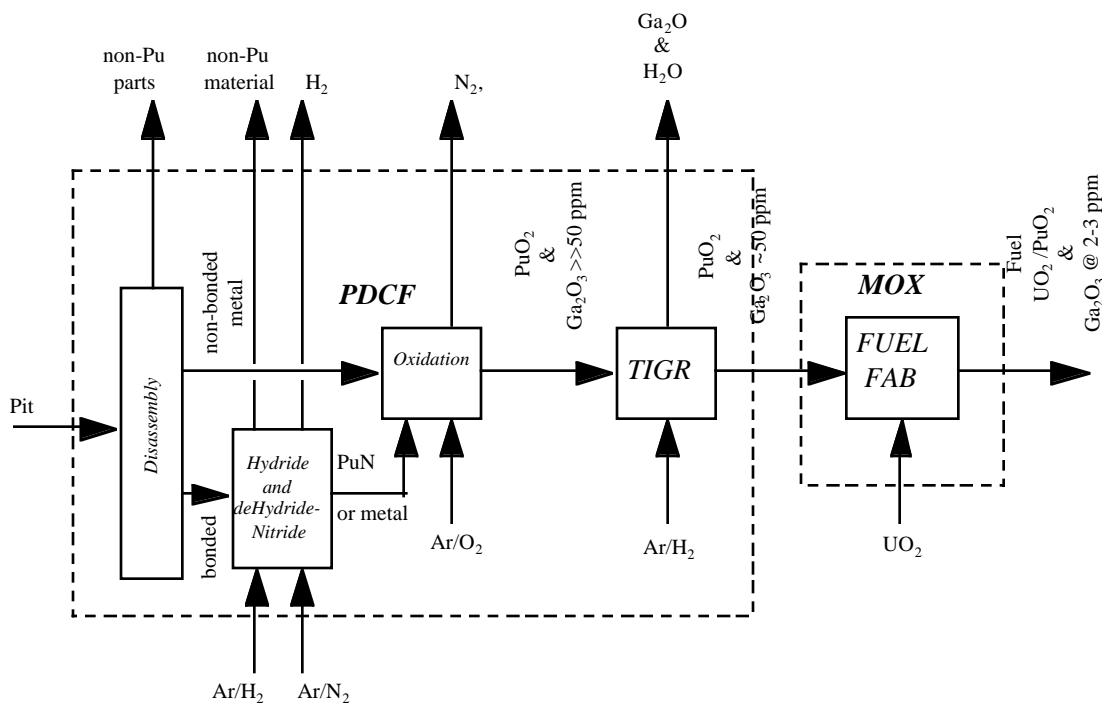


Figure 2.2.4-2. Pits to MOX fuel conversion.

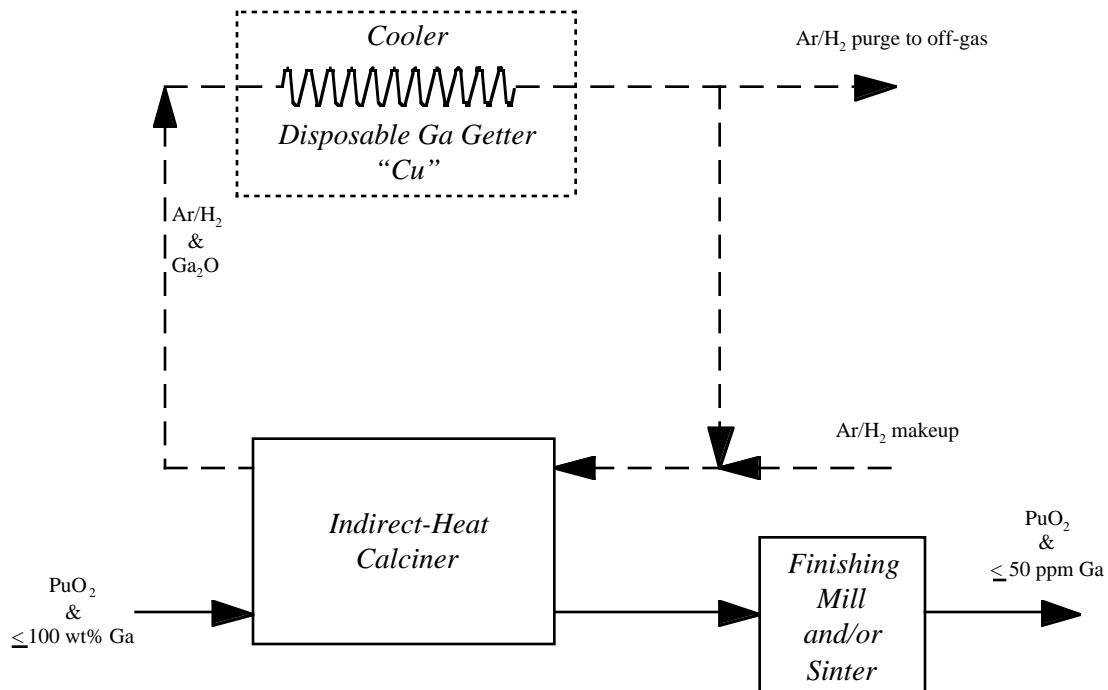


Figure 2.2.4-3. Conceptual TIGR design.

Rotary calciner - achieves better mixing of solids and gas, and can be operated in continuous mode

The higher temperature of the oven calciner can reduce processing time by enhancing the  $\text{Ga}_2\text{O}$  sublimation pressure, whereas the rotary calciner can reduce processing time by increasing the mass transfer rate between the solid particle and gas phase.

**2.2.4.4. Modeling of the Plutonium and Gallium Separation.** The basic principles behind the TIGR process involve selective reduction of  $\text{Ga}_2\text{O}_3$  to  $\text{Ga}_2\text{O}$  by hydrogen followed by sublimation of  $\text{Ga}_2\text{O}$ . The  $\text{Ga}_2\text{O}_3$  reduction is thermodynamically favored over that of  $\text{PuO}_2$  reduction. The sublimation pressure of  $\text{Ga}_2\text{O}$  is much greater than that of  $\text{Ga}_2\text{O}_3$  or  $\text{PuO}_2$ . Consequently, there are three primary mechanisms involved in the TIGR process:

- (1) chemical reduction of  $\text{Ga}_2\text{O}_3$  to  $\text{Ga}_2\text{O}$  within or on the surface of the particle
- (2) diffusion within the particle
  - hydrogen from the surface into the particle
  - $\text{Ga}_2\text{O}$  from within the particle to the surface
- (3) mass transfer from the particle to the gas phase
  - hydrogen from the gas to the particle
  - $\text{Ga}_2\text{O}$  from the particle to the gas

The time dependent nature of these mechanisms is mathematically shown in Figure 2.2.4-4.

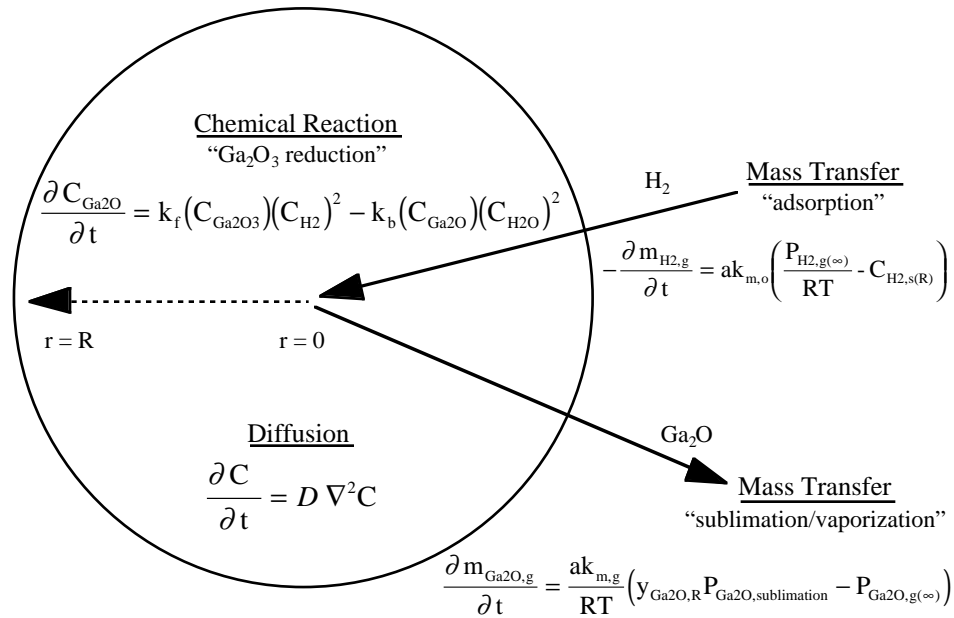


Figure 2.2.4-4. Time dependent nature of TIGR mechanisms.

Nomenclature for Figure 2.2.4-4

$a$  = area  
 $C$  = concentration  
 $D$  = diffusion coefficient  
 $k_m$  = mass transfer coefficient  
 $k_f$  = forward reaction rate constant  
 $k_b$  = backward or reverse reaction rate constant  
 $m$  = mass  
 $P$  = pressure  
 $R$  = gas constant  
 $t$  = time  
 $T$  = temperature  
 $y$  = mole fraction

The predominance of one or more of these three mechanisms will determine how the process can be manipulated to achieve maximum gallium separation with (1) minimum negative impact on powder physical characteristics, (2) minimum dose, and (3) minimum processing waste. Additionally, the predominant mechanisms may change with processing time as the gallium sublimes. For instance, early in the separation, the concentration of  $\text{Ga}_2\text{O}_3$  at the particle surface has not yet been depleted such that diffusion within the particle should be insignificant. As processing time progresses, the  $\text{Ga}_2\text{O}_3$  at the surface of the particle will be depleted such that chemical reaction within the interior of the particle will become more significant, increasing the importance of diffusion within the particle.

The importance of understanding the predominant mechanisms is related to operating the process in a fashion which maximizes gallium separation while minimizing adverse consequences. Increasing temperature, processing time, and gas velocity should all increase the gallium separation; however, (1) high temperatures can create excessive sintering, (2) long processing times can create excessive sintering and excessive dose, and (3) high gas velocities can produce excessive  $\text{PuO}_2$  entrainment.

Determining the predominant mechanisms of Figure 2.2.4-4 can be used to optimize operating parameters as follows:

- If the separation is controlled by the mass transfer rate, then separation can be enhanced by increasing the gas velocity while minimizing the temperature and time.
- If the separation is controlled by the chemical reaction rate, then separation can be enhanced by increasing the hydrogen partial pressure while minimizing temperature, time and gas velocity.
- If the separation is controlled by multiple mechanisms simultaneously or mechanisms that change with processing time, the approach is similar although more complex.

Research and development efforts can be used to (1) determine the predominant mechanisms with bench-scale testing, (2) select the prototypic processing equipment, and (3) determine optimum operating parameters for the prototypic equipment.

For instance:

- If it is determined that the predominant mechanism is mass transfer, then a rotary-type device such as a rotary-calciner may be preferred for enhanced gas/solid mixing.
- If it is determined that the predominant mechanism is chemical kinetics or diffusion, then an oven-type device may be preferred for enhanced temperature.

**2.2.4.5. Preliminary Cost and Schedule Estimates.** Cost and schedule estimates have been completed for the laboratory-scale TIGR unit that will be designed, fabricated and operated during FY98 and FY99. Three identical units will be constructed during the beginning of FY99. One will be used for large batch studies of surrogate fuel, one will be used for testing with PuO<sub>2</sub> derived from the HYDOX units at TA-55, and the third unit will be used for the integration with Phase II of the HYDOX in FY00.

The total estimated costs for the design, fabrication, and operation of the TIGR system, including supporting research, analysis and surrogate studies is \$5M to be split between FY98 and FY99. Additional funding will be required if any of the following steps are required: grinding, blending and sieving. These steps will also affect the plant size and number of required personnel.

The total estimated costs of the TIGR system for integration into the PDCF will not be available until late in FY99 when system studies have been completed.

**2.2.4.6. Conclusions.** The TIGR system is a simple, low-cost method for removing the gallium from the PuO<sub>2</sub> powder derived from weapons plutonium processed through the HYDOX system. It also integrates seamlessly into the current dry conversion process of the PDCF. It has few environmental impacts and little waste generation. The preliminary design is based upon the available data at this time and should remain well within the defined envelope as the final results are obtained from the supporting research. The primary work on the design will be completed during FY98 and the units will be fabricated during the start of FY99.

The system design will continue to be refined as the project continues and additional information becomes available. There are several key issues that must be completed during the next two years to support the final system design and the integration of the TIGR system with HYDOX.

**2.2.4.7. Aqueous Separation of Plutonium and Gallium.** Aqueous separation of plutonium and gallium was studied during FY97 as a backup to the TIGR dry process. In particular, generalized flowsheets were prepared for solvent extraction (SX)<sup>20</sup> and ion exchange (IX).<sup>19</sup> These flowsheets are shown as Figures 2.2.4-5 and 2.2.4-6. Ion exchange was selected as the baseline backup aqueous process since it is currently in use for a similar process in the plutonium facilities at Los Alamos and SRS. The IX generalized flowsheet was elaborated by way of a complete set of material balances for a preconceptual design.<sup>22</sup> This preconceptual design was prepared so that it could provide details required for the preparation of an Environmental Impact Statement (EIS).<sup>23</sup>

Another concept for aqueous separation of plutonium and gallium, which has not yet been studied in detail, is oxalate precipitation of  $\text{Pu}^{\text{VI}}$ . While the ion exchange process utilizes oxalate precipitation of  $\text{Pu}^{\text{III}}$ , precipitation of  $\text{Pu}^{\text{IV}}$ , for which an existing flowsheet has been demonstrated,<sup>24</sup> using this type of process should provide some degree of  $\text{Ga}^{\text{III}}$  separation. In fact, it has been demonstrated that a decontamination factor of 100 has been obtained with the flowsheet shown by Figure 2.2.4-7 for aluminum and chromium, which both have a 3<sup>+</sup> valence like gallium.<sup>24</sup> While data do not exist for gallium decontamination by  $\text{Pu}^{\text{IV}}$  oxalate precipitation, indications from aluminum and chromium suggest that two or three batch-wise precipitation steps in series should achieve a decontamination factor of 100 to 200 as is desired for the MOX fuel.

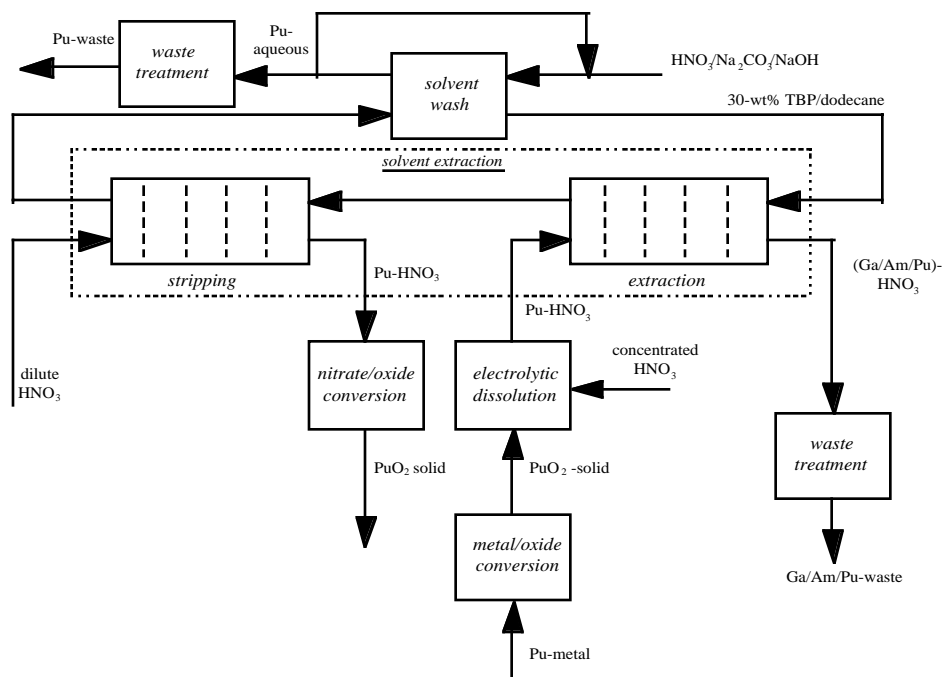


Figure 2.2.4-5. Solvent extraction flowsheet for separating plutonium and gallium.

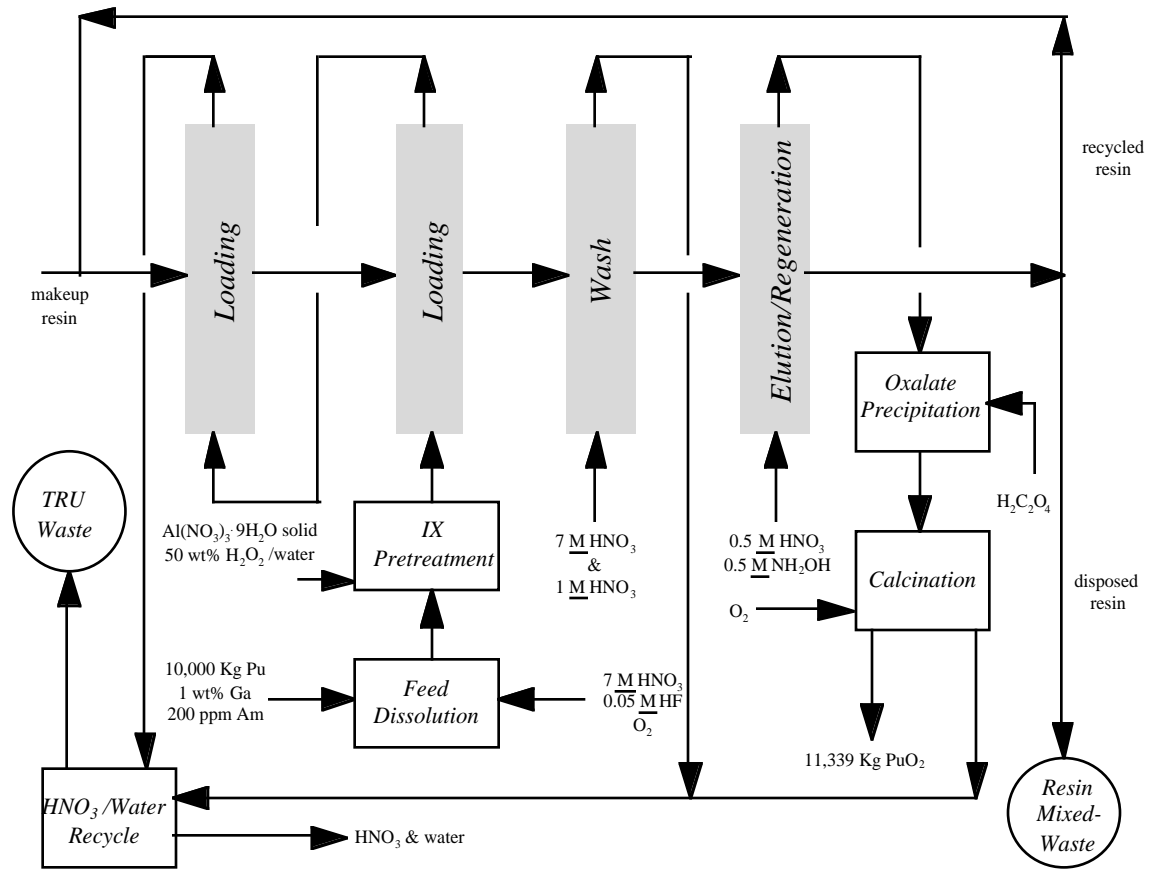


Figure 2.2.4-6. Ion exchange flowsheet for separating plutonium and gallium.

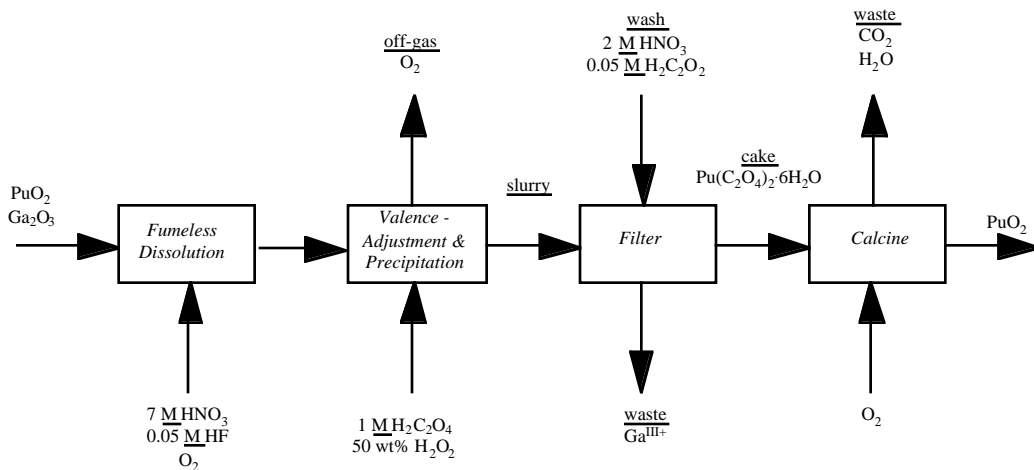


Figure 2.2.4-7. Oxalate precipitation flowsheet for separation of plutonium and gallium.

### 3.0. FUEL FABRICATION DEVELOPMENT

The reactor-option of the MD plutonium disposition program currently calls for fabrication of MOX fuel using weapons-grade plutonium oxide and depleted uranium oxide. Any variation in the fabrication process, including the feed materials, will lead to variations in the final fuel product, and it is important to quantify the effect each variation will have on the quality of the MOX fuel. Thus, experimentation is required to determine the range of acceptable fabrication parameters that will lead to an acceptable fuel product. Further development is also needed in the laboratory to enhance the current techniques available for measurement of certain fuel characteristics.

Consequently, the purposes of the research whose results are captured below are:

- Understand the impact of variations in PuO<sub>2</sub> feedstock (primarily physical characteristics) on fuel fabrication and fuel quality.
- Understand the impact of variations in UO<sub>2</sub> feedstock on fuel fabrication and fuel quality.
- Establish AUC-derived UO<sub>2</sub> as the new baseline UO<sub>2</sub> used in all research, development, and testing activities.
- Understand the impact of gallium on the fuel sintering process and process equipment.
- Develop a technique to measure quickly the spatial distribution of residual gallium in green and sintered MOX fuel pellets.
- Establish an acceptable technique to measure Pu homogeneity.
- Establish an acceptable technique to measure oxygen-to-metal ratio in feedstocks and fuel pellets.
- Establish an acceptable technique to measure fuel pellet surface finish.
- Validate current techniques for measuring the concentration of trace amounts of elements in feedstocks and fuel pellets.

#### 3.1. Fabrication Studies

In Section 2.1.1, results from the characterization of three different PuO<sub>2</sub> powders were presented, and it was observed that powders from different extraction processes have different morphologies as well as other characteristics. Thus, when these powders are sintered with UO<sub>2</sub> during pellet fabrication, they each produce different results. The effects that these three powders have on pellet fabrication processes and the final fuel pellet must be examined. Similarly, the effect of various types of UO<sub>2</sub> on pellet fabrication is also important to pursue. However, final results from only one type of pellet were obtained during FY97, so further experimentation is needed to determine how different types of PuO<sub>2</sub> and UO<sub>2</sub> powders will affect the quality of the final fuel pellet. Additionally, the effects of different sintering times and temperatures on the final pellet density were also examined in FY97 as well as the effects that various H<sub>2</sub>O partial pressures have on Ga evolution.

### 3.1.1. PuO<sub>2</sub> Variability

The original intent of this study was to fabricate pellets using a single UO<sub>2</sub> source (Cameco ADU) while varying PuO<sub>2</sub> feed materials (i.e., LLNL 2-step, LLNL 3-step, and Los Alamos 2-step and aqueous-derived PuO<sub>2</sub>). However, during FY97, only final results from MOX pellets developed for the Parallex project were obtained due to resource and schedule constraints. This powder was developed from Cameco ADU UO<sub>2</sub> that was obtained from AECL (Atomic Energy of Canada, Limited) for the purpose of Parallex fuel fabrication and from the Los Alamos-derived PuO<sub>2</sub> that was discussed in Section 2.1.1. This PuO<sub>2</sub> powder was put through a thermal gallium removal process, heating the material at 1100°C for 2 h in a furnace in a 6% H<sub>2</sub> and 94% argon environment (Ar-6%H<sub>2</sub>) and subsequent heat treatment at 800°C for 2 hours in a different furnace with pure oxygen. The purpose of this secondary heat treatment was to adjust the stoichiometry of the powder (make it as close to PuO<sub>2</sub> as possible), but it was discovered during fabrication that this treatment was unnecessary and does not need to be performed on future PuO<sub>2</sub> powder. Additionally, the powder was passed through a vibratory mill three times to increase the specific surface area after the thermal treatment, which is a common process at Los Alamos for PuO<sub>2</sub> powder.

All pellets produced from this Los Alamos-derived PuO<sub>2</sub> powder have a 3.1 wt % Pu loading. Since four separate batches of pellets were sampled for the Parallex project, four different results appear in Table 3.1.1-1. This table includes results from the following analyses:

- Oxygen-to-metal ratio as measured by modified Lyon's method,
- Density as measured by geometric and Archimedes' methods (green and immersion density respectively),
- Ga concentration as determined by inductively-coupled plasma mass spectrometry (ICPMS), which will be discussed in Section 3.2.3,
- A homogeneity picture from alpha autoradiography (see Figure 3.1.1-1), and
- A microstructure picture from optical microscopy (see Figure 3.1.1-2).

**TABLE 3.1.1-1  
RESULTS OF PELLET MEASUREMENTS FOR PARALLEX  
MOX FUEL PELLETS**

O/M Ratio	Green Density (g/cm <sup>3</sup> )	Immersion Density (% of Theoretical)	Ga Concentration (ppm)
2.0051	52.72	95.96	2.6
2.0038	52.90	95.72	2.4
2.0063	52.72	95.99	2.1
2.0000	52.90	95.98	2.2

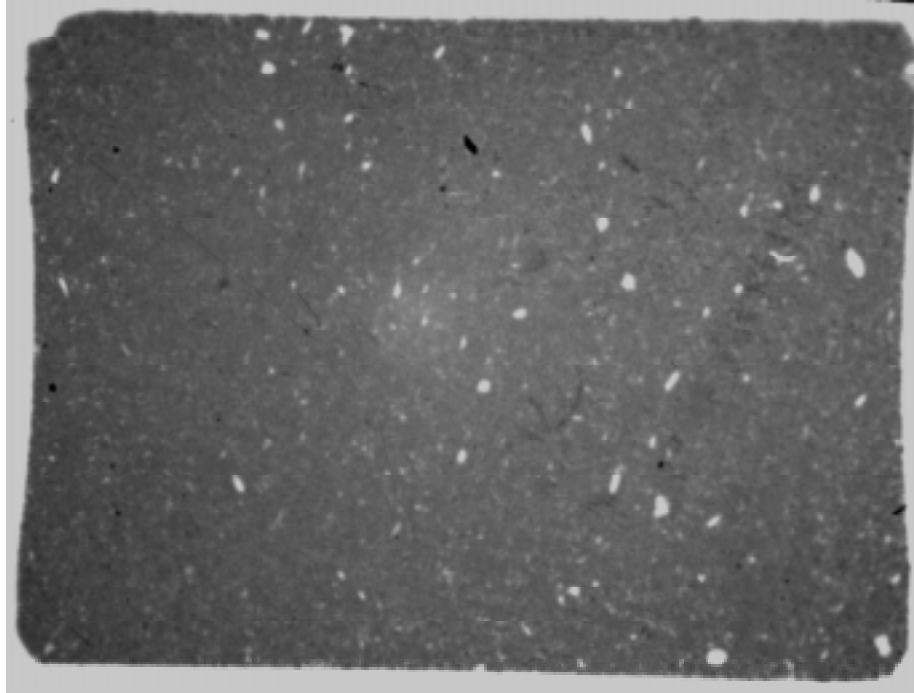


Figure 3.1.1-1. Autoradiograph of a high fired Parallex MOX fuel pellet.

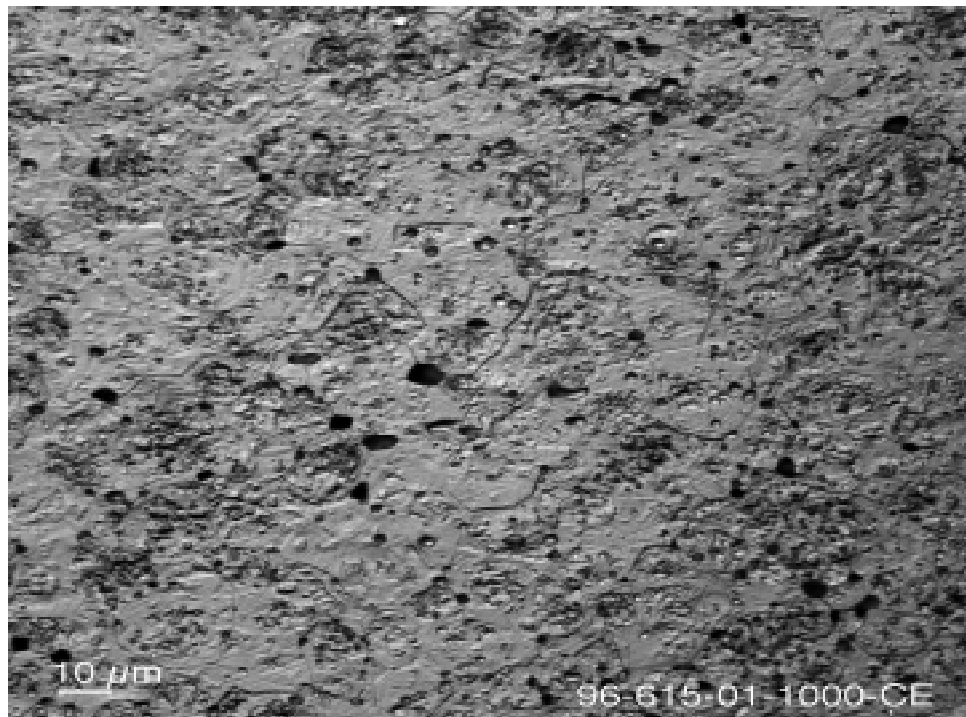


Figure 3.1.1-2. Microstructure of a Parallex MOX fuel pellet.

The oxygen-to-metal ratios, densities, and gallium concentrations of these samples were all fairly similar with only statistical variations. Further studies are currently being conducted to provide more insight about what effects various PuO<sub>2</sub> powders have on MOX fuel pellets.

### **3.1.2. UO<sub>2</sub> Variability**

The purpose of this study was to fabricate MOX fuel pellets using a constant PuO<sub>2</sub> supply and various UO<sub>2</sub> feed materials. Pellets were characterized for density, homogeneity, O/M, and microstructure. However, final pellets with only one type of UO<sub>2</sub> were fabricated during FY97 due to resource and schedule constraints. The characterization of these pellets was presented in Section 3.1.1. and ongoing efforts are currently being made to obtain different types of UO<sub>2</sub> feed material and characterize both the powders and the pellets fabricated from the various powders with a consistent PuO<sub>2</sub> feed material.

### **3.1.3. Sintering Study**

During FY97, Los Alamos conducted pellet preparation and sintering studies using the UO<sub>2</sub> mixed with CeO<sub>2</sub> and Ga<sub>2</sub>O<sub>3</sub>. At the beginning of FY97, there were no furnaces that could be used for these studies. Therefore, one of the largest accomplishments during FY97 was to install a furnace for these purposes. Only one temperature (1700°C) and time (2-3 hours) were used for studies during FY97, but the basis for more studies during FY98 was developed.

The sintering study satisfies several needs: (1) the UO<sub>2</sub> is the same material being used for preparation of the actual MOX fuel; thus the knowledge gained in optimizing sintering conditions for this material can be used as baseline data for fabrication of the actual fuel; (2) the solid pellets produced will be used in studies regarding Ga transport in MOX fuel (radial diffusion studies); and (3) the same powder mixtures will be used for the annular surrogate fuel for the ORNL (Oak Ridge National Laboratory) /Texas A&M (Agriculture and Mining) experiments. Currently, Los Alamos has fully characterized powder characteristics, namely particle size, morphology, and surface area. Figures 3.1.3-1 through 3.1.3-3 show the particle size distributions for the CeO<sub>2</sub>, Ga<sub>2</sub>O<sub>3</sub>, and UO<sub>2</sub> powders respectively, that resulted from a limited number of specimens. Initial studies have provided the data necessary for final design of the pressing dies for the annular pellets (pressure, shrinkage, sintering temperature, and density parameters).

Funding for the fabrication of the annular pellets for Texas A&M arrived at Los Alamos in August 1997. The dies for the pellets should be ready by the middle of December 1997. Fabrication of the pellets will then commence, assuming that the necessary NEPA approval for the ORNL/Texas A&M project is in place. To sinter surrogate pellets, a dedicated 1700°C tube furnace with atmosphere, pressure, and humidity control has been installed at Los Alamos. This furnace has recently become functional and is being used for determining sintering parameters of the surrogate MOX pellets.

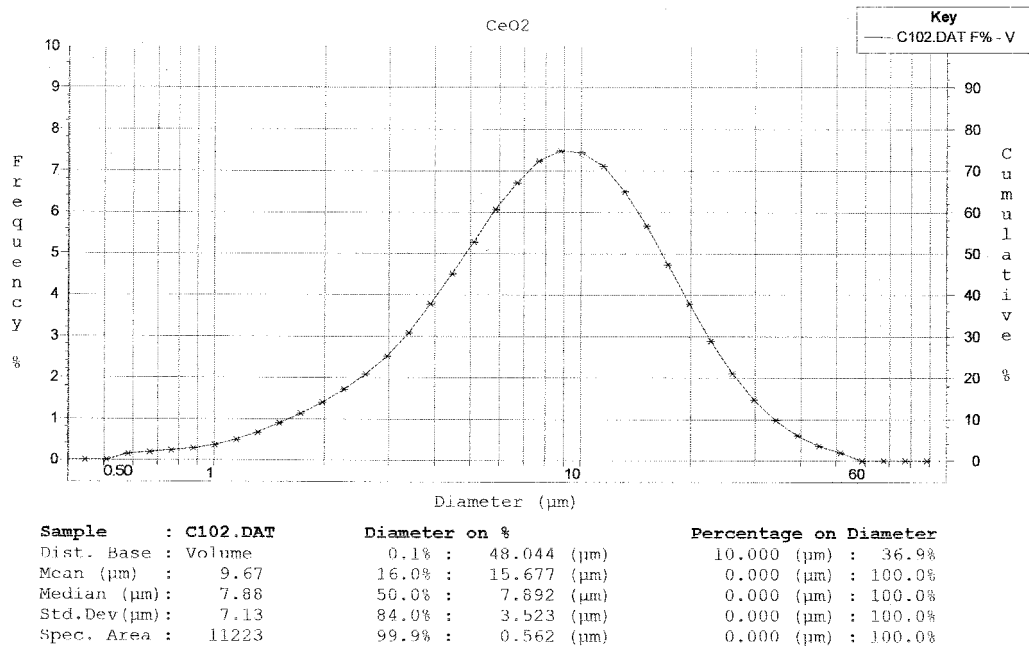


Figure 3.1.3-1. Particle size distribution of CeO<sub>2</sub> powder.

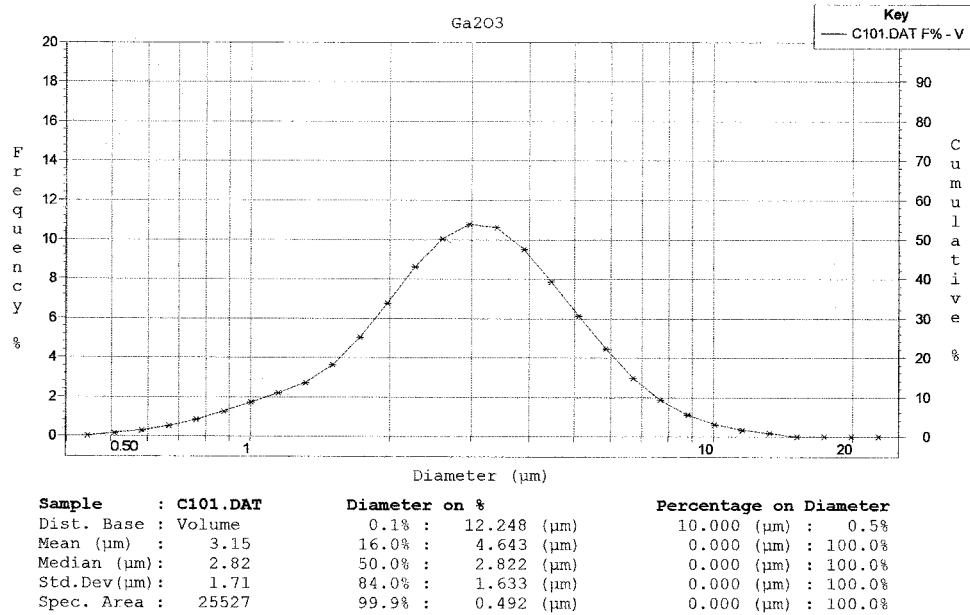


Figure 3.1.3-2. Particle size distribution of Ga<sub>2</sub>O<sub>3</sub> powder.

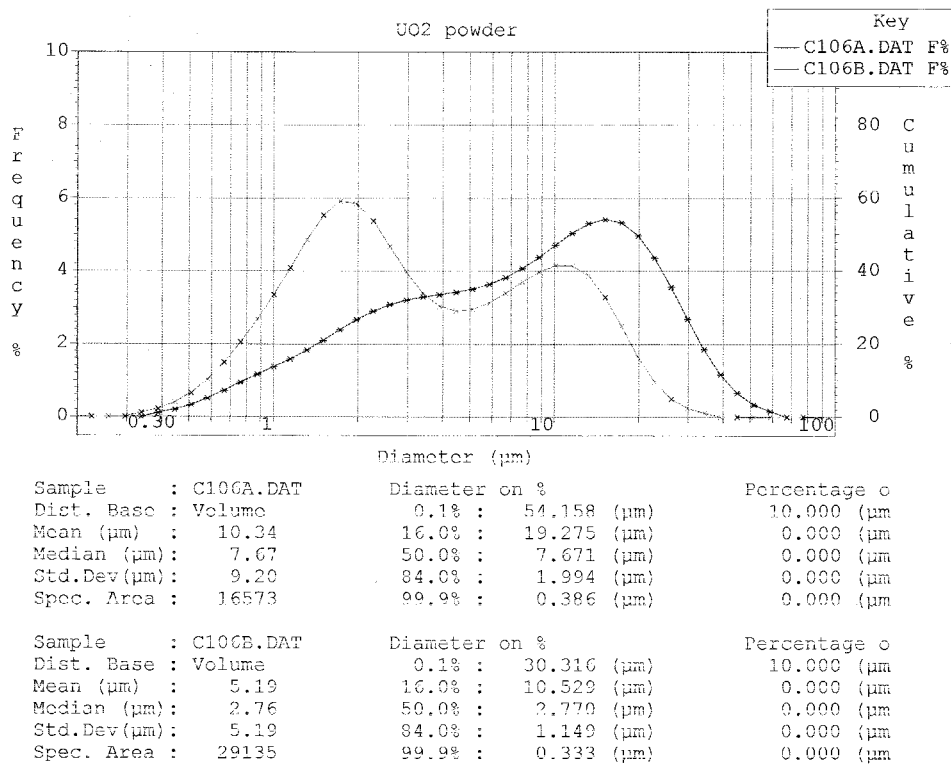


Figure 3.1.3-3. Particle size distribution of UO<sub>2</sub> powder.

Note: the UO<sub>2</sub> powder was relatively agglomerated. Consequently, Los Alamos analyzed the powder before (larger particle size distribution) and after ultrasonication (smaller particle size distribution).

### 3.2. Analytical Development

Development of analytical techniques used in conjunction with the fabrication of MOX fuel was identified as necessary in FY97. Measurement of homogeneity for weapons-grade material was initially found to be more difficult than other types of plutonium. Autoradiography is typically used to measure homogeneity in commercial MOX fabrication, so it was also examined during FY97 to determine its applicability to weapons-grade MOX fuel fabrication at Los Alamos. Additionally, x-ray microfluorescence (XRMF) was found to be another technique that is applicable to the measurement of homogeneity and the spatial determinations of gallium concentrations. Thus, XRMF was further developed during this fiscal year. At the end of FY97, certain existing analytical capabilities were (surface finish measurement) or were known to potentially be (O/M measurement) inadequate for determining if the fuel pellets produced met requirements (especially for production for irradiation experiments). The purchase of a new surface finish measurement device and a limited number of studies regarding the O/M measurement technique helped enhance the analytical capabilities within the laboratory. Finally, results from experiments involving three different types of chemical analyses were compared to determine which most effectively measured gallium concentrations in MOX fuel samples in the ranges that were applicable to this program.

### 3.2.1. Homogeneity

The purpose of the homogeneity analyses were to compare different homogeneity measurement techniques and to determine their relative merits. Initially, experiments with the alpha autoradiography and X-Ray Microfluorescence (XRMF) techniques were to be performed to determine the suitability of each technique with regard to weapons-grade plutonium. However, alpha autoradiography was found to be sufficient for homogeneity measurements, so efforts involving XRMF were refocused on gallium measurement in February 1997. Section 3.2.4 includes more information on XRMF, including these studies.

Instead, a combination of methods were used during FY97 to investigate the homogeneity of mixed plutonium-uranium fuel pellets. The principal method has been the time-tested autoradiograph technique using high-purity cellulose nitrate film sensitive to alpha particles. The additional analysis methods of SEM/EDS and microprobe analysis have also been used to identify the structures recorded in the autoradiographs.

Autoradiographs using the cellulose nitrate film (see Figure 3.1.1-1 as an example) show remarkable detail of plutonium in the fuel pellet. To obtain this autoradiograph, two pellets were examined on the microprobe. Plutonium distribution in both high-fired pellets were essentially uniform at a concentration near the nominal enrichment used to make the pellet. Areas with higher enrichment as well as areas with lower enrichment or essentially no plutonium are then observed. Pellets are generally homogeneous with areas of relatively higher or lower concentrations of plutonium, but discrete  $\text{PuO}_2$  grains are not observed. The bright spots are probably areas containing plutonium concentrations higher than the matrix, the very dark spots are artifacts of the film, and the darker areas are areas of low plutonium concentration.

Improvements have also been made on the autoradiography technique. Traditionally, the autoradiograph film was exposed and developed in the laboratory. The film was then taken from the laboratory, and a negative of it was made by photographic processing personnel. An autoradiograph print was then made from the negative, and the print was scanned to make an electronic image. This process has been improved and simplified. The autoradiograph is now developed in the laboratory, and a direct image of the film is taken on the metallograph. The image is electronically captured and stored in a single-step process. Numerous steps and expenses are eliminated using this procedure and the image quality is better.

Numerous pellets were examined with the SEM/EDS technique. Plutonium-rich regions in one of the early, low-fired pellets was detected in the pellet matrix but the EDS detector was unable to detect discrete  $\text{PuO}_2$  particles in high fired pellets. This is because discrete  $\text{PuO}_2$  particles no longer existed, and the matrix was essentially homogeneous. SEM/EDS analyses can be used when discrete  $\text{PuO}_2$  grains exist, but it is not effective in evaluating homogeneous or nearly homogeneous material. Thus, alpha autoradiography was considered a more acceptable technique for obtaining homogeneity measurements.

Future work involving autoradiography includes:

1. Standards of known  $\text{PuO}_2$  particle size and distribution need to be fabricated and analysis techniques evaluated on such standards.

2. Additional work using the microprobe and autoradiographs must be continued on high fired pellets. Areas of high and low concentrations of plutonium observed on the microprobe must be correlated with features found in the autoradiographs.
3. There is a very limited amount of the cellulose nitrate film available. A new source and/or a new film type needs to be located so that homogeneity with the autoradiography technique can continue to be measured.

### **3.2.2. Upgrade TA-55 Analytical Capability**

In FY97, two specific tasks were undertaken to upgrade the analytical capabilities available in TA-55. The first was to obtain and install a new surface finish measurement device, and the second was to evaluate various O/M measurement techniques in terms of availability and cost for eventual installation in TA-55.

A new surface finish measurement device was required because the existing device no longer yielded accurate data. This analysis is required for fuel fabrication to verify that the fuel meets the required specifications, which is especially important for the fabrication of fuel for irradiation testing. The new surface finish measurement device was purchased and installed in TA-55 in May, 1997. The new device is operational, provides accurate results, and was used to measure the final surface finish of the Paralex production fuel.

A small effort was undertaken to identify potential O/M measurement techniques for eventual use in TA-55. While the existing O/M measurement technique is sufficient for current activities, the potential exists that future efforts could require more accurate measurements. In FY97, information was gathered from various sources on their techniques for measurement of O/M ratio. In FY98, this activity will continue as resources permit.

### **3.2.3. Trace Analysis Validation**

In FY97, experiments were performed to measure Ga concentrations using three different available techniques: (1) x-ray fluorescence (XRF), (2) direct-coupled plasma (DCP) atomic emission, and (3) inductively-coupled plasma mass spectrometry (ICPMS). XRF is a well calibrated technique for determining Ga concentrations within the range of 200 ppm and above, and the purpose of these experiments was to compare it with DCP and ICPMS. When properly calibrated, the DCP and ICPMS techniques should yield accurate gallium concentrations down to the ppb range. However, earlier comparisons between DCP and XRF results for concentrations above 200 ppm showed variation in the results. (This could be due to either the calibration being incorrect or to mistakes in dilution of the sample which is required to get the gallium concentration within the calibrated concentration regime of the DCP.) Consequently, validations were instead performed at higher Ga concentration levels through comparison of the DCP and ICPMS results to those of the XRF.

A "round robin" type analysis for gallium was done on a thermally cleaned plutonium oxide feed and a MOX powder mixture with a common PuO<sub>2</sub> feed material and each of the three of the techniques described above. In each case, the powdered samples were dissolved using standard acid dissolution methods. For XRF and DCP, the dissolved solution was put through an ion exchange column, and the effluent was analyzed for gallium content. This removes a majority of the plutonium matrix, for simpler spectroscopic analysis and lower radiation exposure for the analyst. For ICPMS, the sample was diluted by a factor of almost 1000 to get the concentration into a range acceptable to the instrument.

The results in mg/mL (ppm) of the round robin are shown in Table 3.2.3-1. The XRF data is for three separate samples run in duplicate, so the six results were averaged. The DCP analyses are for a single determination on three samples, while the ICP is a duplicate analysis on one sample. The results show good agreement among the three methods for the “cleaned” plutonium oxide. The MOX and uranium samples contained an amount of gallium below the detection limits for XRF. A spectroscopic interference from uranium was discovered on the gallium emission line, and this prevented the DCP from doing a gallium analysis on any samples for which uranium was present. It may be feasible to get around this interference; however, this avenue was not pursued in FY97.

**TABLE 3.2.3-1  
RESULTS FROM GALLIUM CONCENTRATION ANALYSES**

mg/mL						
	XRF	std dev	DCP	std dev	ICPMS	std dev
MOX Powder	bdl		na		5.5	0.4
Uranium Powder	bdl		na		1.2	0
Pu Oxide “clean”	243	7	245	3	206	20

This “round robin” analysis demonstrated that XRF is good for detecting gallium to at least 100 ppm in the solid. It also means that XRF would be best for determination of gallium in the plutonium oxide feed prior to gallium removal and for checking the cleanliness of the plutonium oxide feed after gallium removal down to a minimum level of 100 ppm. This would be a rapid, accurate and precise method for gallium determination in the feed plutonium oxide. ICPMS should be utilized for certifying specification levels of impurities and determining gallium concentrations expected to be below 100 ppm in the solid.

Additionally, new methods of XRF analysis are also being pursued, which may allow gallium to be detected in concentrations below 100 ppm in the solid both directly and through the use of a dissolution method.

#### **3.2.4. X-Ray Microfluorescence Gallium Measurement.**

Overall, most of the tasks initially projected for this activity were achieved. The first half of the year was directed towards Pu homogeneity. After the DOE European MOX fuel fabricator review in February, the focus was shifted from Pu homogeneity to gallium detection, both in the feed and final fuel pellets. The basis for this re-direction was the need for a sensitive, spatially resolved method for gallium detection, while homogeneity was found to be determined adequately by alpha autoradiography. Studies with XRMF then involved: (1) element detection capabilities of the technique including spatial resolution, (2) demonstrating phase identification abilities, and (3) developmental work for XRMF as a more widely-known measurement technique, especially for gallium in MOX fuel surrogates.

This re-direction accounted for changes in accomplished tasks, but resulted in more significant accomplishments by collaborating the X-Ray Microfluorescence (XRMF) technique more closely with gallium removal studies. The purpose of XRMF in these studies is to provide the concentration of gallium in MOX fuel pellets (and/or associated powders) where other techniques may be insufficient (see Section 3.2.3 for more information) or too time consuming. The XRMF technique is discussed further in Section 3.2.4.

The XRMF method demonstrated its unique ability to rapidly provide elemental information that cannot be obtained with any other analytical method in elucidating the movement of gallium in surrogate MOX fuel pellets under reducing conditions. XRMF analyses using point spectra of the internal cross sections, line scans of the external surface, and elemental maps of the cross section and end surfaces showed that the volatile gallium species diffuses out and up within the pellet. The gallium then concentrates on the exterior of the pellet, on the upper exterior portions, and on the top of the pellet. Subsequent work with micro Raman spectroscopy, micro-x-ray diffraction, and scanning electron microscopy shows that there is a mixed phase of gallium and cerium forms with no apparent pure gallium phases. It is surmised that the mixed phase is a gallate, but its composition is uncertain at this time.

#### **3.2.4.1. Elemental Detection.**

##### Radioactivity

Radioactive burden studies during FY97 exhibited success in detecting and mapping plutonium in a 3% PuO<sub>2</sub> pellet. This demonstrated that the Pu and potentially the gallium could be detected directly in the MOX fuel pellets with the energy dispersive detector and micro-x-ray excitation. Additional work will be necessary to establish limits on radioactive burden and improve masking and shielding of the detector.

##### Sensitivity

As a result of re-direction, XRF sensitivity experiments were directed toward gallium detection in MOX surrogates. First, a series of Ga-spiked CeO<sub>2</sub> micropellet standards (3 mm in diameter and sub-mm thick) were prepared ranging from 10 to 10,000 ppm Ga. Due to a cerium interference peak, no Ga could easily be discerned at concentrations below 500 ppm. Then, to avoid the gallium interference peak, Y<sub>2</sub>O<sub>3</sub> rather than CeO<sub>2</sub> was used as the gallium-spiked micropellet matrix. With this matrix 100 ppm Ga was directly detected in the powder. A continuation of these studies will determine the actual Ga limit of detection in Y<sub>2</sub>O<sub>3</sub>. Yttrium is relevant to the MOX project since its K line is close in energy to the L lines of Pu and U. Thus, no Ga interference lines should be observed from Pu or U in MOX fuel samples, and the background levels should be similar.

##### Spatial Resolution

During FY97, it was discovered that gallium detection using a 50 micron aperture was feasible for the MOX surrogates and the real MOX pellet. The tradeoff in spatial resolution is longer scan times and slower rates, but it does provide for a factor of two improvement in resolution over the 100 micron aperture.

##### Evaluate Quantitative Imaging

Various work was also performed while evaluating quantitative imaging techniques. Resulting determinations from these activities include:

- Pu quantification could not be pursued due to the termination of the Pu heterogeneity funding and the dearth of available samples.
- XRF elemental critical thicknesses, defined as the sample surface depth from which 99.9% of the measured analyte intensity originates, were calculated.
- Using the case of MOX fuel consisting of 4% PuO<sub>2</sub>, thicknesses around 15 mm were calculated for the U and Pu main x-ray lines, and about 8 mm for Ga.
- In comparison, the SEM maximum electron range (analysis depth for emitted x-rays) was determined to be about 1 mm for typical electron beam energy of 25 keV. Hence, the sample probing depth is at least 10 times greater with XRF than SEM for X-Ray analyses.

#### High Power Tube

An evaluation task with a high power tube was also performed in FY97. This was primarily an evaluation task that involved comparing data from the 50 W tube at Los Alamos to the system operated at Oak Ridge. Oak Ridge's system generated higher flux using electron excitation of different anode materials, resulting in higher sensitivity values for the higher flux when directly compared the Los Alamos's tube. Future plans at Los Alamos are to purchase a 100 W x-ray tube for the Omicron in FY98. This should boost both the flux and the sensitivity.

#### X-Ray Optics

Collaborative efforts with X-Ray Optical Systems, Inc. (XOS) were pursued to design a capillary optic which could be utilized with Los Alamos's Kevex Omicron XRMF spectrometer. First, a capillary optic was purchased and installed on the instrument used at Los Alamos, and preliminary efforts to align the optic with the x-ray source were partially successful. Low energy x-rays were able to traverse the optic, and up to a five fold gain in low Z elemental sensitivity was observed compared with using the largest aperture available (3 mm in diameter). According to XOS, the throughput of high energy x-rays is extremely sensitive to the capillary-source alignment, and fine tuning this alignment will be pursued in FY98. This is important in gaining sensitivity for the gallium detection, which requires higher energy excitation.

**3.2.4.2. Demonstrate Phase Identification.** All XRMD (X-Ray Microdiffraction) work was performed by Don Carpenter at Oak Ridge Center for Manufacturing Technology through a collaborative project with Los Alamos. This work showed that no definitive crystalline phases were observed from a surrogate pellet reduced at 1200 °C; only amorphous regions were found.

The presence of CeO<sub>2</sub> was detected wherever high concentrations of gallium were located. The formation of a cerium gallate has been proposed as the phase that was observed. Future spectroscopic studies of the fundamental processes involved in surrogate reduction will attempt to verify the formation of a gallate.

Pellet reduction at 1200 °C was also analyzed by EDX with an SEM because the pellet was amply conductive and did not require a conductive coating. Micro-domains were observed with gallium concentrated in the grain boundaries, and no apparent pure phases of gallium were found either at the grain boundaries or within grains. Identification of this mixed

phase material will be pursued in FY98 as it may be a stable phase, which may limit the ultimate amount of gallium, that can be thermally removed in one step.

In the area of molecular spectroscopy, IR and Raman studies were undertaken to complement the XRD and XRF analyses. Literature searches as well as preliminary experiments demonstrated that the surrogate  $\text{Ga}_2\text{O}_3$  and  $\text{CeO}_2$  exhibit characteristic bands in both techniques. Future studies will focus on any shifts of these bands to indicate changes in molecular states following reduction processes. Raman images of the  $\text{Ga}_2\text{O}_3$  obtained through collaboration with Professor Patrick Treado at the University of Pittsburgh showed a different phase distribution on the top surface of the 1200 °C reduced surrogate pellet. The Raman images and light microscope examinations revealed localized heterogeneity. Further studies of the Raman spectrum for the pure gallium and cerium oxides, as well as sintered mixtures of these oxides, will aid in elucidating the composition of these unknown phases.

**3.2.4.3. XRMF of MOX Fuel Surrogates.** X-ray fluorescence (XRF) is well established as a method for providing qualitative and quantitative elemental information about a sample.<sup>25</sup> Two primary advantages of XRF include its nondestructive elemental analysis and the need for little or no sample preparation. Within the past decade, x-ray microfluorescence (XRMF) has also evolved into a significant analytical tool, whereby analyte fluorescent x-rays are monitored as a function of position in a sample. Several methods can be used to obtain a microfocused x-ray source. One way is to place an aperture in front of the source.<sup>26,27</sup> Glass capillaries can also be employed to focus x-rays from either a commercial anode or from a synchrotron source for a higher x-ray flux,<sup>28-36</sup> and recently a point-focusing diffractor was used to generate a small spot monochromatic beam with a very low background signal.<sup>37</sup>

In addition to being nondestructive and requiring minimal sample preparation, XRMF offers a number of other advantages over conventional electron microprobe techniques for acquiring elemental distributions from a sample<sup>38</sup> including higher sensitivity, greater penetration depth, the ability to operate in air, and large area sample analysis. Hence, XRF and XRMF are ideally suited for a plethora of materials where elemental information is needed. In the present work, mixed oxide fuel surrogates consisting of  $\text{Ga}_2\text{O}_3$  in a  $\text{CeO}_2$  matrix were characterized by both XRMF and bulk analysis XRF.

The ultimate objective of this work is to demonstrate the analytical capabilities of XRF and XRMF in providing unique elemental information about a sample. Three modes of operation were incorporated, including: (1) single spot analysis, (2) line scans, and (3) two-dimensional elemental mapping (XRMF). Each mode offers unique but complementary information about a sample, which when combined, provided a more complete elemental characterization of the samples.

#### **3.2.4.3.1. Experimental Parameters**

*Instrumentation.* All XRF data were acquired with a Kevex Omicron spectrometer using a 50 W rhodium x-ray anode oriented at a 45° angle with the sample stage, and the exit angle to the detector was also 45°. A liquid nitrogen cooled lithium-drifted silicon detector with an active area of 50 mm<sup>2</sup> was employed. Apertures were used to restrict the primary beam diameter for XRMF studies, with a minimum achievable spot diameter of 50 μm. To scan

the x-ray beam across a sample for imaging, the sample stage was moved while the primary beam remained stationary.

*Surrogate Sample Preparation.* All the MOX surrogates consisted of 2% Ga<sub>2</sub>O<sub>3</sub> in a CeO<sub>2</sub> matrix. Cylindrical pellets of this material 1 cm long and 0.7 cm in diameter were prepared according to the following protocol. A 30g mixture composed of CeO<sub>2</sub> with 2 wt.% Ga<sub>2</sub>O<sub>3</sub>, 0.2 wt.% stearic acid, and 0.2 wt.% polyethylene glycol prepared and mixed for 15 min with a SPEX mixer 8000. Approximately 2g of this material were then pressed to between 30 and 40 percent of the sample theoretical density with a Carver model-6 press. The resulting powder was sifted through a 150 μm mesh screen and pressed into a pellet at 60 – 70 percent of the theoretical density. The pellet was then heated at 450°C for 4 h to remove the binder and sintered at 1650°C for 4 h to homogenize the mixture.

Seven of these sintered pellets were reduced by heating in Ar-6% H<sub>2</sub> for 0.5 h at 600°C, 700°C, 800°C, 900°C, 1000°C, 1100°C, and 1200°C respectively. For baseline comparison purposes, a pellet that was only sintered was also included for analysis. Surrogate powders reduced at the above-mentioned temperatures were synthesized by crushing sintered pellets and heating the resulting powders in 6% hydrogen in argon for 0.5 h. Three different powder sample lots (0.3g, 0.9g, and 2.5g) were reduced at each temperature to study the effect of sample mass as well as temperature on gallium removal.

*Sample Acquisition Parameters.* The instrumental voltage, current, and aperture size were optimized for each mode of analysis to provide the highest available signal while maintaining the instrument dead time at 50 %.

#### Pellet Interior

To examine the pellet interiors, they were cut in half parallel to the long cylinder axis using a diamond saw. The interiors were then imaged by XRMF for gallium, cerium, and zirconium as impurities in a dynamic mode where the x-ray beam was continuously rastered over the sample, and the emitted x-rays were simultaneously detected. All XRMF analyses were performed with the samples under vacuum to improve the signal-to-noise ratio. A 50 μm aperture was employed, and the x-ray tube was operated at 50 kV and 1 mA. The interior of the pellet reduced at 1200°C was also imaged in a microprobe mode, whereby a 300 μm diameter incident x-ray beam was maintained over sample regions for 100 sec each and sequentially rastered in 250 μm increments laterally and horizontally over a ~36 mm<sup>2</sup> area. This image was obtained with the x-ray anode operated at 50 kV and 0.5 mA. Single spots 3 mm in diameter were also examined from the bottom and top of the pellet interiors relative to their orientation in the reducing furnace to semi-quantify any internal gallium migration. These spectra were acquired with the x-ray tube operated at 20 kV and 8 μA. After background subtraction and compensating for escape peaks, the gallium Kα peak from each of these spectra was integrated using the Kevex Omicron instrument software.

#### Pellet Exterior

Gallium migration gradients were detected on the pellet exteriors by rastering the primary beam in a line from the pellet bottom to the top in 100 μm increments with a 100 sec acquisition time per step, and the gallium intensity was monitored at each analysis point along the scan line. A 100 μm beam diameter was used, and the x-ray anode was operated at 50 kV and 1 mA. In addition to the interior, the top exterior of the pellet reduced at 1200°C was also imaged for gallium content with a 50 μm beam at 50 kV and 1 mA.

### Powders

Equal 0.25g aliquots from the surrogate powders (0.3g, 0.9g, and 2.5g lots) reduced from 600-1200°C in 100°C increments (21 samples total) were analyzed by bulk XRF. Since the powders were examined for bulk gallium content, the largest available beam aperture of 3 mm in diameter was utilized to provide the highest possible signal. All the powders were examined under helium. The x-ray anode was operated at 20 kV and 28  $\mu$ A, and each sample was analyzed for 200 sec. From the spectra obtained, the gallium  $K\alpha$  and cerium  $L\alpha$  lines were then background and escape peak subtracted and integrated for quantification purposes using the Kevex Omicron instrument software.

### **3.2.4.3.2. Results and Discussion**

*Pellet Analysis.* The series of surrogate pellets reduced at temperatures from 600°C to 1200°C were examined by XRMF both internally and externally with three different modes of analysis including: (1) elemental mapping, (2) single spot spectra, and (3) elemental line scans.

#### Elemental Mapping

Using the XRMF dynamic imaging mode, color-coded gallium maps of the surrogate pellet interiors were acquired, whereby the total gallium counts detected at each sample location (image pixel) are represented by a distinct color shade. Black regions correspond to 0 counts per second (cps) intensity values, while the areas where the maximum counts were detected are white, and the intensities measured between the maximum and minimum values are represented in a linear manner by a thermal color spectrum (with the red end corresponding to high count rates and the violet end representing low count rates).

Localized regions of high gallium concentration are observed throughout the pellets reduced at and above 900°C by comparing the XRMF gallium images acquired from the 600°C - 1200°C reduced surrogate pellet interiors shown in Figure 3.2.4.-1. The temperature regime from 600°C - 800°C was apparently not high enough for any preferential gallium migration to occur. Further evidence for this gallium migration temperature dependence will be presented in later discussions of the pellet single spot and line scan analyses. Recent and ongoing work to determine the phase diagram of the  $CeO_2/Ga_2O_3$  binary system (see Section 2.2.1) indicates that cerium gallates can form during reduction with hydrogen.<sup>39</sup> Hence, the gallium inclusions observed in the pellets reduced at 900°C-1200°C could correspond to the presence of these gallates. Additional x-ray microdiffraction (XRMD) studies to definitively identify the gallium phases present are currently being pursued and will be reported in a future publication.

A homogeneous gallium distribution is seen throughout the interior of the pellets reduced from 600°C – 800°C except at the bottom of the pellets (in relation to their orientation in the reducing furnace) where a high localized gallium concentration is present. The locations of these gallium hot spots appear to correlate with zirconium impurities that diffused into the pellet ends which rested on a zirconium-containing sand in the furnace. Figure 3.2.4-2 shows a localized zirconium hot spot detected by XRMF from the interior of a pellet reduced at 600°C, which is similar to the zirconium images from the pellets reduced at the other temperatures.

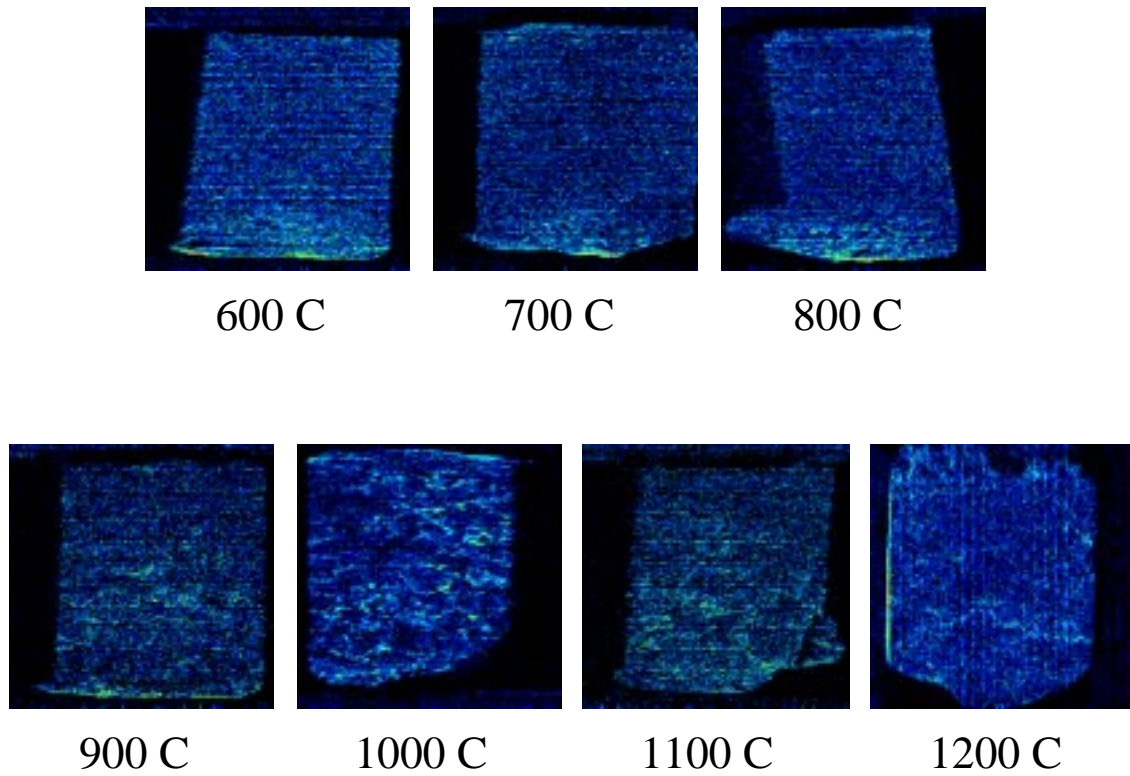


Figure 3.2.4-1. Interior dynamic mode XRMF gallium images acquired of the surrogate pellets reduced from 600°C - 1200°C. The bottoms of the pellet images correspond to the pellet ends resting on the furnace floor.

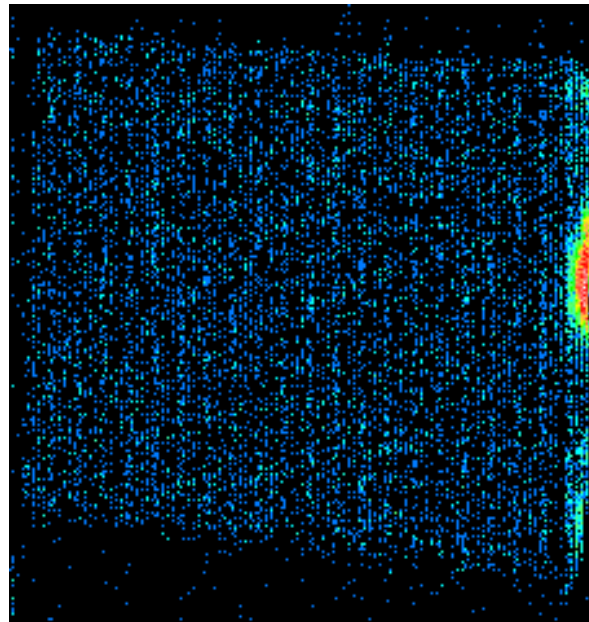


Figure 3.2.4.-2. Interior dynamic mode XRMF zirconium image of a surrogate pellet reduced at 600°C. The bottom of the image corresponds to the end of the pellet contacting the furnace floor.

Another interesting observation is the high gallium content seen on the exterior skin of the pellet reduced at 1200°C. (A gallium gradient was only observed on the left edge of the sample because it was aligned in a more direct path with the detector than the right edge, and higher count rates were therefore detected.) This gallium heterogeneity is illustrated in greater detail in Figure 3.2.4-3 which contains both a white light image and the XRMF dynamic mode gallium map of the 1200°C reduced pellet interior. At this high reduction temperature, a majority of the gallium apparently migrated outward to the pellet exterior. (The XRMF gallium image depicted in Figure 3.2.4-3B corresponds to the entire sample shown in Figure 3.2.4-3, but its dimensions are slightly distorted.) This migration information is significant to the MOX project since any gallium on the exterior of a fuel pellet might interact undesirably with the fuel cladding material. There appears to be some correlation between the location of the white regions in the white light image and the gallium inclusions identified in the elemental map. Ongoing XRMD, Raman, and IR studies of these surrogate samples should provide information about the phase of this white material.

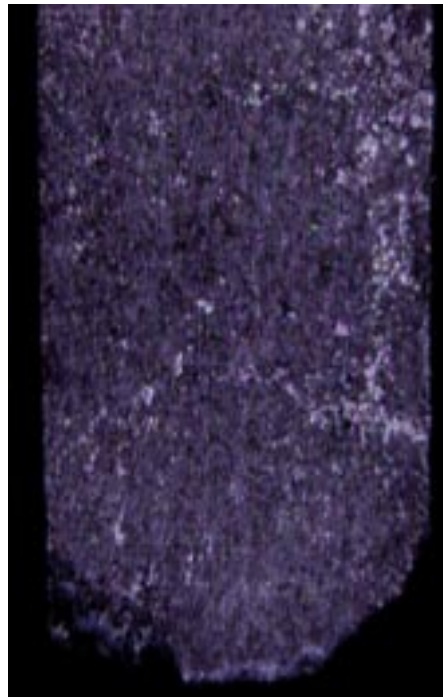


Figure 3.2.4-3. White light of the internal surface of the surrogate pellet reduced at 1200°C. The bottoms of the pellet images correspond to the pellet ends resting on the furnace floor.

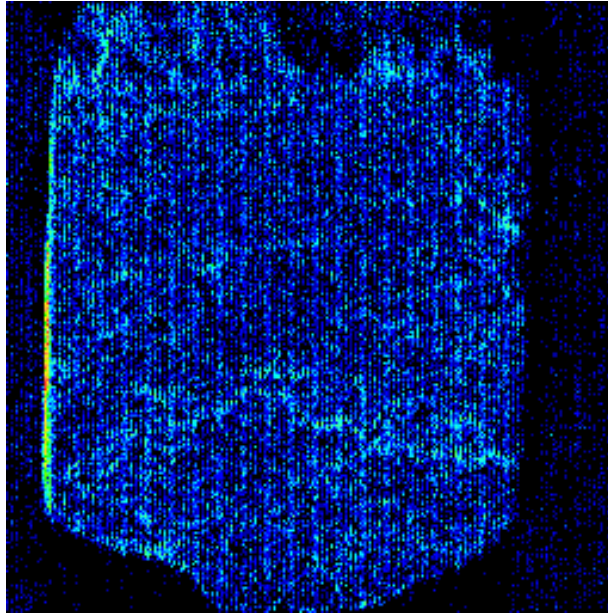


Figure 3.2.4-3B. Dynamic mode XRMF gallium image of the internal surface of the surrogate pellet reduced at 1200°C. The bottoms of the pellet images correspond to the pellet ends resting on the furnace floor.

The interior of this same pellet reduced at 1200°C was also examined by XRMF operated in the microprobe mode shown in Figure 3.2.4-4, where the image pixel intensity values were color-coded in the same manner as the dynamic mode image. With images acquired in the microprobe fashion, higher elemental sensitivity is achieved compared to dynamic imaging. However, the acquisition time can approach 24 h compared with 4 to 8 h for a dynamic image, and microprobe images will exhibit lower lateral resolution than that achieved with a dynamic image, where fluoresced x-rays are continuously monitored while the beam is rastered over the sample.

Both the white light image and the XRMF microprobe gallium map are shown in Figure 3.2.4-4. The gallium image corresponds to the boxed region denoted in green on the white light picture. (The scanned region was maintained within the pellet edges, and the entire pellet was not imaged because of instrumental problems if the x-ray beam moves off the sample edge where the count rate falls to 0 in the microprobe mode.) With the greatly improved gallium sensitivity of this microprobe image, concentrated regions of gallium can now clearly be discerned along both pellet edges as well as toward the top. This XRMF data provides unique and direct evidence for the Ludwig-Soret effect<sup>40</sup> in which a volatile species, such as the  $\text{Ga}_2\text{O}$  generated from the reduction of  $\text{Ga}_2\text{O}_3$ , follows a thermal gradient to higher temperature regions. The furnace used for pellet reduction contained a temperature gradient in which the temperature increased with distance above the oven floor. As the surrogate pellets were placed vertically on the furnace floor, the pellet tops were exposed to a higher temperature than the bottoms; thus, the  $\text{Ga}_2\text{O}$  liberated was expected to migrate up the pellets as well as outward to the hotter exterior surface, as was demonstrated by the XRMF microprobe image of the 1200°C pellet.

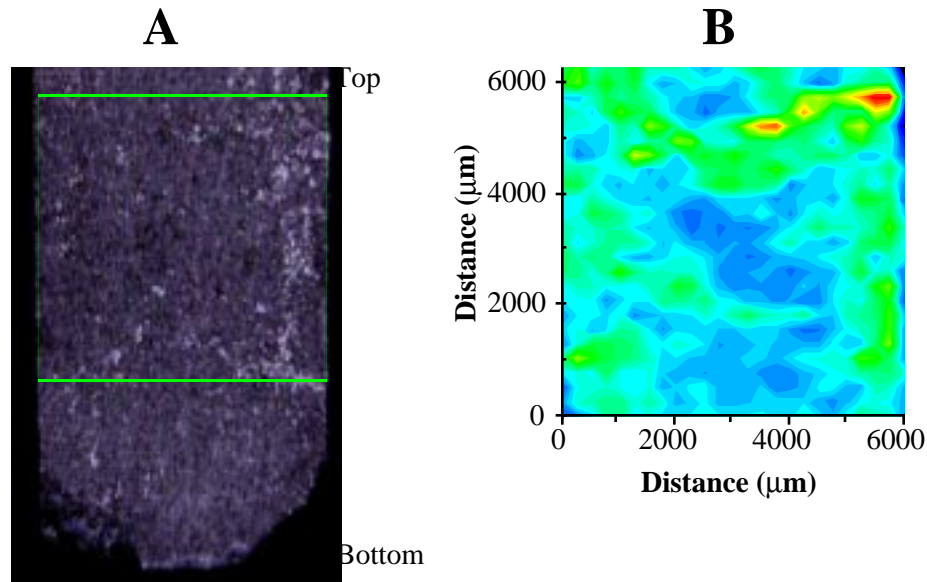


Figure 3.2.4-4. White light image (A) and microprobe mode XRMF gallium image (B) of the internal surface of the surrogate pellet reduced at 1200°C. The bottoms of the pellet images correspond to the pellet ends resting on the furnace floor. The sample region scanned in the microprobe mode is denoted with a green box on the white light image.

In addition to the gallium images, cerium was also mapped by XRMF in the dynamic mode. Figure 3.2.4-5 contains the interior cerium image of a surrogate pellet reduced at 900°C. As a majority of the pellet material is composed of cerium, high cerium counts are observed over a majority of the sample. Such an image is useful in detecting physical features such as cracks in the pellet because the sample topography in these regions results in lower cerium count rates being detected. Hence, the pellet cracks are imaged directly.

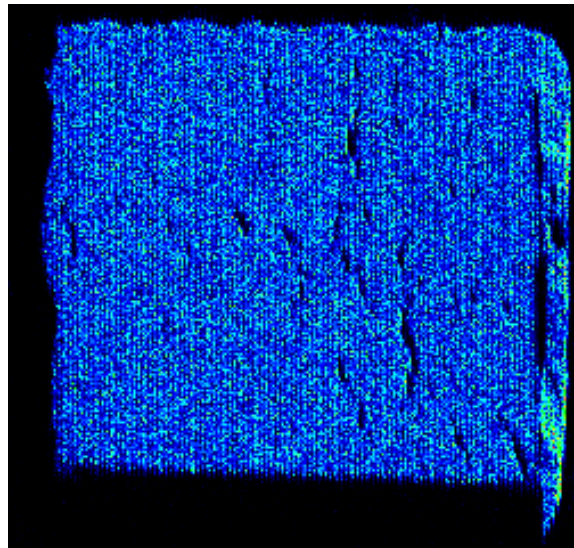


Figure 3.2.4-5. Interior dynamic mode XRMF cerium image of a surrogate pellet reduced at 900°C. The bottom of the image corresponds to the end of the pellet contacting the furnace floor.

### Interior Spot Analysis

Single spot spectra were also acquired from the reduced pellet interior bottom and tops to quantify internal gallium migration gradients. The gallium  $K\alpha$  peak top/bottom intensity ratio was determined for each pellet as shown in Figure 3.2.4-6. (The pellet reduced at 1100°C was damaged before the single spot analyses were performed and, therefore, was not included in the Figure 3.2.4-6 plot.) As the reduction temperature increases, the top/bottom gallium ratio also rises, indicative of the gallium increasingly migrating toward the top of the pellets. A pellet that was only sintered and not reduced was also analyzed to serve as a control and is included on the far right of Figure 3.2.4-6. The gallium top/bottom ratio in this case was found to be almost unity (1.04), verifying that gallium was evenly dispersed throughout the pellet prior to reduction and the formation of migrating  $Ga_2O$ .

### Exterior Line Scans

The external surface of the temperature-dependent reduced pellets was analyzed by XRMF gallium intensity line scans to probe any external migration gradients. By scanning the x-ray beam from the bottom of a pellet to the top, a typical gallium intensity profile was observed as illustrated in Figure 3.2.4-7. A high concentration was found at the pellet bottom region resulting in an intensity spike, and after falling to a plateau (P1), the intensity sharply increased before reaching a second plateau (P2) at the top of the pellet. The spike at the pellet bottom is attributed to the absence of significant gallium migration, as the furnace was relatively cool in this region. Toward the top of the pellet, the oven temperature was higher, and, thus, the rise in intensity and formation of P2 is indicative of the Ludwig-Soret Effect in which  $Ga_2O$  followed the oven thermal gradient to higher temperature regions.

The gallium line scan profiles from the pellets reduced at 600°C, 800°C, and 1200°C are overlaid in Figure 3.2.4-8. Clearly, the gallium migration is different when reduced at 600°C than at 1200°C. At 600°C no significant gallium was found at the top of the pellet because the temperature was too low for substantial movement over the experimental timeframe; however, at 1200°C, a majority of the gallium was kinetically able to move toward the top of the pellet as seen by the sharp rise in the P2 intensity. The gallium spike present at the bottom of the pellets also was found to migrate upward to a greater extent at higher reduction temperatures.

From each of the 600°C-1200°C pellet line scans, an average P2 gallium intensity was calculated, and these values are plotted versus pellet reduction temperature in Figure 3.2.4-9. (An anomalous gallium line scan was observed from the 900°C reduced pellet with no P1 or P2 regions present; thus, no P2 intensity value could be determined or included in the Figure 3.2.4-9 graph.) This P2 average gallium intensity increases linearly ( $r^2 = 0.912$ ) with reduction temperature, which quantitatively demonstrates that more gallium moved to the top of the pellet external surfaces which were reduced at higher temperatures. The distance from the bottom of each pellet to the start of the P2 region was also plotted versus pellet reduction temperature (Figure 3.2.4-10), and a linear increase was again observed ( $r^2 = 0.988$ ). Hence, in addition to more gallium migrating toward the top of the pellets reduced at higher temperatures, the gallium moved further up these pellets as well. (The P2 starting distance from the pellets reduced at 600°C and 900°C could not be determined and were not included in Figure 3.2.4-10 because both pellet line scans were flat and did not exhibit any plateaus.)

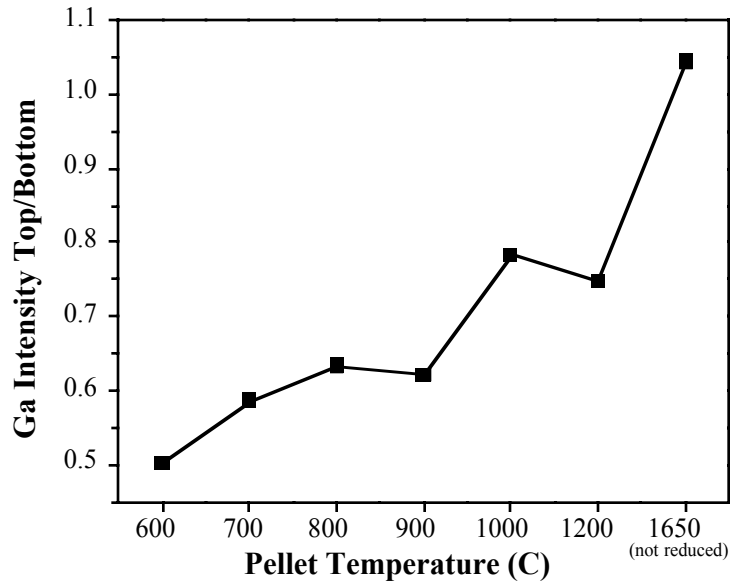


Figure 3.2.4-6. Plot of the gallium XRF intensity ratio vs. reduction temperature from single spot analyses at the top and bottom of the inside of the reduced surrogate pellets. The data point at the far right corresponds to the top/bottom intensity ratio observed from a pellet only sintered and not reduced.

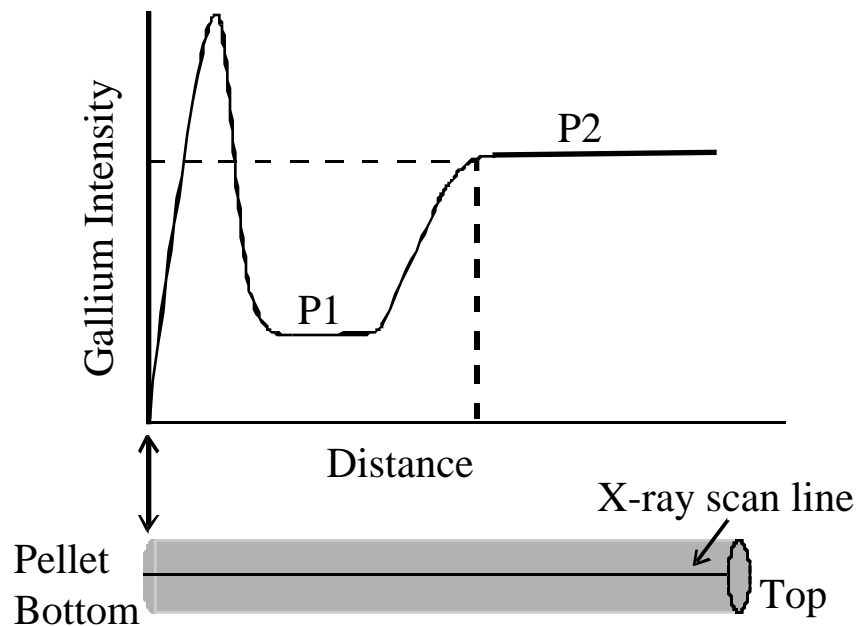


Figure 3.2.4-7. Typical gallium line scan intensity profile observed from the external skin of the reduced surrogate pellets.

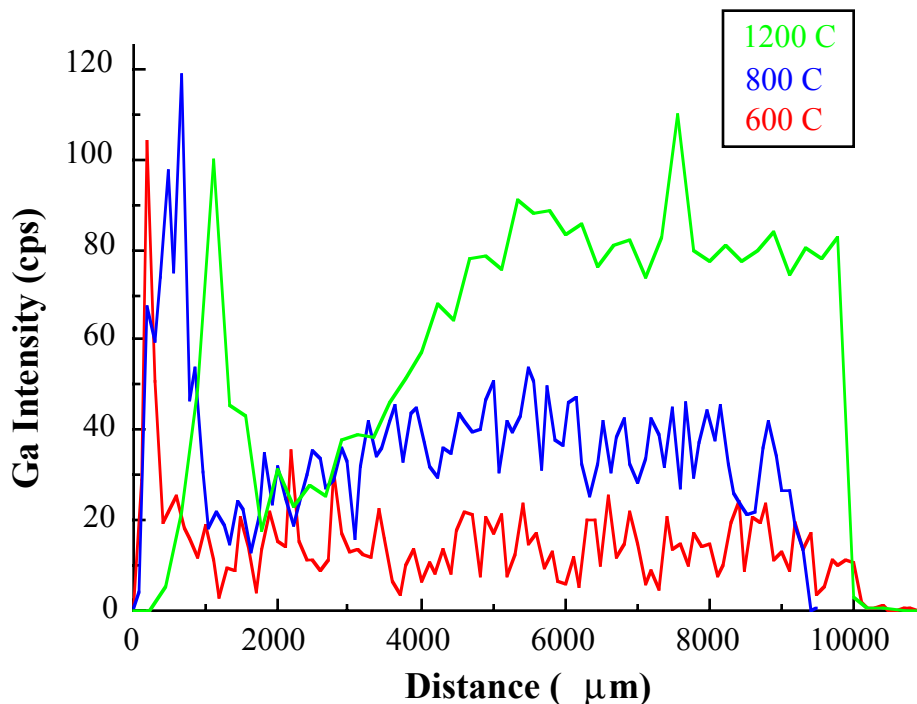


Figure 3.2.4-8. Gallium line scan profiles acquired from the outside of the surrogate pellets reduced at 600°C, 800°C, and 1200°C.

In addition to the line scans, the top external surface of the pellet reduced at 1200°C was mapped for gallium by XRMF. As expected, a high concentration of gallium was detected over the entire top surface (image not shown) which supports the previously discussed gallium migration profile. At such a high reduction temperature, a substantial amount of gallium traveled to the top of the pellet.

*Powder Analysis.* As the  $\text{Ga}_2\text{O}_3$  is removed from MOX fuel while in a powder form, surrogate powders reduced at temperatures from 600°C to 1200°C were examined by XRF to quantify the gallium present in each sample. In addition to determining the effect of temperature on gallium removal, different sample masses were also studied at each temperature to see if any correlation existed between sample mass and the extent of gallium extraction.

Figure 3.2.4-11 is a plot of the Ga/Ce intensity ratios measured from each powder sample versus reduction temperature. As expected, based on the surrogate pellet observations, more gallium was generally removed from the powders as the reduction temperature was raised, and the sample mass was also found to significantly affect the extent of gallium extracted. Essentially no gallium remained in the 0.3g and 0.9g samples reduced at 1200°C (both with a Ga/Ce intensity ratio of 0.002), but a significant gallium signal was detected from the 2.5g powder (Ga/Ce = 0.016). The hydrogen apparently did not effectively diffuse throughout the entire 2.5g powder lot, and, therefore, some  $\text{Ga}_2\text{O}_3$  was not converted to volatile  $\text{Ga}_2\text{O}$  but remained in the powder. In the case of the smaller 0.3g and 0.9g powders, however, essentially all of the  $\text{Ga}_2\text{O}_3$  was converted to the suboxide and was released from the powders.

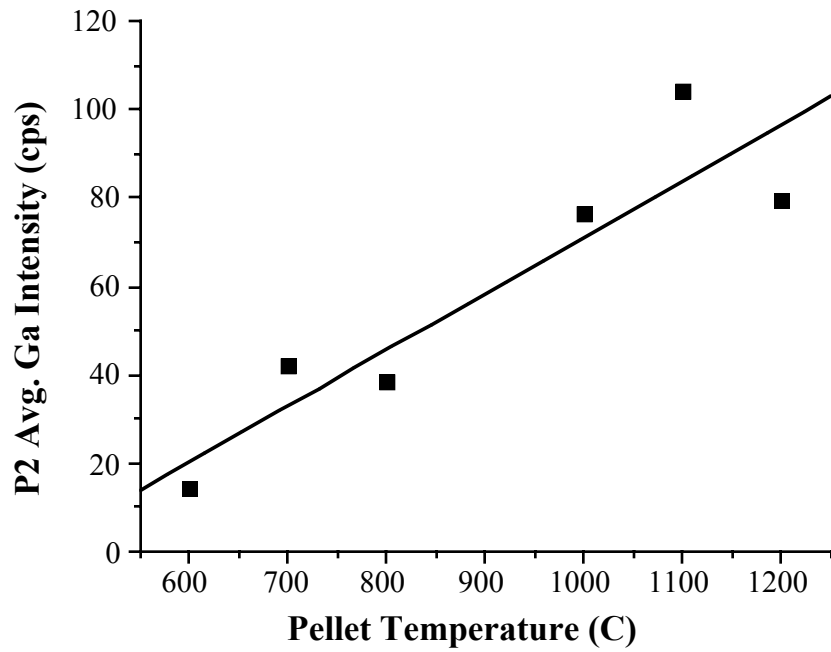


Figure 3.2.4-9. Plot of the average P2 gallium intensity vs. reduction temperature from the external line scans of the reduced surrogate pellets.

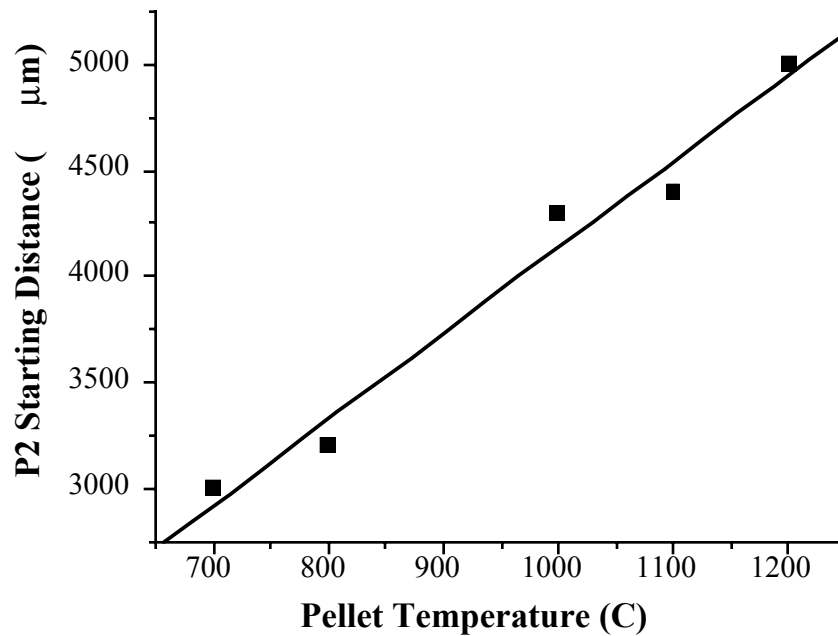


Figure 3.2.4-10. Plot of the distance from the pellet bottom to the start of the P2 region vs. reduction temperature from the external line scans of the reduced surrogate pellets.

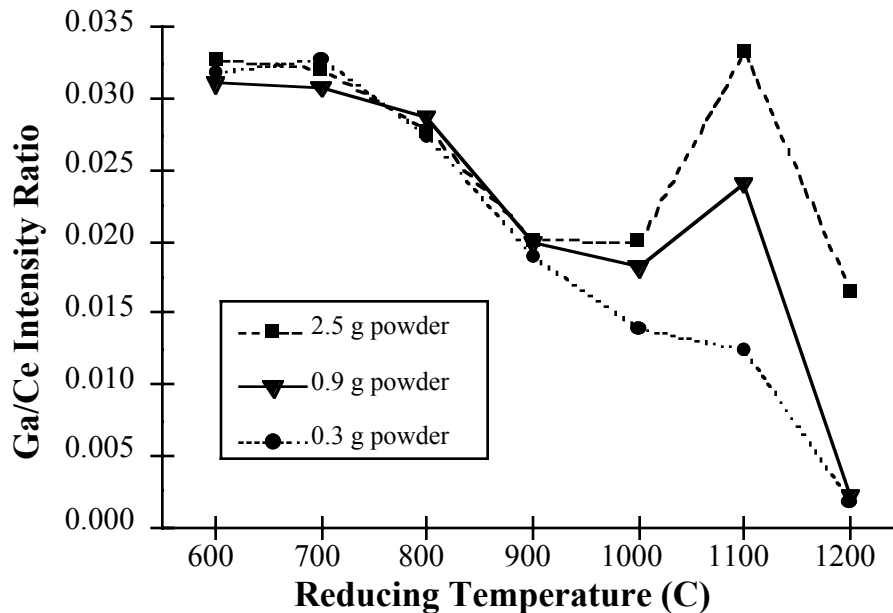


Figure 3.2.4-11. Plot of the XRF gallium/cerium intensity ratio from the reduced surrogate powders vs. reduction temperature.

A note should also be made concerning the powders reduced at 1000°C and 1100°C. The steady decline in the Ga/Ce ratio observed from the powders reduced at lower temperatures began to plateau at 1000°C and actually increased at 1100°C. One possible explanation for this is that a competition occurred between the  $Ga_2O_3$  leaving and the hydrogen diffusing into the powders in this temperature regime which inhibited the gallium removal process. This theory has not been verified, however. Nevertheless, the finding that the powder mass affects the magnitude of gallium removed is vital information to the MOX production process because it indicates that sample loads more effectively exposed to the hydrogen reducing atmosphere need to be implemented to maximize gallium extraction.

### 3.2.4.3.3 Conclusions

This work has demonstrated the utility of XRF and XRMF in providing elemental information about MOX surrogate samples. Such data would not be attainable by other methods with the elemental sensitivity of XRF when acquired over a comparable period of time. By using single spot analyses, line scans, and two dimensional elemental maps in a complementary manner, a better understanding of the elemental distributions as well as quantitative information was obtained.

XRMF experiments are presently underway to examine the gallium diffusion profile of MOX surrogates after reducing a sample consisting of an inclusion of  $Ga_2O_3$  located in the interior of a  $CeO_2$  pellet. In addition the fundamental processes involved during the reduction of the  $Ga_2O_3/CeO_2$  surrogate system will be studied by Raman, IR, XRD, and XPS to provide molecular and chemical state information that will complement the XRF elemental data already obtained.

#### 4.0 SUMMARY OF ACTIVITIES IN FY97

Table 4.0-1 contains a summary of the activities that were proposed for FY97 as well as the status of these activities.

**TABLE 4.0-1  
FISCAL YEAR 1997 R&D MILESTONE SUMMARY**

Applicable Section	Milestone	Expected Completion Date for FY97 Activities	Status
2.1.1	Define Required HYDOX-Derived PuO <sub>2</sub> Amounts and Desired Characteristics	1 December 1996	Completed. Definition used in LLNL request for PuO <sub>2</sub> .
2.1.1	Obtain HYDOX-Derived Feed Materials	1 March 1997	Completed. Materials were received.
2.1.1	Complete Characterization of HYDOX-Derived Feed Material	1 May 1997	Completed and reported in Section 2.1.1 and LA-UR-97-2863
2.1.2	Define Required Aqueous-Derived PuO <sub>2</sub> Amounts and Desired Characteristics	14 February 1997	Completed. Definition used to locate source and obtain permission for use.
2.1.2	Obtain Aqueous-Derived Feed Materials	1 March 1997	Completed. Permission and material received. Waiting for room in gloveboxes.
2.1.2	Complete Characterization of Aqueous-Derived Feed Material	1 May 1997	Delayed or eliminated. Waiting for samples to be made after glovebox entry.
2.2.1	Complete Critical Assessment of Ga <sub>2</sub> O <sub>3</sub> -PuO <sub>2</sub> Thermodynamic Data	1 March 1997	Completed and reported in Section 2.2.1.
2.2.1	Optimize Ga <sub>2</sub> O <sub>3</sub> -PuO <sub>2</sub> Phase Diagram	30 September 1997	Underway and reported in Section 2.2.1; will be completed in FY98.
2.2.1	Complete Critical Assessment of PuO <sub>2</sub> -UO <sub>2</sub> Thermodynamic Data	1 August 1997	Completed and reported in Section 2.2.1.
2.2.1	Optimize PuO <sub>2</sub> -UO <sub>2</sub> Phase Diagram	30 September 1997	Underway and reported in Section 2.2.1; will be completed in FY98.

**TABLE 4.0-1 (con't)**  
**FISCAL YEAR 1997 R&D MILESTONE SUMMARY**

<b>Applicable Section</b>	<b>Milestone</b>	<b>Expected Completion Date for FY97 Activities</b>	<b>Status</b>
2.2.1	Optimize Ga <sub>2</sub> O <sub>3</sub> -PuO <sub>2</sub> -UO <sub>2</sub> Phase Diagram	30 September 1997	Underway and reported in Section 2.2.1; will be completed in FY98.
2.2.2	Complete Time, Temperature, and Sample Size Studies on Surrogates	1 July 1997	Completed and reported in Section 2.2.2.
2.2.2	Complete Surrogate Gallium Removal Studies	30 September 1997	Underway and reported in Section 2.2.2; will be completed in FY98.
2.2.3	Complete PuO <sub>2</sub> gallium removal studies	30 September 1997	Delayed - awaiting facility availability; will be initiated in FY98.
2.2.4	Generate Throughput Requirements and Surplus Inventory Effects	28 February 1997	Completed except for inventory effects. Reported in Section 2.2.4.
2.2.4	Identify Thermal Treatment Equipment and Sizing	31 July 1997	Completed and reflected in TIGRS demo plan.
2.2.4	Complete Thermal Treatment Cost Estimates	31 August 1997	Delayed - pending TIGRS design effort.
2.2.4	Complete Thermal Treatment Industrialization Study Report	30 September 1997	Underway and reported in Section 2.2.4.
2.2.4	Create Block Diagram of Aqueous Removal Concept	31 December 1996	Completed and reported in Section 2.2.4.
2.2.4	Develop Aqueous Removal Process Specifics	31 December 1996	Completed and reported in Section 2.2.4.
2.2.4	Determine Materials Balances for Aqueous Removal	31 March 1997	Completed and reported in Section 2.2.4.
2.2.4	Estimate Aqueous Removal Equipment Sizing	30 June 1997	Completed and reported in Section 2.2.4.
2.2.4	Perform Aqueous Removal Cost Estimation	30 June 1997	Delayed - insufficient funds.
2.2.4	Complete Aqueous Removal Report	30 September 1997	Completed and reported in Section 2.2.4 and LA-UR-97-181 and 685.

**TABLE 4.0-1 (con't)**  
**FISCAL YEAR 1997 R&D MILESTONE SUMMARY**

<b>Applicable Section</b>	<b>Milestone</b>	<b>Expected Completion Date for FY97 Activities</b>	<b>Status</b>
3.1.1	Characterize Samples	1 May 1997	Delayed - waiting for pellet fabrication; included in FY98 plan.
3.1.1	Complete PuO <sub>2</sub> Variability Study	1 May 1997	Delayed - waiting for pellet fabrication/analysis; included in FY98 plan
3.1.2	Obtain Various UO <sub>2</sub> Feed	14 March 1997	Underway. Permission obtained for new UO <sub>2</sub> from ABB/CE. Working on details to assure that material is "useful"; included in FY98 plan
3.1.2	Fabricate Pellets with Various UO <sub>2</sub> Feed	14 April 1997	Delayed - waiting for prototypic UO <sub>2</sub> feed material; will be included in FY98 plan
3.1.2	Characterize Samples	15 May 1997	Delayed - waiting for pellet fabrication; included in FY98 plan.
3.1.2	Complete UO <sub>2</sub> Variability Study	15 May 1997	Delayed - waiting for pellet fabrication/analysis; included in FY98 plan
3.1.3	Complete Temperature Effect Study Using UO <sub>2</sub> -based Surrogates	1 July 1997	Completed and reported in Section 3.1.3.
3.1.3	Complete H <sub>2</sub> O Partial Pressure Effect Study Using UO <sub>2</sub> -based Surrogates	30 September 1997	Underway and reported in Section 3.1.3; will be completed in FY98.
3.1.3	Complete Sintering Study	30 September 1997	Underway and reported in Section 3.1.3; will be completed in FY98.
3.2.1	Identify Autoradiograph Techniques, Obtain Films and Visual Standards	1 March 1997	Underway and reported; more films need to be obtained
3.2.1	Fabricate Homogeneity Standards with Reactor-grade Pu	31 May 1997	Delayed/Canceled. Consortium funded activity.

**TABLE 4.0-1 (con't)**  
**FISCAL YEAR 1997 R&D MILESTONE SUMMARY**

<b>Applicable Section</b>	<b>Milestone</b>	<b>Expected Completion Date for FY97 Activities</b>	<b>Status</b>
3.2.1	Complete Autoradiograph Study	15 July 1997	Underway - and reported in Section 3.2.1; will be completed in FY98.
3.2.1	Compare XRMF Aperture with Capillary Optics	15 November 1996	Underway - and reported in Section 3.2.1; will be completed in FY98.
3.2.1	Determine XRMF Radioactive Burden Limit	1 March 1997	Delayed/Canceled.
3.2.1	Determine XRMF Limits of Detection for Ga and Pu	1 June 1997	Underway - and reported in Section 3.2.1- focuses on Ga detection; will be completed in FY98.
3.2.1	Determine Resolution of 50 $\mu$ m X-Ray Beam	1 September 1997	Underway - and reported in Section 3.2.1; will be completed in FY98.
3.2.1	Complete XRMF Study	1 September 1997	Underway - and reported in Section 3.2.1; will be completed in FY98.
3.2.2	Obtain New Surface Finish Measurement Device	1 February 1997	Completed. Used in Parallax fabrication campaign.
3.2.2	Investigate Alternative O/M Measurement Techniques	30 September 1997	Underway - and reported in Section 3.2.2; will be completed in FY98.
3.2.3	Validation of Trace Analysis	1 March 1997	Completed and reported in Section 3.2.3.

## 5.0. REFERENCES

1. DOE, Office of Fissile Materials Disposition, "General Requirements Document," DOE/MD-0007, October 1, 1997, Rev. 0.
2. C. A. Beard et al., "Nuclear Fuels Technologies Fiscal Year 1996 Research and Development Test Results," Los Alamos National Laboratory report LA-UR-97-440, November 8, 1996.
3. G. Arthur and D. Scott, "The Effect of TiO<sub>2</sub> Additions on the Sintering of UO<sub>2</sub>," *Trans. Brit. Ceram. Soc.*, **63** [4] 417-429 (1964).
4. T. D. Chikalla, C. E. McNeilly and R. E. Skavdahl, "The Plutonium-Oxygen System," *J. Nucl. Mater.*, **12**, 131-141 (1964)
5. F. L. Oetting, "The Chemical Thermodynamic Properties of Plutonium Compounds," *Chem. Rev.*, **67**, 262-295 (1967).
6. I. Barin, *Thermochemical Data of Pure Substances*, 3rd Edition, Vols. 1 and 2, Meinheim VCH (New York, 1995).
7. T. M. Besmann and T. B. Lindemer, "Chemical Thermodynamic Representations of PuO<sub>2-x</sub>(s) and U<sub>1-z</sub>Pu<sub>z</sub>O<sub>w</sub>(s)," *J. Nucl. Mater.* **130**, 489-504 (1985).
8. M. H. Rand, "Thermochemical Properties," *Plutonium: Physico-Chemical Properties of Its Compounds and Alloys*, IAEA Review of Atomic Energy. Vol. 4, Special Issue **1**, 5-51 (Vienna, 1966).
9. R. J. Ackerman, R. L. Faircloth, and M. H. Rand, "A Thermodynamic Study of the Vaporization Behavior of the Substoichiometric Plutonium Dioxide Phase," *J. Phys. Chem.*, **70**, 3698 (1966).
10. L. M. Foster and J. Scardefield, "Oxygen Doping of Solution-Grown GaP," *J. Electrochem. Soc.: Solid State Sci.*, **116**, 494-498 (1969).
11. I. A. Sheka, I. S. Chaus and T. T. Mityureva, *The Chemistry of Gallium*, Elsevier Publishing Company (New York, 1966).
12. D. P. Butt personal database, MTA. Within MTA it is referenced to Ruzinov L. P. and Guljanickij B. S.: Ravnovesnye prevrasoenija metallugiceskin reaktseij, Moskva, 1975 (Russian).
13. C. Sari, U. Benedict, and H. Blank, "Metallographic and X-ray Investigation of the Pu-O and U-Pu-O Systems," *Thermodynamics of Nuclear Materials*, IAEA, 541-611, (Vienna, 1968).
14. Jean-Claude Boivinequ, "Etude Par Rayons X du Diagramme Plutonium -Oxygene de la Temperature Ambiante Jusqu'e a 1100°C," *J. Nucl. Mater.* **60**, 31-38 (1976).
15. P. E. Potter and M. H. Rand, "Thermodynamic Aspects of the Use of Oxides as Nuclear Reactor Fuels," *High Temp. Sci.*, **13**, 315-329 (1980).
16. R. D. Shannon, "Revised Effective Ionic Radii and Systematic Studies of Interatomic Distances in Halides and Chalcogenides," *Acta Cryst.* (1976), **A 32**, 751.
17. A. I. Leonov and E K. Keler, "High Temperature Reactions Between Ce<sub>2</sub>O<sub>3</sub> and Al<sub>2</sub>O<sub>3</sub>, and the Properties of the Cerium Aluiminates Formed," *Izv. AN SSR. Otd. Khim. N.* (English Translation), **11**, 1819-1823 (1962).
18. D. F. Wilson, et al., "Interactions of Zircaloy Cladding with Gallium—1997 Status," Oak Ridge National Laboratory report ORNL/TN-13505, November 1997.

19. S. DeMuth, "Technical Basis for Separation of Plutonium from Gallium by Ion Exchange," Los Alamos National Laboratory report LA-UR-97-685, 2/24/97.
20. S. DeMuth, "Conceptual Design for Separation of Plutonium and Gallium by Solvent Extraction," Los Alamos National Laboratory report LA-UR-97-181, 4/4/97.
21. R.H. Perry and C.H. Chilton, *Chemical Engineers' Handbook*, 5th Edition, McGraw-Hill Book Company, New York, (1973).
22. S. DeMuth, "Preconceptual Design for Separation of Plutonium from Gallium by Ion Exchange, Rev. 1," Los Alamos National Laboratory report LA-UR-97-3767, 9/97.
23. S. DeMuth, "Ion Exchange Separation of Plutonium from Gallium (1) Resource and Inventory Requirements, (2) Waste, Emissions, and Effluent, and (3) Facility Size, Rev. 1," Los Alamos National Laboratory report LA-UR-97-3902, 9/97.
24. M. Benedict, T. H. Pigford, and H. W. Levi, *Nuclear Chemical Engineering*, 2nd Edition, McGraw-Hill, 1981, Section 4.7.
25. E. P. Bertin, *Principles and Practice of X-ray Spectrometric Analysis*, 2nd ed.; Plenum Press: New York, 1975.
26. M. C. Nichols, D. R. Boehme, R. W. Ryon, D. Wherry, B. Cross, G. Aden, *Adv. X-ray Anal.* **1987**, *30*, 45-51.
27. D. C. Wherry, B. J. Cross, T. H. Briggs, *Adv. X-ray Anal.* **1988**, *21*, 93-98.
28. A. Rindby, *Nucl. Instrum. Methods Phys. Res.* **1986**, *A249*, 536-540.
29. N. Yamamoto, Y. Hosokawa, *Jpn. J. Appl. Phys. Part 2* **1988**, *27*, L2203-L2206.
30. D. A. Carpenter, M. A. Taylor, C. E. Holcombe, *Adv. X-ray Anal.* **1989**, *32*, 115-120.
31. Y. Kobayashi, N. Fukumoto, M. Kurahashi, *Meas. Sci. Technol.* **1991**, *2*, 183-184.
32. K. Janssens, L. Vincze, J. Rubio, F. Adams, G. Bernasconi, *J. Anal. At. Spectrom.* **1994**, *9*, 151-157.
33. D. A. Carpenter, M. A. Taylor, R. L. Lawson, *J. Trace Microprobe Tech.* **1995**, *13*, 141-161.
34. A. Attaelmanan, P. Voglis, A. Rindby, S. Larsson, P. Engstrom, *Rev. Sci. Instrum.* **1995**, *66*, 24-27.
35. V. A. Arkadiev, A. A. Bjeoumikhov, H. E. Gorny, M. Schiekkel, R. Wedell, *J. Trace Microprobe Tech.* **1996**, *14*, 131-135.
36. A. Rindby, P. Engstrom, K. Janssens, J. Osan, *Nucl. Instrum. Methods Phys. Res.* **1997**, *B124*, 591-604.
37. Z. W. Chen, D. B. Wittry, *Appl. Phys. Lett.* **1997**, *71*, 1884-1886.
38. R. W. Ryon, H. E. Martz, J. M. Hernandez, J. J. Haskins, R. A. Day, J. M. Brase, B. Cross, D. Wherry, *Adv. X-ray Anal.* **1988**, *31*, 35-52.
39. D. P. Butt, Y. Park, *Thermodynamics, Phase Relationships, and the Kinetics of Gallium Removal from Mixed Oxide Fuel Fabricated with Weapons Grade Plutonium*; Internal Report, Los Alamos National Laboratory; 1997.
40. P. Kofstad, *High Temperature Corrosion*; Elsevier Applied Science: London, 1988.

